Photon Scattering in Semiconductor Nanostructures

David L. Hurst
MPhys

Submitted for the Degree of
Doctor of Philosophy
July 2019

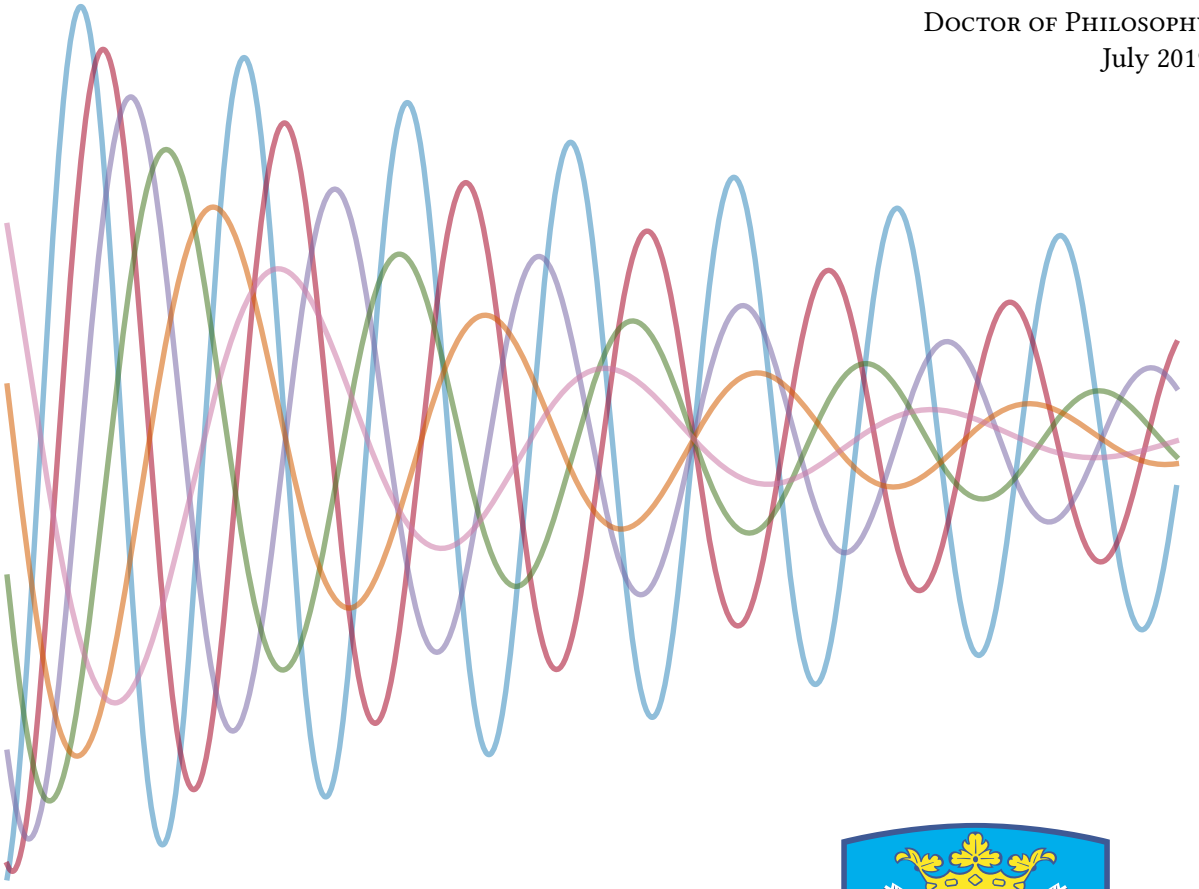

Department of Physics and Astronomy
The University of Sheffield

theoretical physics

*How do I define ~~history~~? It's just one f*cking thing after another.*

-Alan Bennett, The History Boys

Abstract

Quantum technologies promise to revolutionise the world we live in, with improvements in computing, metrology and secure communication all promised in the future. However, despite decades of developmental work, these technologies are not yet ubiquitous in even industrial settings and this is because of the inherent difficulties in physically realising a scalable, high-fidelity qubit. Solid-state qubits have a number of advantages over their trapped ion and photonic counterparts in terms of potential scalability but several challenges remain unaddressed. These qubits, primarily in the form of the semiconductor quantum dot, are the subject of this thesis.

We begin by reviewing the mathematical foundations of quantum mechanics and discuss the key feature of 'entanglement,' which we show forms a resource for communication protocols. We then discuss the broad field of quantum optics and show how the master equation and Input-Output formalism can be used to model various simple quantum systems. For quantum information applications however, neither of these techniques is ideal and this motivates us to find a novel technique for calculating S-matrices in waveguide QED. This is important because of the advantages associated with integrating quantum dots into waveguide structures, such as the ability to enhance the light-matter interaction. We derive the single and two-photon S-matrices for both two-level and Λ-system emitters.

We then move on to describe how a solid-state quantum emitter can be coupled to a waveguide in a non-reciprocal manner and study experimental results obtained for such a system. We produce a theoretical model to describe the system and determine that the dynamics are dominated by noise processes, which we are able to quantify. We conclude by studying a second experiment and use a transfer-matrix technique to reproduce the observed asymmetric lineshapes in the transmission geometry experiments.

Finally, we note that one major disadvantage of solid-state qubits is that their spectral properties can vary considerably even between emitters of the same species. We show how a protocol for entangling such emitters can fail when we input only a single photon into the system but succeed if we are able to engineer a suitable two-photon state. We study a wide section of the total emitter parameter space and are able to specify whether a given pair of emitters will be more strongly entangled by the one or two-photon protocol. Our work indicates that the technical challenge of locating spectrally identical emitters may be relaxed in favour of optical state optimisation.

Declaration of Authorship

I, David L. Hurst, declare that the work presented here is my own and has not been previously submitted for award at this or any other institution. Wherever the work of another author is shown, it is appropriately referenced. Parts of this thesis are based upon published articles or manuscripts submitted for publication.

Publications

1. D.L. Hurst and P. Kok. "Analytic few-photon scattering in waveguide QED." *Phys. Rev. A* **97** 043850 (2018).
   I designed this project collaboratively with P. Kok. I performed the calculations and wrote the manuscript with input from P. Kok.

2. D. Hallett, A.P. Foster, D.L. Hurst, B. Royall, P. Kok, E. Clarke, I.E. Itskevich, A.M. Fox, M.S. Skolnick and L.R. Wilson. "Electrical control of nonlinear quantum optics in a nano-photonic waveguide." *Optica* **5**(5) 644 (2018).
   I developed a theoretical model of the system studied experimentally by D. Hallett and A.P. Foster. I contributed sections to the manuscript written by A.P. Foster.

3. D.L. Hurst, D.M. Price, C. Bentham, M.N. Makhonin, B. Royall, E. Clarke, P. Kok, L.R. Wilson, M.S. Skolnick and A.M. Fox. "Non-Reciprocal transmission and reflection of a chirally-coupled quantum dot." *Nano. Lett.* **18**(9) 5475 (2018).
   I interpreted the experimental data collected by D.M. Price, C. Bentham and M.N. Makhonin. I developed a theoretical model of the system and wrote the manuscript with input from: A.M. Fox, M.N. Makhonin, D.M. Price and M.S. Skolnick.

4. D.L. Hurst, K.B. Joanesarson, J. Iles-Smith, J. Mørk and P. Kok. "Generating maximal entanglement between spectrally distinct solid-state emitters." *Phys. Rev. Lett.* **123** 023603 (2019).
   I designed this project collaboratively with P. Kok. I performed the single and two photon calculations together with K.B. Joanesarson. I wrote large parts of the manuscript, which was collaboratively produced with input from all authors.

Signed: .....

Dated: .....

Acknowledgements

Thanks are firstly and crucially due to my supervisor, Pieter Kok, without whom this PhD would not have been possible. When I think back to how he persuaded me to start the project in the first place, chivvied me along through the rough times and got me to the point I'm at today, I could honestly beat him to death with a cricket bat. Occasionally my maverick ways or general misery would prove too much for even Pieter and at various points I received additional and extremely useful guidance from: Mark Fox, Maurice Skolnick and Luke Wilson.

I want to extend huge thanks to Kristoffer Joanesarson, who made our collaboration not only extremely productive but also extremely enjoyable. Without his ability to write code at super-human speeds, the sixth chapter of this thesis would not be so interesting. And without his ability to drink beer at super-human speeds, many of my Friday nights would not have been so interesting. I have had the (sometimes dubious) pleasure of collaborating with a number of great experimentalists over the course of my PhD and I want to specifically acknowledge their contribution to this thesis. Without the hard work of: Chris Bentham, Andrew Foster, Dom 'Doom' Hallett, Maxim Makhonin and Dave Price, my models would have remained untested and useless—as opposed to merely useless.

My only hope is that this thesis is more neatly organised than the office in which it was written. However, like an old, mouldy teddy bear, the outer appearance of E13a stands in stark contrast to the emotional value it holds. It was an honour to call a desk on that hallowed ground my own and I sincerely hope I didn't set anybody's career or science in general too far back during my time here. Please be assured that, were I a rich man, I'd have bought everyone a pair of 'David-cancelling headphones.' Giuseppe Buonaiuto, Emiliano Cancellieri, Luke Heyfron, Mark Howard, Zixin Huang, Mark Pearce, Jasminder Sidhu and Scott Vinay have all earned my love and gratitude and I regret that I cannot spend more time getting to know the new inhabitants of 'The Mind Palace:' Cosmo Lupo, Armanda Quintavalle and Joschka Roffe.

It's customary to thank your friends and say that 'this thesis would not have been possible without them' at this point. To be honest I'm fairly confident that, as none of my friends are quantum opticians, this statement would be a lie. Of course that isn't to say that I'd have wanted to do this PhD without the rogues' gallery of freaks and misfits that I often find myself in the company of. I am going to avoid the problem of forgetting to mention somebody by mentioning nobody at all but please be aware that if you're reading this and have put up with my inconsistent personal hygiene and sobriety over the last few years, you occupy a special place in my heart. It would be remiss of me to not acknowledge the Capybros and Grenoside Working Men's Club specifically.

It is however possible that this thesis really would not have been produced without the support of my family. Mum, Dad and Rachel all share a common contempt for the entire subject of physics and I firmly believe this had the healthy effect of preventing me becoming too wrapped up in my own bullsh*t. On a more practical note, I thank my parents for housing me for the last six months of the PhD and for feeding me at various points throughout—the very real threat of starvation was subsequently averted. On the subject of housing, I thank James Bishop, Rob Elgar and Joe

Maguire for living with me while most of this work was completed. I think anybody who knows me sufficiently well understands the sacrifice they all made.

The contribution of another cannot be ignored and I want to extend thanks to my girlfriend, who's been with me throughout the PhD. Without her lack of existence and subsequent inability to distract me from the project, there's a chance I would have completed a year and not merely six months late.

Financial support from EPSRC made this PhD possible and is gratefully acknowledged. I sincerely hope that the UK taxpayer never fully realises just how much money this all cost…

Contents

Chapter 1

Introduction

1.1 Motivation—Quantum Technologies

The world we live in today is the product of decades of relentless technological advancement. In particular, our ability to engineer ever more powerful micro-processors has rendered tasks with massive computational complexity almost trivial. This increase in processing power is captured phenomenologically by Moore's Law, which predicts a doubling in the transistor count of a typical micro-processor over a period of eighteen to twenty-four months [1]. We see in Fig. 1.1a that Moore's Law has proven wonderfully prescient over the past half century but we must also be mindful that this cannot continue indefinitely. At the time of writing, state of the art computer chips have transistors with physical dimensions on the nanometre scale [2]. We are entering the regime where a processor's transistors cannot be made smaller—being constrained from below by the size of a single atom.

In order to solve problems of increasing complexity, a new approach to computing is necessary and fortunately a promising avenue presents itself to us. It has been known for many years that algorithms exist, which can drastically reduce the number of steps a given calculation requires to complete. Arguably the most famous example of such a protocol is Shor's Algorithm for finding the prime factors of an integer [3]. We see in Fig. 1.1b that Shor's algorithm, running at a million operations per second, could factor a thousand bit number in a few hours. In contrast, current algorithms running on modern supercomputers could take hundreds of millions of years. The difficulty of prime factorisation forms the basis for many current security protocols and such a dramatic speed-up would prove massively disruptive to our current communication paradigms. Shor's Algorithm is just one example of a wider class of protocols, which achieve similar dramatic results. Algorithms for e.g. database searching [4], simulation of physical systems [5] and the solution of algebraic problems [6] are all known to exist.

These massively efficient algorithms are distinct from those employed in a modern "classical"[1] computer in that they rely on a new computing architecture; that of the quantum computer [9]. This is a device designed to utilise the features of quantum mechanics for advantage and is just one instance of a broader class of quantum technologies, with quantum-enhanced measurement devices [10] and cryptography systems [11] being two notable others. The first quantum devices were proposed many decades ago [12] and quantum theory was developed nearly a century before even that. The fact that these devices are not yet commonplace is testament to the huge challenges we face in their creation and overcoming these hurdles is one of the over-arching goals of modern physics. Progress towards this has accelerated in recent years and we are entering what is sometimes termed the "Second Quantum Revolution."

[1] Here and throughout this thesis we use "classical" to simply mean "not quantum."

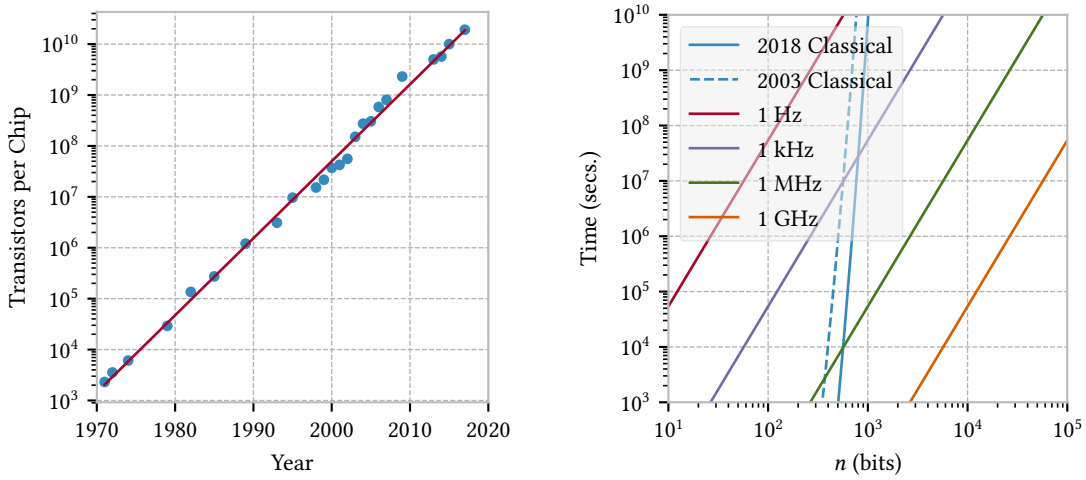

(a) Moore's Law.

(b) Quantum-classical scaling.

Figure 1.1: (a) Typical transistor count for a micro-processor manufactured in a given year. (b) Time to factor an n-bit prime number using either a classical computer or Shor's algorithm at a given clock speed. Data for Fig. 1.1a can be found in Ref. [7] and the expressions used to create Fig. 1.1b in Ref. [8].

1.2 Qubits and Entanglement

In classical technologies the fundamental unit of information is the "bit" and takes one of two distinct values, conventionally labelled as 0 and 1. These values can be physically represented by e.g. the absence or presence of an electrical pulse (as in a computer processor) and combinations built up to form large data structures. In quantum technologies the base unit of information is fundamentally different and takes into account our understanding of the world in terms of quantum theory. Here the quantum bit or "qubit" can take the 0 and 1 values of the classical bit but also any combination of these. Conventionally we represent the state of a qubit by the vector $|\psi\rangle = \alpha|0\rangle + \beta|1\rangle$, where α and β are complex numbers and $|0\rangle$ and $|1\rangle$ form an orthonormal basis. When normalised to unit length, this vector can conveniently be represented as a point on the "Bloch Sphere" as shown in Fig. 1.2a.

As quantum technologies develop, it seems likely that different physical implementations of the qubit will be used in conjunction with one another. This is because no implementation considered so far is free from disadvantages, which preclude its use for a given purpose. For example, qubits formed from the orthogonal polarisation states of a photon have large velocities and coherence times, which makes them ideal for long-distance communication. The photon-photon interaction strength is extremely low however and this makes two photon logic gates and subsequent photonic quantum computation challenging. By contrast, qubits formed from superconducting circuits interact with control photons strongly but lose their quantum information or 'decohere' in a matter of microseconds. Potential qubit candidates that have been experimentally realised to date include: NV colour centres in diamond [13], semiconductor quantum dots [14], trapped ions [15], optical photons [16] and superconducting circuits [17].

Systems of multiple qubits can exhibit so-called entanglement, a property with no classical analogy. Entanglement is a fundamental feature of quantum theory and the one which Einstein famously objected to, terming it "spooky action at a distance" [18]. Essentially quantum theory allows two physically distinct and spatially separated systems to share a common state and, crucially, the state of one sub-system can be instantaneously changed via a measurement on

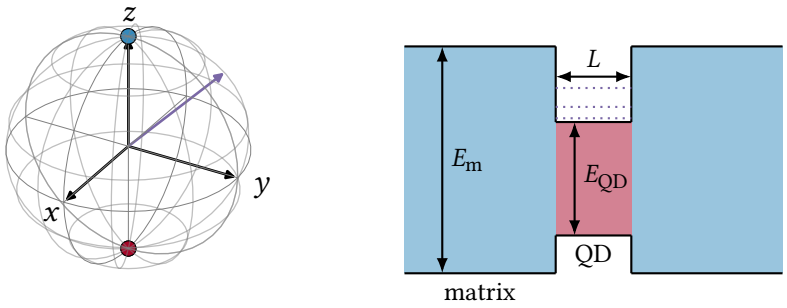

(a) Bloch sphere.

(b) QD energy level schematic.

Figure 1.2: (a) Any possible pure qubit state can be mapped to a point on the Bloch Sphere and any location on the sphere mapped to a qubit state. The states $|0\rangle$ and $|1\rangle$ are represented by the blue and red markers respectively and the purple arrow shows some arbitrary state $|\psi\rangle$. (b) QD energy level diagram. The host material is characterised by some band-gap E_m, with the QD having a smaller gap E_{QD}. The size of the QD, L is small such that energy levels are discrete, similar to the infinite potential well model.

the other. This property can actually be thought of as a resource for quantum technologies [19], with technologies employing more highly entangled states of qubits enjoying a greater advantage over their classical counterparts. In recent years entanglement has been experimentally observed between qubits embedded in diamonds physically separated by more than a kilometre [20].

1.3 Semiconductor Nanostructures and Quantum Dots

Quantum technologies cannot out-perform their classical counterparts with arbitrarily few qubits. The protocol shown in Fig. 1.1b would require $\mathcal{O}(n)$ qubits to factor an n bit number for example and we therefore require a scalable implementation of the qubit. Furthermore, for the reasons discussed in Sec. 1.2, we would like to use light as the medium for inter-qubit communication—in analogy to our use of electrical pulses for inter-bit communication in a computer chip. We need then to confine a large number of qubits to a small area and have photons routed between them. This is where our interest in semiconductor technology arises and in particular we note the recent and rapid developments in the area of nanostructure fabrication. These sub-wavelength scale structures, constructed from high-refractive index semiconductor, both guide light and enhance the interaction between the light and an object or 'emitter' embedded inside the material [21]. Emitters in these structures would then form an extremely convenient qubit, having both scalability and strong interactions with control photons.

There has been success in coupling many types of emitters to semiconductor nanostructures, including cold atoms [22] and silicon colour centres [23] but the emitter we will discuss throughout most of this thesis is the semiconductor quantum dot (QD). These objects are sometimes referred to as 'solid-state atoms' and are islands of one semiconductor species located inside a large matrix of a different species. An electron can then be confined to the host island and, assuming the confinement volume is sufficiently small, will exhibit atomic properties with well-defined energy states. In addition to the fundamental physics and quantum information applications discussed in this thesis, QDs are of interest to physicists working in a diverse range of fields. For example QD lasers operate at much lower threshold currents than traditional devices [24], QD solar cells can be more efficient than those made from bulk semiconductors [25] and QD photodetectors have the potential to operate at high, previously inaccessible, temperatures [26].

1.4 Outline of the Thesis

We have determined that quantum technologies could revolutionise the world but that they require many physical qubits, which are hard to implement. Photons form the ideal carriers of quantum information, can be guided in small scale semiconductor structures and made to interact with embedded emitters. These considerations motivate this thesis, which is concerned primarily with the creation of entanglement between solid-state qubits, embedded in nanophotonic structures. We begin with a summary of the key concepts in quantum mechanics and in Chapter 2 describe the postulates upon which it is based. We explain how these postulates develop into predictions for experimental results and show how to calculate the dynamics of a system evolving over time. From these foundations, we move into more advanced topics in Chapter 3 and review some useful tools in quantum optics. In particular we discuss the master equation, input-output and scattering matrix treatments of quantum optical systems. A strong understanding of these techniques informs and guides the rest of our endeavour.

We turn to original work in Chapter 4 and develop a theory to describe few-photon scattering from emitters embedded in nanophotonic waveguides. We calculate the transition amplitudes for one and two photon states scattering from two-level and Λ-type emitters and compare the pole structures of these quantities. In Chapter 5 we move on to the analysis of realistic systems and produce models that capture the physics of two recent QD photon scattering experiments. Having determined that experimental systems are dominated by noise and imperfections, we move on to a final project in Chapter 6 and construct an entanglement generation protocol, which is robust to some of these defects. In particular we find that we can overcome spectral mismatch and perfectly entangle two distinct emitters using multi-photon probe states. Chapter 7 is reserved for a summary, discussion and some suggestions for further research.

Chapter 2

Quantum Mechanics

In this Chapter we review briefly some basic concepts in quantum mechanics in order to prepare ourselves for the more advanced topics we describe in Chapter 3. Firstly, in Sec. 2.1, we detail the axioms upon which quantum mechanics is based and in Sec. 2.2 we examine the consequences of these in terms of calculating physical quantities. In Sec. 2.3 we discuss general strategies for computing the time evolution of quantum systems and treat the specific example of angular momentum in Sec. 2.5. We conclude in Sec. 2.6 with a description of 'entanglement' and explain how we can quantify the amount of this property that a system of two qubits exhibits.

2.1 Postulates

Quantum mechanics is the jewel in the crown of modern physics and, along with relativity, one of the most rigorously experimentally verified theories in history. Quantum mechanics was born out of the fact that irreconcilable divergences between experimental results and the predictions of classical physics became more pronounced in the early 1900s. Specifically, physicists lacked convincing explanations for phenomena including: the spectrum of radiation emitted by a black-body, the photo-electric effect and the structure of the atom [27]. Quantum theory emerged as a unified framework in which these, and many other, observations could be consistently explained. Quantum mechanics is the most rigorously probed scientific theory in history and evidence for the requirement for an alternative description of reality is thus far lacking [28].

The postulates of quantum mechanics are the axioms upon which the theory is built and form the minimum set of statements required to give us a set of tools with predictive power. These postulates cannot be mathematically derived and we instead infer their validity from the predictions made by quantum theory. Quantum mechanics correctly predicts experimental results with extraordinary accuracy and we therefore assume that the axioms used in its derivation are correct. The minimum five postulates required to construct quantum theory are as follows [29].

I The state of any physical system at time t is given by the vector $|\psi(t)\rangle$, which inhabits an N-dimensional Hilbert space. A Hilbert space is a complex, multi-dimensional generalisation of the familiar three-dimensional Euclidean space and the vector $|\psi(t)\rangle$ contains all the information required to predict an arbitrary system property.

II Any observable property of the system, A is represented by the Hermitian operator $\hat{A}$[1] and the eigenvectors of this operator form a complete, orthonormal basis. An operator is an object that acts on a state vector, $|\psi\rangle$ and in general returns a new vector $|\phi\rangle$ such that $\hat{A}|\psi\rangle = |\phi\rangle$. If the equation $\hat{A}|\psi\rangle = a|\psi\rangle$, where a is some complex number, is satisfied then we say that $|\psi\rangle$ is an 'eigenvector' of A with the corresponding 'eigenvalue' a.

[1] In non-relativistic quantum mechanics, operators are differentiated from complex numbers via the addition of a ˆ or 'hat.' This is not the convention in quantum field theory, with the context providing enough information to determine the class of object and throughout this thesis we generally do not endow operators with hats.

III The eigenvalues of $\hat{A}$ are labelled as $\{a_1, a_2 \ldots a_n\}$ and represent possible outcomes of an experiment measuring the property A. We can calculate the probability of these outcomes via

$$\Pr_{a_i}(t) = |\langle a_i|\psi(t)\rangle|^2 , \tag{2.1}$$

where $|a_i\rangle$ is the eigenvector corresponding to the a_i eigenvalue and $\langle x|y\rangle$ is the notation we adopt to describe the inner product between the vectors $|x\rangle$ and $|y\rangle$.

IV Quantum systems evolve in time via unitary transformations satisfying $U(t)^\dagger U(t) = 1$. I.e. the state of a quantum system at some time t is related to its state at the earlier time t_0 by

$$|\psi(t)\rangle = U(t, t_0)\,|\psi(t_0)\rangle . \tag{2.2}$$

V Following a measurement on a system described by $|\psi(t)\rangle$, the state of the system immediately collapses to the eigenstate corresponding to the measurement outcome. This is referred to as the 'projection postulate' and has been the cause of much debate over the years, famously leading to the 'Schrödinger's Cat' thought experiment [30].

Researchers continue to debate the necessity of each of these postulates [31] but they are generally agreed upon and certainly suffice for the purposes of this thesis. The precise nature of the quantum state and how it relates to any kind of deeper physical 'reality' is an active area of research [32].

2.2 States and Density Matrices

Postulate I tells us that the state of a physical system is represented by a vector in some N-dimensional Hilbert space and it's therefore important to understand the properties of these vectors. The first point we note is that operators in quantum mechanics are linear [33] and therefore if $|\psi_1\rangle$ and $|\psi_2\rangle$ describe quantum states then the superposition

$$|\psi\rangle = c_1\,|\psi_1\rangle + c_2\,|\psi_2\rangle , \tag{2.3}$$

where c_1 and c_2 represent complex numbers, is also a valid state. Conventionally the $|\psi\rangle$ vector or 'ket' refers to an N-entry column vector and the 'bra,' $\langle\psi|$ is the corresponding Hermitian conjugate row vector. This means that the inner product $\langle\psi|\phi\rangle$ is a scalar by the rules of matrix multiplication. Note that the Hermitian conjugate operation both transposes and complex-conjugates a vector, which ensures that the inner-product $\langle\psi|\psi\rangle$ is real. If $\langle\psi|\psi\rangle = 1$ then we say that the vector $|\psi\rangle$ is 'normalised.'

In the vast majority of cases we want to choose the quantum states from which we construct a superposition to be 'orthonormal.' For an N-dimensional system the total state is given by

$$|\psi\rangle = \sum_{i=0}^{N} c_i\,|\psi_i\rangle \tag{2.4}$$

and the orthonormality condition is that $\langle\psi_i|\psi_j\rangle = \delta_{ij}$, where c_i gives some complex number and δ_{ij} is the Kronecker delta function [34]. The reason we do this is because, by Postulate III, the inner product $\langle\psi_i|\psi\rangle = c_i$ gives the probability amplitude for a measurement on the system to reveal the state $|\psi_i\rangle$. Strictly this only holds if the state $|\psi\rangle$ is normalised such that $\sum_i |c_i|^2 = 1$ but a state can always be normalised through division of the constituent probability amplitudes by $\sqrt{\langle\psi|\psi\rangle}$.

There is a fundamental randomness associated with quantum mechanics and, unlike in classical physics, we cannot deterministically predict the result of a given measurement. We can however find the average or 'expectation' value that a measurement would tend to if performed an infinite number of times. Suppose we measure the observable associated with the operator A; it is clear that the expectation is simply the probability of each outcome, multiplied by the value associated with said outcome. This can be compactly written

$$\langle A \rangle = \langle \psi | A | \psi \rangle = \mathrm{Tr}\left[A | \psi \rangle \langle \psi | \right], \tag{2.5}$$

where the 'trace' operator, $\mathrm{Tr}[M]$ of a matrix M sums diagonal elements in any orthonormal basis, $\mathrm{Tr}[M] \equiv \sum_n \langle \lambda_n | M | \lambda_n \rangle$. The trace operation is basis independent [35] but the statement in Eq. (2.5) is most easily seen in the orthonormal basis associated with the operator A.

We have to be careful not to confuse the fundamental quantum randomness of a measurement with any classical uncertainty associated with a system. Suppose somebody prepares a quantum state dependant on the result of a coin flip. If the coin lands on heads then they prepare the state $|\psi\rangle$ and on tails they prepare $|\phi\rangle$; there is no requirement for $|\psi\rangle$ and $|\phi\rangle$ to be orthonormal. Consider the case where one state corresponds to an atom in its ground state, $|\psi\rangle = |g\rangle$ and the other to an atom prepared in an equal superposition of ground and excited states, $|\phi\rangle = 1/\sqrt{2}\,(|g\rangle + |e\rangle)$. By simple probability theory we must have a 25% chance of finding the atom excited but this is not captured by our state vector formalism. If we proceed in the naive manner of simply adding the state vectors we have

$$|\psi_{\mathrm{total}}\rangle = \frac{1}{\sqrt{2}}\left(|\psi\rangle + |\phi\rangle\right) = \frac{1}{2}\left[\left(\sqrt{2}+1\right)|g\rangle + |e\rangle\right]. \tag{2.6}$$

Ignoring the fact that this state is not normalised, we nevertheless find that the probability of finding the atom excited is ~ 15%, which is clearly incorrect.

To rectify this problem we start from the requirement that expectation values must obey the principles of probability. Namely we have that

$$\langle A \rangle = \frac{1}{2}\left(\langle A \rangle_{|\psi\rangle} + \langle A \rangle_{|\phi\rangle} \right), \tag{2.7}$$

i.e. that the expectation of some operator A has to be the weighted sum of the expectations for the states $|\psi\rangle$ and $|\phi\rangle$. We can use the fact that the trace operator is linear to determine

$$\langle A \rangle = \frac{1}{2}\left(\mathrm{Tr}\left[A | \psi \rangle \langle \psi | \right] + \mathrm{Tr}\left[A | \phi \rangle \langle \phi | \right] \right) = \mathrm{Tr}\left[A \frac{1}{2}\left(|\psi\rangle\langle\psi| + |\phi\rangle\langle\phi| \right) \right] \equiv \mathrm{Tr}\left[A\rho \right], \tag{2.8}$$

where we defined the 'density matrix,' $\rho = 1/2\,(|\psi\rangle\langle\psi| + |\phi\rangle\langle\phi|)$. This is the fundamental object in quantum mechanics when classical probability is incorporated. In the general case where we have N possible states, $|\phi_i\rangle$ in our preparation, each with an associated classical probability P_i, the density matrix is given by

$$\rho = \sum_{i=0}^{N} P_i \, |\phi_i\rangle\langle\phi_i|, \tag{2.9}$$

where there is no requirement for the $|\phi_i\rangle$ vectors to be orthonormal.

It is important to understand the fundamental difference between classical mixtures and quantum superposition states. We consider again the two-level atom, with states

$$|g\rangle \equiv \begin{pmatrix} 0 \\ 1 \end{pmatrix} \qquad \text{and} \qquad |e\rangle \equiv \begin{pmatrix} 1 \\ 0 \end{pmatrix} \tag{2.10}$$

and prepare the atomic state according to a classical probability distribution as in the coin flip example above, realising the density matrix

$$\rho = \frac{1}{2}\left(|g\rangle\langle g| + |e\rangle\langle e|\right) = \frac{1}{2}\begin{pmatrix}1 & 0\\ 0 & 1\end{pmatrix}. \tag{2.11}$$

If we measure the excitation of an atom prepared in this state, we would expect to find it excited 50% of the time, as if it were prepared in the superposition state $|\psi\rangle = 1/\sqrt{2}\left(|g\rangle + |e\rangle\right)$. However in this case the associated density matrix is given by

$$\rho = |\psi\rangle\langle\psi| = \frac{1}{2}\left(|g\rangle\langle g| + |g\rangle\langle e| + |e\rangle\langle g| + |e\rangle\langle e|\right) = \frac{1}{2}\begin{pmatrix}1 & 1\\ 1 & 1\end{pmatrix}, \tag{2.12}$$

which is clearly different to that in Eq. 2.11. The expectation value of one particular measurement on a single system does not tell us anything about the 'quantumness' of a given state. We note that in Eq. (2.12) the resulting density matrix has non-zero off-diagonal elements and these are sometimes referred to as the coherences of a system. A state that can be written as a vector, without any classical probability distribution, is referred to as 'pure' and one that cannot is called 'mixed.'

A final point to note is that the examples featured in this section for the purposes of illustration have concerned single quantum systems. This is not generally the case and the Hilbert space $\mathscr{H}$, on which the state vectors lie is most often a product of smaller sub-spaces $\mathscr{H}_i$. For a total system of n sub-systems, the Hilbert space is given by

$$\mathscr{H} = \mathscr{H}_1 \otimes \mathscr{H}_2 \otimes \mathscr{H}_3 \otimes \ldots \otimes \mathscr{H}_n, \tag{2.13}$$

where $A \otimes B$ gives the tensor product between A and B [36]. The action of the tensor product means that the dimension of $\mathscr{H}$ is given by the product of the dimensions of the constituent spaces. It is not generally the case that vectors on the space $\mathscr{H}$ are products of vectors on the smaller spaces (see Sec. 2.6) but it is true that the vectors $|\psi_i\rangle$ lying on the spaces $\mathscr{H}_i$ combine as

$$|\Psi\rangle = |\psi_1\rangle \otimes |\psi_2\rangle \otimes |\psi_3\rangle \otimes \ldots \otimes |\psi_n\rangle \equiv |\psi_1, \psi_2, \psi_3 \ldots \psi_n\rangle\,. \tag{2.14}$$

Operators may act on any combination of the sub-spaces but commonly correspond to a single Hilbert space and subsequently obey

$$(A_1 \otimes A_2 \otimes \ldots \otimes A_n)\,|\psi_1\rangle \otimes |\psi_2\rangle \otimes \ldots \otimes |\psi_n\rangle = A_1\,|\psi_1\rangle \otimes A_2\,|\psi_2\rangle \otimes \ldots \otimes A_n\,|\psi_n\rangle\,. \tag{2.15}$$

As a concrete example, consider a composite system of two two-level-atoms prepared in the product state $|\Psi\rangle = |g, e\rangle$, such that the first atom is in the ground state and the second is excited. We show in the next section that the excitation of the atom corresponds to the Hermitian σ_z operator and that $\sigma_z\,|g\rangle = -\,|g\rangle$ and $\sigma_z\,|e\rangle = |e\rangle$. We can calculate the expectation of this operator on either of the two atoms, e.g. for the first

$$\langle\sigma_z \otimes I\rangle = \langle g, e|\,(\sigma_z \otimes I)\,|g, e\rangle = -\,\langle g, e|g, e\rangle = -1 \tag{2.16}$$

and for the second

$$\langle I \otimes \sigma_z\rangle = \langle g, e|\,(I \otimes \sigma_z)\,|g, e\rangle = \langle g, e|g, e\rangle = 1, \tag{2.17}$$

as expected. We have used I to represent the identity operator, which maps any state $|\psi\rangle$ to itself such that $I\,|\psi\rangle = |\psi\rangle$.

2.3 Time Evolution

2.3.1 The Hamiltonian

We discussed how Postulate IV demands that the time evolution of quantum systems is unitary but we have not yet specified a form for the operator $U(t, t_0)$. We are guided here by the 'correspondence principle,' which demands that in the macroscopic limit, the predictions of quantum mechanics must be consistent with those of classical physics [37]. In classical mechanics, time evolution is generated by the Hamiltonian operator, and we therefore contend that the same should be true in our quantum theory. The Hamiltonian operator is formally the Legendre transformation of the Lagrangian and in many situations represents the total energy of a given system [38].

From these considerations we can derive the famous Schrödinger equation, which gives the time evolution of a system's state vector $|\psi(t)\rangle$ when evolving under the Hamiltonian $H(t)$. We have for a state evolving from time t to $t + \delta t$ that

$$|\psi(t + \delta t)\rangle = U(t + \delta t, t)\,|\psi(t)\rangle = e^{-i\frac{H(t)}{\hbar}\delta t}\,|\psi(t)\rangle\,, \tag{2.18}$$

where we introduced the reduced Planck constant $\hbar$ to ensure that the generator of the evolution remains dimensionless. Expanding Eq. 2.18 to first-order in δt we find that

$$|\psi(t)\rangle + \delta t\frac{\mathrm{d}}{\mathrm{d}t}|\psi(t)\rangle + \ldots = |\psi(t)\rangle - i\frac{H(t)}{\hbar}\delta t\,|\psi(t)\rangle + \ldots \tag{2.19}$$

so in the limit $\delta t \longrightarrow 0$

$$i\hbar\frac{\mathrm{d}}{\mathrm{d}t}|\psi(t)\rangle = H(t)\,|\psi(t)\rangle\,, \tag{2.20}$$

which is the time-dependent Schrödinger equation. The Schrödinger equation is employed extensively in non-relativistic quantum mechanics and can be used to find e.g. the energy spectra of the hydrogen atom with great accuracy.

It is helpful at this point to define the 'Pauli operators,' which are used extensively throughout this thesis. The matrix representations of the three basis operators are given by

$$\sigma_x = \begin{pmatrix} 0 & 1 \\ 1 & 0 \end{pmatrix}, \qquad \sigma_y = \begin{pmatrix} 0 & -i \\ i & 0 \end{pmatrix}, \qquad \sigma_z = \begin{pmatrix} 1 & 0 \\ 0 & -1 \end{pmatrix} \tag{2.21}$$

and we additionally define

$$\sigma_+ \equiv \frac{1}{2}\left(\sigma_x + i\sigma_y\right) = \begin{pmatrix} 0 & 1 \\ 0 & 0 \end{pmatrix} \qquad \text{and} \qquad \sigma_- \equiv \frac{1}{2}\left(\sigma_x - i\sigma_y\right) = \begin{pmatrix} 0 & 0 \\ 1 & 0 \end{pmatrix}. \tag{2.22}$$

The Pauli operators are important and useful for a number of reasons but in this case they are helpful in understanding the dynamics of a two-level-system. We can show that $\sigma_z\,|g\rangle = -\,|g\rangle$ and $\sigma_z\,|e\rangle = |e\rangle$ so that the expectation value of this operator tells us about the populations of the two energy levels. Furthermore we find that $\sigma_+\,|g\rangle = |e\rangle$ and $\sigma_-\,|e\rangle = |g\rangle$, which means that population altering operations can be represented by application of these operators.

We introduced the abstract concept of the qubit in Sec. 1.2 but we can use the Schrödinger equation to describe a concrete example. Suppose we form a qubit from the ground and excited states of a two-level-atom such that $|0\rangle \equiv |g\rangle$ and $|1\rangle \equiv |e\rangle$. We deduce the Hamiltonian for a two-level-atom qubit in the absence of external forces and write down the corresponding Schrödinger equation for the state vector $|\psi(t)\rangle$

$$-i\hbar\frac{\mathrm{d}}{\mathrm{d}t}|\psi(t)\rangle = \frac{1}{2}\hbar\Omega\sigma_z\,|\psi(t)\rangle \tag{2.23}$$

where Ω gives the frequency of the atomic transition. The solution is readily arrived upon and we find

$$|\psi(t)\rangle = \alpha(0)e^{-it\Omega/2}|g\rangle + \beta(0)e^{it\Omega/2}|e\rangle, \tag{2.24}$$

where the probability amplitudes $\alpha(0)$ and $\beta(0)$ describe the configuration of the system at time, $t = 0$. We can use this solution to find the expectation value for an observable operator and find e.g.

$$\langle\sigma_x\rangle = \alpha^*(0)\beta(0)e^{it\Omega} + \alpha(0)\beta^*(0)e^{-it\Omega}, \tag{2.25}$$

which we note is zero when the system is not prepared in a superposition state. Intuitively this tells us that $\langle\sigma_x\rangle$ is related to the electric dipole moment of the system, as we do not expect states of well defined parity to couple to external fields.

2.3.2 Dynamical Pictures

The method of calculating time evolution as presented above appeals to us intuitively. We take some system, associate with it a quantum state and solve a differential equation for the state vector. This may not be the most convenient representation for the dynamics however and there are other 'pictures' of quantum mechanics, which reproduce the same results. Consider the expression for the expectation value of A as in Eq. (2.5)

$$\begin{aligned}\langle A(t)\rangle =& \mathrm{Tr}\left[A|\psi(t)\rangle\langle\psi(t)|\right] = \mathrm{Tr}\left[AU(t,0)|\psi(0)\rangle\langle\psi(0)|U^\dagger(t,0)\right]\\ =& \mathrm{Tr}\left[U^\dagger(t,0)AU(t,0)|\psi(0)\rangle\langle\psi(0)|\right] \equiv \mathrm{Tr}\left[A_{\mathrm{H}}(t)|\psi_{\mathrm{H}}\rangle\langle\psi_{\mathrm{H}}|\right],\end{aligned} \tag{2.26}$$

where we used the cyclic property of the trace [39]. We thus define the 'Heisenberg picture,' where time-dependent operators are related to their 'Schrödinger picture' counterparts by the transformation $A_{\mathrm{H}}(t) = U^\dagger(t,0)AU(t,0)$ and states satisfy $|\psi_{\mathrm{H}}\rangle = |\psi(0)\rangle$. We see that expectation values, the things we can actually measure, don't change if we view quantum states as stationary and instead employ time-dependent observable operators.

There exists a Heisenberg picture equivalent of Eq. (2.20), which we can deduce by differentiation of the operator,

$$\frac{\mathrm{d}}{\mathrm{d}t}A_{\mathrm{H}}(t) = \frac{\mathrm{d}}{\mathrm{d}t}U^\dagger(t,0)AU(t,0) = \dot{U}^\dagger(t,0)AU(t,0) + U^\dagger(t,0)A\dot{U}(t,0) = \frac{i}{\hbar}\left[H, A_{\mathrm{H}}(t)\right], \tag{2.27}$$

where we have assumed the Schrödinger picture operator to be free from explicit time-dependence and recalled the definition of the commutator, $[A,B] \equiv AB - BA$. We can treat the isolated two-level-system example of the previous section within this new framework and find an equation for the Heisenberg picture Pauli operator

$$\dot{\sigma}_x^{\mathrm{H}}(t) = -\frac{i}{\hbar}\left[\sigma_x^{\mathrm{H}}(t), H\right] = -\frac{i\Omega}{2}\left[\sigma_x^{\mathrm{H}}(t), \sigma_z\right] = -\frac{i\Omega}{2}U^\dagger(t,0)\left[\sigma_x, \sigma_z\right]U(t,0) = -\Omega\sigma_y^{\mathrm{H}}(t), \tag{2.28}$$

which we see is dependent upon the Heisenberg picture σ_y operator. We similarly derive an equation for the motion of this operator and find that $\dot{\sigma}_y^{\mathrm{H}} = \Omega\sigma_x^{\mathrm{H}}(t)$. The coupled differential equations can be solved with relative ease and we find that

$$\langle\sigma_x^{\mathrm{H}}(t)\rangle = Ce^{it\Omega} + De^{-it\Omega} = \alpha^*(0)\beta(0)e^{it\Omega} + \alpha(0)\beta^*(0)e^{-it\Omega}, \tag{2.29}$$

where we deduced the constants C and D from the requirement that dynamic pictures are equivalent at $t = 0$. We note that as expected, the expectation values calculated in Eqs. (2.25) and (2.29) agree exactly.

In the simple qubit example the Hamiltonian produced exactly solvable dynamics but there are very few interesting situations in which this is the case. Often, when the dynamics of a system are complicated, neither the Heisenberg nor Schrödinger pictures are the most convenient to work in and we choose instead a hybrid frame. Suppose that the total Hamiltonian for a system is given by $H = H_0 + H_{\text{int}}$, where H_0 is the 'free' Hamiltonian, which is exactly soluble and H_{int} is the 'interaction' Hamiltonian, which generates non-trivial evolution. It turns out that the 'interaction picture,' where operators evolve according to H_0 and states H_{int}, is the most convenient frame for this purpose. To see why, we derive the interaction picture equivalent to the Schrödinger equation, which begins from the definition of an interaction picture operator $A_{\text{I}}(t) \equiv e^{iH_0 t/\hbar} A e^{-iH_0 t/\hbar}$. From the requirement that expectation values agree in all frames we have then that states obey $|\psi_{\text{I}}(t)\rangle = e^{iH_0 t/\hbar} |\psi(t)\rangle$ and we can differentiate this with respect to time to obtain

$$i\hbar \frac{\mathrm{d}}{\mathrm{d}t} |\psi_{\text{I}}(t)\rangle = -e^{iH_0 t/\hbar} H_0 |\psi(t)\rangle + e^{iH_0 t/\hbar} i\hbar \frac{\mathrm{d}}{\mathrm{d}t} |\psi(t)\rangle = H_{\text{I}}(t) |\psi_{\text{I}}(t)\rangle , \tag{2.30}$$

where we defined the 'interaction Hamiltonian' by $H_{\text{I}}(t) \equiv e^{iH_0 t/\hbar} H_{\text{int}} e^{-iH_0 t/\hbar}$. Eq. (2.30) is exact and we see then that, if H_{int} is zero, the state vector in the interaction picture does not evolve with time and that the magnitude of the evolution is directly related to the strength of the interaction. This lends itself to a perturbative treatment and is particularly employed in e.g. quantum electrodynamics where the coupling between light and matter is weak compared to their respective free energies.

2.4 Light as a Harmonic Oscillator

2.4.1 Ladder Operators

We will see shortly that a quantum description of light is best formulated in terms of 'ladder operators' and we therefore briefly introduce these operators and the algebra that they obey. Our starting point is the harmonic oscillator and, more specifically, the Hamiltonian describing the quantum analogy of this system. We deduce that this is given by

$$H = \frac{1}{2m} p^2 + \frac{1}{2} m\omega^2 x^2 = \hbar\omega \left(a^\dagger a + \frac{1}{2} \right), \tag{2.31}$$

where m gives the oscillating mass, ω the resonance frequency and x and p are the position and momentum operators respectively. We simplified the Hamiltonian in Eq. (2.31) by defining the ladder operator

$$a \equiv \sqrt{\frac{m\omega}{2\hbar}} \left(x + \frac{i}{m\omega} p \right) \tag{2.32}$$

along with its Hermitian conjugate. The canonical commutation relation is $[x, p] = i\hbar$ and imposes the condition $[a, a^\dagger] = 1$ on the ladder operators [40]. The crucial thing to note is that if the operator $a^\dagger a$ has some set of eigenstates $|n\rangle$, then the Hamiltonian H shares this eigenbasis, with each vector corresponding to the eigenvalue $\hbar\omega(n + 1/2)$.

The algebra imposed on the ladder operators by the commutator imbues them with some interesting properties. We first apply a to some eigenvector $|n\rangle$ of $a^\dagger a$ and note that

$$a^\dagger a a |n\rangle = \left(a a^\dagger a - a \right) |n\rangle = (n - 1) a |n\rangle , \tag{2.33}$$

meaning $a|n\rangle$ is also an eigenvector of the Hamiltonian. From the normalisation condition we can deduce that $a|n\rangle = \sqrt{n}\,|n-1\rangle$ and find in the same manner that $a^\dagger |n\rangle = \sqrt{n+1}\,|n+1\rangle$. This means that the operators a and $a^\dagger$ remove and add $\hbar\omega$ units of energy to eigenstates of H respectively

and we therefore term them the 'annihilation' and 'creation' operators for the system. The next items to note are that $n = \langle n| a^\dagger a |n\rangle = |a|n\rangle|^2 \geq 0$ and that it can be shown that the ground state wavefunction of H has $\hbar\omega/2$ units of energy. Therefore n takes positive integer values and the operators a and $a^\dagger$ correspond to operations where we remove and add one quantum of energy to the oscillator.

2.4.2 Quantising the Electromagnetic Field

What is the physical significance of the ladder operators? There are a number of possible ways to answer this question and we might for example note that the photonic nature of light has been demonstrated experimentally. The composition of the electromagnetic field, from indivisible photons of energy, intuitively suggests that a description of the field in terms of the ladder operators should be possible [41]. We could equally consider a specific system and solve Maxwell's equations for the electromagnetic field inside an optical cavity [42]. We would find that the coefficients for each mode of the field satisfy a classical Hamiltonian, which following canonical quantisation, takes the form of Eq. (2.31). We adopt a different approach however and consider the case of a wave propagating in free-space.

In the Coulomb gauge, where the scalar potential $\Phi(\mathbf{r}, t) = 0$, and in the absence of free charges and currents we can show that the vector potential of the electromagnetic field, $\mathbf{A}(\mathbf{r}, t)$ obeys the wave equation

$$\nabla^2 \mathbf{A}(\mathbf{r}, t) = \frac{1}{c^2} \frac{\partial^2 \mathbf{A}(\mathbf{r}, t)}{\partial t^2}, \tag{2.34}$$

where c is the speed of light. The general solution to this equation in free-space is given as an integral over Fourier components and we find that [43]

$$\mathbf{A}(\mathbf{r}, t) = \sum_\lambda \int \mathrm{d}\mathbf{k}\; a_\lambda(\mathbf{k}) \mathbf{u}_\lambda(\mathbf{r}) e^{i(\mathbf{r}\cdot\mathbf{k} - \omega_k t)} + \text{H.c.}, \tag{2.35}$$

where $\lambda = 1, 2$ labels the two orthogonal polarisations, $\mathbf{k}$ the wave-vector, $\omega_k = ck$ is the dispersion relation and H.c. represents the Hermitian conjugate. The vector $\mathbf{u}_\lambda(\mathbf{k})$ is the function for the mode of the field with polarisation λ and wave-vector $\mathbf{k}$. The corresponding Fourier coefficient is $a_\lambda(\mathbf{k})$ and this gives the amplitude of these modes of the vector field. We next note that the Hamiltonian for the field over the volume V is given by

$$H = \int_V \mathrm{d}V \left(\frac{\epsilon_0}{2} E(\mathbf{r}, t)^2 + \frac{1}{2\mu_0} B(\mathbf{r}, t)^2, \right) \tag{2.36}$$

where $\mathbf{E}(\mathbf{r}, t)$ and $\mathbf{B}(\mathbf{r}, t)$ are the electric and magnetic fields respectively. The Lagrangian from which the Hamiltonian Eq. (2.36) is derived is a function of the scalar and vector potentials and subsequently the Hamiltonian is a function of these fields and their corresponding canonical momenta. For example we can express the electric and magnetic fields in terms of the vector potential with $\mathbf{E}(\mathbf{r}, t) = -\partial_t \mathbf{A}(\mathbf{r}, t)$ and $\mathbf{B}(\mathbf{r}, t) = \nabla \times \mathbf{A}(\mathbf{r}, t)$.

To quantise a field theory, we promote the expressions for field position and momentum to operators and impose the canonical commutation relation upon these operators. It can be shown that when one performs this procedure, the Fourier coefficients in Eq. (2.35) must also be promoted to operators and obey the algebra [44]

$$\left[a_\lambda(\mathbf{k}), a^\dagger_{\lambda'}(\mathbf{k}') \right] = \delta_{\lambda\lambda'} \delta^{(3)}(\mathbf{k} - \mathbf{k}'), \tag{2.37}$$

where $\delta^{(3)}(\mathbf{k} - \mathbf{k}')$ is the three-dimensional Dirac delta function.[2] The ladder operators in this context then have a clear interpretation in terms of creation and destruction of excitations of

[2] Actually the situation is slightly more complicated than this and the delta function must be subtly modified for consistency with Gauss's Law [45]. In the one-dimensional case this is completely correct however.

the electromagnetic field. In particular, the 'number operator,' $n \equiv \sum_\lambda \int \mathrm{d}\mathbf{k}\, a_\lambda(\mathbf{k})^\dagger a_\lambda(\mathbf{k})$ counts the total number of photons in the system. In general, through the remainder of this thesis, we will neglect polarisation and assume propagation in a single spatial dimension. In this case the commutation relation for ladder operators takes the form $[a(k), a^\dagger(k')] = \delta(k - k')$ and the associated free Hamiltonian is

$$H = \int \mathrm{d}k\, \hbar\omega(k) a_k^\dagger a_k, \tag{2.38}$$

where the dispersion relation, $\omega(k)$ may not be linear if the wave propagates in a finite region. We can derive the Hamiltonian Eq. (2.38) by algebraic substitution of the field quadratures into Eq. (2.36), replacement of these quadratures with ladder operators as in Eq. (2.32) and subtraction of the infinite zero-point-energy [46].

2.4.3 Coherent States

A final important point to note about the quantum description of light relates to the fact that, in the macroscopic world, we don't experience light on the individual energy quanta level. We might expect that the limit $n \longrightarrow \infty$ somehow reproduces the expected behaviour but we note that $\langle n| a |n\rangle = 0$ for all n. This means that states of light with one photon subtracted are always orthogonal to the original state and therefore should be distinguishable for even large n. This motivates our search for a 'classical' state of light $|\alpha\rangle$ that, restricting ourselves to a single mode, is an eigenstate of the annihilation operator a so that $a|\alpha\rangle = \alpha|\alpha\rangle$. We expand $|\alpha\rangle$ in the basis of number states, $|\alpha\rangle = \sum_n C_n |n\rangle$ and determine the recursion relation $\alpha C_{n-1} = \sqrt{n} C_n$, which means that $C_n = C_0 \alpha^n / \sqrt{n!}$. We then find the constant C_0 by normalising the total state and arrive upon

$$|\alpha\rangle = e^{-|\alpha|^2/2} \sum_{n=0}^{\infty} \frac{\alpha^n}{\sqrt{n!}} |n\rangle, \tag{2.39}$$

which is referred to as the 'coherent' state. Using the fact that $\langle\alpha| a^\dagger = \langle\alpha| \alpha^*$, we note that $\langle n\rangle = |\alpha|^2$ and deduce that α represents the amplitude of a coherent state. We also derive the variance of the photon number operator

$$\Delta n = \sqrt{\langle n^2\rangle - \langle n\rangle^2} = \sqrt{\langle a^\dagger a a^\dagger a\rangle - \langle a^\dagger a\rangle^2} = |\alpha|, \tag{2.40}$$

and see that for high intensity fields the uncertainty increases as expected. We note finally that coherent states often allow us to reduce the dimensionality of the Hilbert space in which we work. Suppose we have some combined light-matter state $|\alpha, \psi\rangle$, where ψ gives the matter wavefunction. If we act on this state with the annihilation operator, we know that the only consequence is the replacement $a \longrightarrow \alpha$ and we can therefore do this for all operators, including the total system Hamiltonian. If we assume that all optical system states are at all times coherent and make such a replacement then we say we have made the 'semiclassical' approximation.

2.5 Angular Momentum

When we come to describe semiconductor quantum dots in Chapter 5 we make predictions about the expected physics based on conservation of angular momentum arguments. We therefore briefly detail the quantum mechanical treatment of angular momentum for the sake of completeness. We begin by recalling that, in classical mechanics, the orbital angular momentum of a single particle is given by $\mathbf{L} = \mathbf{r} \times \mathbf{p}$. The vector describing the motion is the cross product between the particle's position and momentum vectors in some fixed coordinate system. We can use Einstein summation notation to compactly express each component and find that $L_i = \epsilon_{ijk} r_j p_k$, where ϵ_{ijk}

is the Levi-Civita symbol. Following standard canonical quantisation protocol, we take the position and momentum variables, promote them to operators and impose the commutation relation $\left[r_i, p_j\right] = i\delta_{ij}\hbar$. This leads to the following algebra for angular momentum operators

$$\left[L_i, L_j\right] = i\hbar\epsilon_{ijk}L_k, \tag{2.41}$$

which we see do not commute.

Operators that do not commute do not share an eigenbasis and this means that if a state is an eigenstate of any one of the angular momentum operators, it is necessarily not an eigenstate of the remaining two [47]. There is another operator however, which does commute with all components of angular momentum and this is defined by $L^2 \equiv L_x^2 + L_y^2 + L_z^2$. We can therefore simultaneously know two pieces of information about a given state: a) the component of angular momentum in one direction, conventionally L_z and b) the magnitude of the system's total angular momentum, L^2. We search for a basis of states $|l, m\rangle$, which are eigenvectors of L^2 and L_z and describe the structure of the allowed values of angular momentum.

We begin by demanding $L_z|l, m\rangle = \hbar m|l, m\rangle$ so that m is the eigenvalue of L_z but rendered dimensionless by the factor of $\hbar$. We go on to define raising and lowering operators in much the same manner as for the harmonic oscillator of the previous section and setting $L_\pm \equiv L_x \pm iL_y$, we deduce the commutation relation $[L_z, L_\pm] = \pm\hbar L_\pm$. This allows us to prove that $L_+|m, l\rangle$ is also an eigenstate of L_z with eigenvalue $m' = m + 1$, i.e. that $L_+|l, m\rangle \propto |l, m + 1\rangle$ and we can repeat the same procedure for L_-. Now, we know that any one component of the angular momentum cannot be greater than the total and so if we define $l\hbar$ as the total angular momentum, we have that $-l \leq m \leq l$, or

$$L_-|l, -l\rangle = L_+|l, l\rangle = 0. \tag{2.42}$$

This immediately tells us that m takes on $2l + 1$ potential values; or that l is either an integer or half-integer. We can use the fact that $L_-L_+|l, l\rangle = 0$ to further show that $L^2|l, m\rangle = \hbar^2 l(l+1)|l, m\rangle$.

We do not repeat the procedure here and refer to e.g. Ref. [48] for details but at this point we could take the known operators for position and momentum and substitute them into the eigenvalue equations for the state $|l, m\rangle$. We would then be able to deduce that, from the requirement that physics is unchanged under rotations of 2π radians, that m (and subsequently l) must be integers. However, we have seen that the angular momentum algebra is obeyed by a set of operators $\{S_x, S_y, S_z\}$, which behave in the same way as $\{L_x, L_y, L_z\}$ but with $l = s = 1/2, 3/2, 5/2 \ldots$ and $m = m_s = \ldots - 5/2, -3/2, -1/2, 1/2, 3/2, 5/2 \ldots$. It turns out that this type of 'angular momentum' is just as physically real as the integer variety [49], though it cannot correspond to any classical analogies we may wish to draw. We term this 'intrinsic' angular momentum 'spin' and note that it is an internal property of any sub-atomic particle, which must be accounted for when e.g. generalising the Schrödinger equation to a relativistic regime [50].

This means that even for a single particle system, we have to consider two contributions to the total angular momentum, which we label j. It is clear that $|l - s| \leq j \leq l + s$ and we can also show that if we define $J = L\otimes I + I\otimes S$ then $\left[J_i, J_j\right] = i\hbar\epsilon_{ijk}J_k$. In other words, that the total angular momentum operator obeys the same algebra as the spin and orbital angular momentum operators do individually. The important point to note here for our purposes is that there are a variety of possible spectra resulting from the addition of orbital and spin angular momenta. For example, if we have an electron, which has $s = 1/2$ orbiting a nuclei with $l = 2$ then the possible values of j are 5/2 and 3/2, with associated projections onto J_z of $m_J = -5/2, -3/2, -1/2, 1/2, 3/2, 5/2$ and $m_J = -3/2, -1/2, 1/2, 3/2$ respectively. We know that circularly polarised light carries one unit of angular momentum and so we can say that optical transitions from $J = 0$ states to such orbitals are forbidden.

2.6 Entanglement

2.6.1 Emergence of Entanglement

Suppose we have a quantum system composed of two sub-systems such that the total Hilbert space $\mathscr{H}$ is given by $\mathscr{H} = \mathscr{H}_1 \otimes \mathscr{H}_2$. Further suppose that the set of vectors $|\psi_i\rangle$ forms a complete basis on $\mathscr{H}_1$ and $|\phi_i\rangle$ does the same on $\mathscr{H}_2$. This means that an arbitrary total system state $|\Psi\rangle$ can be written as

$$|\Psi\rangle = \sum_{i=0}^{n} \sum_{j=0}^{m} c_{i,j} \, |\psi_i, \phi_j\rangle \,, \tag{2.43}$$

where the dimension of $\mathscr{H}_1$ is assumed to be n, that of $\mathscr{H}_2$ is m and the $c_{i,j}$s are to be specified. Now suppose there are two observers, Alice and Bob, who each have access to only one portion of the total state, on $\mathscr{H}_1$ for Alice and $\mathscr{H}_2$ for Bob. How do they each describe the system? We know that each observer has access to a reduced density matrix on their respective sub-space so that Alice has ρ^{A} and Bob ρ^{B}. If the total density matrix is $\rho \equiv |\Psi\rangle\langle\Psi|$ we find e.g. Alice's state by taking the 'partial trace' over Bob's states

$$\rho^{\mathrm{A}} = \mathrm{Tr}_{\mathrm{B}} \left[\rho\right] \equiv \sum_{k=0}^{m} \langle \phi_k | \, \rho \, | \phi_k \rangle \,. \tag{2.44}$$

The partial trace operation makes intuitive sense in that Alice has the set of density matrices, each corresponding to a state of Bob's system, weighted by the probabilities of these states. It can be shown however that the partial trace is the unique operation that preserves the expectation value of an arbitrary operator [51].

A concrete example of this occurs when Alice and Bob share a state composed of e.g. two atomic spins. We can prepare the spins in an arbitrary state [52] and choose $|\Psi\rangle = \frac{1}{\sqrt{2}} \left(|\uparrow\downarrow\rangle + |\downarrow\uparrow\rangle\right)$, where the first label in the ket corresponds to Alice's spin and the second to Bob's. We use the $\uparrow$ arrow to indicate a spin in one direction and $\downarrow$ to denote the anti-parallel version such that $\langle\uparrow \mid \downarrow\rangle = 0$. This state in density matrix form is

$$\rho = \frac{1}{2} \left(|\uparrow\downarrow\rangle\langle\uparrow\downarrow| + |\uparrow\downarrow\rangle\langle\downarrow\uparrow| + |\downarrow\uparrow\rangle\langle\uparrow\downarrow| + |\downarrow\uparrow\rangle\langle\downarrow\uparrow|\right) \tag{2.45}$$

and we can easily find the reduced density matrices for the systems held by Alice and Bob

$$\rho^{\mathrm{A}} = \frac{1}{2} \left(|\uparrow\rangle\langle\uparrow| + |\downarrow\rangle\langle\downarrow|\right) \tag{2.46}$$

$$\rho^{\mathrm{B}} = \frac{1}{2} \left(|\downarrow\rangle\langle\downarrow| + |\uparrow\rangle\langle\uparrow|\right) . \tag{2.47}$$

We can try to reconstruct the original density matrix in Eq. (2.45) and find that

$$\rho_{\mathrm{reconstructed}} = \rho^{\mathrm{A}} \otimes \rho^{\mathrm{B}} = \frac{1}{4} \left(|\uparrow\downarrow\rangle\langle\uparrow\downarrow| + |\uparrow\uparrow\rangle\langle\uparrow\uparrow| + |\downarrow\downarrow\rangle\langle\downarrow\downarrow| + |\downarrow\uparrow\rangle\langle\downarrow\uparrow|\right) \neq \rho, \tag{2.48}$$

which we see is clearly not equivalent to the original state. This means that somehow, in reducing the density matrices, we have lost information contained in the original state. States that behave in this way, with quantum correlations between systems on different sub-spaces, are called 'entangled.'

In fact there are a number of ways we could have pre-judged the outcome $\rho_{\mathrm{reconstructed}} \neq \rho$. For a start we note that both ρ^{A} and ρ^{B} are mixed states, while the original density matrix was constructed from the pure state $|\Psi\rangle$. This means that both Alice and Bob inherited classical uncertainty from their lack of access to the whole state. We further note that both Alice and Bob have the power to deterministically predict the measurement outcomes of the other observer through an experiment on their own sub-system. Bob could measure his spin before Alice made

a measurement and, from the collapse Postulate V, be sure that Alice would measure her spin in the anti-parallel direction. Finally, and crucially, we see that the state $|\Psi\rangle$ cannot be written as a tensor product of pure states $|\psi\rangle \otimes |\phi\rangle$ on Alice and Bob's sub-spaces. This means that they each hold a state that is somehow conditional on the state held by their partner.

2.6.2 Teleportation

Entanglement can be thought of as a resource for quantum technologies and we illustrate this through the example of 'teleportation,' the protocol for which was created by Bennett *et al.* in 1993 [53]. The aim of the procedure is for Alice to send the qubit state $|\psi\rangle = \alpha|0\rangle + \beta|1\rangle$ to Bob *without* physically transferring a quantum system to him.[3] It turns out that this can be achieved if Alice and Bob share a quantum system in a 'maximally entangled' state and are allowed to communicate classically. A maximally entangled, bi-partite, pure state is one in which the reduced density matrix ρ for either observer is diagonal in some measurement basis, possessing only classical correlations. The state we choose for this protocol is the Bell state

$$|\Phi^+\rangle = \frac{1}{\sqrt{2}}\left(|00\rangle + |11\rangle\right), \tag{2.49}$$

where the first label corresponds to Alice's qubit and the second to Bob's. Note that this choice is somewhat arbitrary and the procedure can be modified to use any of the four maximally entangled Bell pairs. The total state for the entire system is

$$|\Psi\rangle = |\psi\rangle \otimes |\Phi^+\rangle = \frac{1}{\sqrt{2}}\left(\alpha|000\rangle + \alpha|011\rangle + \beta|100\rangle + \beta|111\rangle\right) \tag{2.50}$$

and the task is to somehow transfer the state of qubit one (the first label in the ket), which is held by Alice to the state of qubit three (the third label), which is held by Bob.

Alice is free to operate on the first two qubits in the state Eq. (2.50) and performs a joint measurement in the Bell basis such that her system is projected onto one of the states $|\Phi^+\rangle$, $|\Phi^-\rangle$, $|\Psi^+\rangle$ or $|\Psi^-\rangle$, where

$$|\Phi^\pm\rangle = \frac{1}{\sqrt{2}}\left(|00\rangle \pm |11\rangle\right) \qquad \text{and} \qquad |\Psi^\pm\rangle = \frac{1}{\sqrt{2}}\left(|01\rangle \pm |10\rangle\right). \tag{2.51}$$

This change of basis would e.g. in the spin example previously, correspond to measuring the magnitude of the spin along a different axis and is a legitimate choice of basis because Bell states are orthogonal to one another. We can rewrite the state in Eq. (2.50) in the Bell basis and find that

$$|\Psi\rangle = \frac{1}{2}\left[|\Phi^+\rangle\left(\alpha|0\rangle + \beta|1\rangle\right) + |\Phi^-\rangle\left(\alpha|0\rangle - \beta|1\rangle\right) + |\Psi^+\rangle\left(\alpha|1\rangle + \beta|0\rangle\right) + |\Psi^-\rangle\left(\alpha|1\rangle - \beta|0\rangle\right)\right], \tag{2.52}$$

which means that if Alice measures e.g. $|\Phi^+\rangle$ she knows that Bob's qubit is in the state $|\psi\rangle$ as desired and can communicate this to him. In fact, once Alice has a measurement outcome and communicates with Bob, Bob can deterministically create the state $|\psi\rangle$ using only local operations on his single qubit. If Alice measures $|\Psi^+\rangle$ then Bob knows to apply a spin-rotation operation such that $|0\rangle \longrightarrow |1\rangle$ and $|1\rangle \longrightarrow |0\rangle$ to his qubit to recover the state $|\psi\rangle$.

In teleportation we really do transmit the quantum state $|\psi\rangle$ from one location to another without any transfer of matter. Classically we can only imagine this being possible if we had N copies of the initial state and were allowed to interrogate it an arbitrary number of times. We could in this case estimate the parameters α and β and transmit them classically to Bob in order

[3] Note that we have now adopted a bit-like notation of 0 and 1 to refer to orthogonal qubit states but this could easily be replaced by the arrows of the previous section.

to achieve the same result, though Bob's state would only be an exact copy of the original in the limit $N \longrightarrow \infty$. In the teleportation protocol neither Alice nor Bob gained any knowledge about the parameters α and β and this gives us some sense as to why quantum cryptography is expected to be such a powerful technology in the near future. We finally note that, even though at first glance it might appear that super-luminal communication is achieved here, it most certainly is not. This is ensured by the probabilistic nature of Alice's measurement outcomes and the subsequent necessity to communicate via a classical channel.

2.6.3 Entanglement Measures

We have demonstrated that quantum entanglement can be used as a resource for quantum technologies and we therefore want to quantify the 'amount' of entanglement exhibited by a given state. This is important for several reasons and we first note that e.g. the state

$$|\Phi\rangle = \frac{1}{10}\left(|\uparrow\downarrow\rangle + 3\sqrt{11}\,|\downarrow\uparrow\rangle\right) \tag{2.53}$$

is entangled in the same way as the state $|\Psi\rangle$ in Eq. (2.45) is. We cannot write either as a product of states on the individual sub-spaces and yet $|\Phi\rangle$ is somehow less entangled than $|\Psi\rangle$ is. The separable product state $|\chi\rangle = |\downarrow\uparrow\rangle$ is very close to $|\Phi\rangle$ and they only behave differently ~ 1% of the time. Furthermore, in more complex situations, it is not always obvious how to check for separability and this is especially true when we allow the states to be mixed. Confirming that

$$\rho \neq \sum_i P_i(\rho_i^{\mathrm{A}} \otimes \rho_i^{\mathrm{B}}) \tag{2.54}$$

for all ρ_i^{A} and ρ_i^{B} in any measurement basis is not a trivial exercise. We therefore search for an algorithm capable of: a) discriminating between entangled and separable states and b) increasing monotonically as the difference between an entangled state and the 'closest' separable state increases. This problem is difficult for 'multipartite' entanglement, where the number of sub-systems is greater than two, and we therefore consider from now on only systems of two qubits.

We're searching for a 'measure' of entanglement, which quantifies the ability of a state to perform a certain task. In particular, we suppose that two parties are given n copies of the pure state $|\Psi\rangle$, which is partly entangled, and asked to use local operations and classical communication to produce the maximum number m of maximally entangled states. It was shown by Bennett *et al.* [54] that this can be achieved and that the ratio m/n is given by the 'von Neumann entropy'

$$E(|\Psi\rangle) = -\mathrm{Tr}\left[\rho^{\mathrm{A}} \log_2 \rho^{\mathrm{A}}\right] = -\mathrm{Tr}\left[\rho^{\mathrm{B}} \log_2 \rho^{\mathrm{B}}\right]. \tag{2.55}$$

The matrices ρ^{A} and ρ^{B} are the reduced density matrices describing the systems held by the first and second parties, which are defined by Eq. (2.44). The von Neumann entropy measures the amount of classical uncertainty in a state [55] and we therefore understand that it tells us how much information was contained in the quantum correlations between the two sub-systems. It has been further shown that we can extend this idea to the mixed state

$$\rho = \sum_i P_i\,|\Psi_i\rangle\langle\Psi_i| \tag{2.56}$$

by defining

$$E(\rho) = \min \sum_i P_i E(|\Psi_i\rangle), \tag{2.57}$$

where the minimisation is taken over all possible decompositions of ρ [56]. This means that we have to find every single pure state decomposition of ρ, i.e. all the possible combinations of P_i and

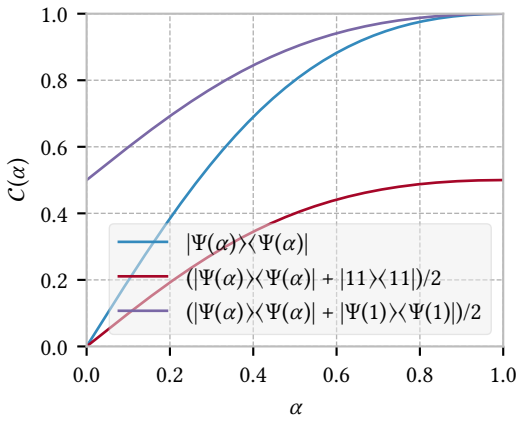

Figure 2.1: Concurrence as a function of the parameter α for three states defined in terms of the pure state $|\Psi(\alpha)\rangle \equiv 1/\sqrt{1+\alpha^2}\,(|00\rangle + \alpha\,|11\rangle)$. The red curve shows the concurrence when this state is in equal mixture with a separable partner state and the purple when the partner is maximally entangled.

$|\Psi_i\rangle$ that reproduce the state, calculate the average entanglement in each decomposition and take the minimum value. This 'entanglement of formation' is a faithful measure of entanglement but the minimisation step in the algorithm renders it extremely costly to compute for the majority of two qubit states.

The measure of entanglement that we adopt throughout the remainder of this thesis is the 'concurrence,' $\mathscr{C}(\rho)$, first introduced by Hill and Wootters in 1997 [57]. The concurrence is not so intuitive to understand as an entanglement measure and we note instead that it is bounded from below by 0, from above by 1 and scales monotonically with the entanglement of formation; if we find the entanglement of formation for an arbitrary pair of states and discover $E(\rho_2) > E(\rho_1)$, we will always find that $\mathscr{C}(\rho_2) > \mathscr{C}(\rho_1)$. We will discuss the mixed case momentarily but it is instructive to note that in the pure state case the concurrence takes a simple form. For the arbitrary two-qubit state

$$|\Psi\rangle = a\,|00\rangle + b\,|01\rangle + c\,|10\rangle + d\,|11\rangle\,, \tag{2.58}$$

where a, b, c and d are complex numbers, the concurrence is $\mathscr{C}(|\Psi\rangle) = |\,\langle\Psi|\tilde{\Psi}\rangle\,|$, where $|\tilde{\Psi}\rangle$ is the 'spin-flipped' version of $|\Psi\rangle$, defined by $|\tilde{\Psi}\rangle \equiv \left(\sigma_y \otimes \sigma_y\right)|\Psi^*\rangle$. This means that

$$\mathscr{C}(|\Psi\rangle) = |\,\langle\Psi|\left(\sigma_y \otimes \sigma_y\right)|\Psi^*\rangle\,| = 2\,|ad - bc|\,, \tag{2.59}$$

which is extremely simple to evaluate. Note that this formula makes good intuitive sense because we can easily show that $|\Psi\rangle$ is only separable in the case where $ad = bc$ and so the concurrence in some sense measures the distance to separability.

For mixed states, the concurrence is more difficult to calculate but does not rely on the minimisation algorithm employed by the entanglement of formation. The procedure for arbitrary two qubit states was derived by Wootters in 1998 and we refer to Ref. [58] for the mathematical details. The protocol is as follows; for the density matrix ρ, we calculate the new matrix

$$R(\rho) = \sqrt{\sqrt{\rho}(\sigma_y \otimes \sigma_y)\rho^*(\sigma_y \otimes \sigma_y)\sqrt{\rho}} \tag{2.60}$$

and find its four eigenvalues λ_i. We arrange these eigenvalues in decreasing order such that $\lambda_1 \geq \lambda_2 \geq \lambda_3 \geq \lambda_4$ and the concurrence is subsequently found as

$$\mathscr{C}(\rho) = \max(0, \lambda_1 - \lambda_2 - \lambda_3 - \lambda_4), \tag{2.61}$$

which is hard to interpret intuitively. We do not prove this result here but it does seem prudent to show how the concurrence behaves for some prototypical states and check that it gives the expected behaviour. We take the state

$$|\Psi(\alpha)\rangle = \frac{1}{\sqrt{1+\alpha^2}}\left(|00\rangle + \alpha\,|11\rangle\right), \tag{2.62}$$

which is separable for $\alpha = 0$ and maximally entangled for $\alpha = 1$ and plot its concurrence as a function of α in Fig. 2.1. We see that, as expected, the concurrence increases monotonically as α is increased. We also take equal mixtures of this state with both maximally entangled and separable states and find that the concurrence does indeed behave exactly as we would expect. In the case of a mixture with a separable state, the concurrence does not become greater than 0.5 and, in the situation where both states in the mixture are maximally entangled, the concurrence becomes unity as $\alpha \longrightarrow 1$.

2.7 Summary

In summary, we have described the postulates of quantum mechanics and seen how these translate into descriptions of experiments in terms of states and operators. We showed how to compute the time-evolution of these objects in the Schrödinger, Heisenberg and interaction pictures. We then saw that quantisation of the electromagnetic field naturally leads to a description of light in terms of photons and that states of the field are conveniently described in terms of ladder operators. Finally, we discussed the strange prediction of entanglement, showed how it can form a resource for quantum technologies and introduced the concurrence, which measures the amount of this resource in a given state.

Chapter 3

Quantum Optics

In this chapter we expand upon the fundamental principles of quantum mechanics discussed in Chapter 2 with a particular focus on systems involving light-matter interactions—the field of 'quantum optics.' We first discuss the Hamiltonian we will commonly employ to describe such systems and justify the often utilised 'rotating-wave-approximation.' We go on to discuss the master equation approach to analysing a system's dynamics and use some example calculations to show how the Lindblad form of the time evolution generator can be used to model dissipative processes. An alternative treatment of some quantum optical set-ups is then given in Sec. 3.3 and we focus on the Input-Output Formalism developed in the 1980s. We conclude this chapter by describing the S-matrix object and show how it can be calculated using the input-output equations.

3.1 A Light-Matter Hamiltonian

We saw in Sec. 2.3.1 that, in order to find how a system evolves over time, we need to find the Hamiltonian operator for the system. As we are ultimately interested in coupling solid-state qubits to optical waveguides, it seems prudent to find the Hamiltonian for such a setup. The point here is that the Hamiltonian comprises three parts $H = H_{\text{atomic}} + H_{\text{optical}} + H_{\text{coupling}}$, where the first two components are Hamiltonians for the free emitter and waveguide respectively and the third component describes the coupling. It is generally relatively easy to find the first two Hamiltonians but unsurprisingly the interesting dynamics are found in H_{coupling}. In general we make a simplifying assumption about the form of this Hamiltonian in order to model the total system dynamics and this is the subject of the following section.

3.1.1 Rotating Wave Approximation

Throughout this thesis we refer to the 'rotating-wave-approximation.' This is a widely made assumption, famously applied in the derivation of the Jaynes-Cummings Hamiltonian [59] and now ubiquitous in the literature. In order to understand the approximation we first consider the classical term for the energy coupling an electric dipole to an external field [60]

$$E_{\text{dipole}} \propto -\mathbf{E} \cdot \mathbf{x}, \tag{3.1}$$

where $\mathbf{E}$ is the field vector and $\mathbf{x}$ indicates the dipole direction. In the 'dipole approximation' this term can be used to describe the coupling of an emitter to a propagating optical wave, as the electric field associated with the wave excites the dipole formed by creating e.g. an electron-hole pair.

We consider the electric field associated with a monochromatic, coherent light source with amplitude α and frequency ω_0 and the dipole generated by the two-level-atom with ground state $|g\rangle$ and excited state $|e\rangle$. By recalling the selection rules for optical transitions [61], we can

deduce that diagonal elements of the dipole operator are zero and therefore the semi-classical Hamiltonian corresponding to the energy in Eq. (3.1) is

$$H_{\text{dipole}} \propto -(\sigma_- + \sigma_+)(e^{-i\omega_0 t}\alpha + e^{i\omega_0 t}\alpha^*). \tag{3.2}$$

We leave the proportionality constant undefined, referring to e.g. Ref. [62] for a more detailed derivation and the Pauli operators σ_+ and σ_- are defined as in Chapter 2. We can transform the Hamiltonian Eq. (3.2) into the interaction picture with respect to the free atomic Hamiltonian $H_0 = \hbar\omega_0\sigma_z/2$ and find that

$$H_{\text{dipole:int}} \propto \left(e^{-i\omega_0 t}\sigma_- + e^{i\omega_0 t}\sigma_+\right)\left(e^{-i\omega_0 t}a + e^{i\omega_0 t}a^\dagger\right). \tag{3.3}$$

We immediately identify four terms in $H_{\text{dipole:int}}$, two of which oscillate rapidly at the frequency $2\omega_0$. For processes occurring on relatively long time-scales it is justified to neglect these rapidly oscillating terms as they will have undergone many rotations and averaged to zero over the course of the interaction. This is the rotating wave approximation and leaves

$$H_{\text{coupling}} \propto e^{i\omega_0 t}\sigma_-\alpha^* + e^{-i\omega_0 t}\alpha\sigma_+ \tag{3.4}$$

in the non-rotating frame. Generalising this Hamiltonian to the situation where the light is non-classical we find that

$$H_{\text{RWA}} = ga\sigma_+ + g^* a^\dagger \sigma_-, \tag{3.5}$$

where we set the coupling constant as g and a is the annihilation operator for the optical field. This assumes a single mode field but readily generalises to a set of modes with wave-number k

$$H_{\text{RWA}} = \sum_k g_k a_k \sigma_+ + g_k^* a_k^\dagger \sigma_-, \tag{3.6}$$

where the coupling between the optical field and atom, g_k, is generally wavelength-dependent.

An important and useful property to notice about the Hamiltonian (3.5) is the fact that it is excitation number conserving. The field annihilation operator is paired with the spin up Pauli matrix and vice-versa. This makes a good deal of physical sense and in many ways justifies our liberal application of the rotating-wave-approximation. That is not to say that the approximation is universally applicable however [63] and the 'ultra-strong coupling' regime [64], where quickly oscillating terms cannot be ignored, has already been realised experimentally [65].

3.1.2 Two-Level-System Coupled to an Optical Waveguide

We follow Ref. [66] and use the rotating-wave-approximation to deduce an interaction Hamiltonian describing a two-level-system coupled to an optical waveguide. We begin by dividing the total Hamiltonian into free and interacting parts, H_0 and H_{int} respectively. The dynamics of an isolated emitter and bare waveguide are described by H_0, while the coupling between them, which we assume is of dipole form, is specified by H_{int}. We take a limit where the waveguide supports a continuum of optical modes with wavenumber k and apply the rotating-wave-approximation. This leads to

$$H = H_0 + H_{\text{int}} = \frac{1}{2}\hbar\Omega\sigma_z + \int_0 \mathrm{d}k\, \hbar\omega(k)\tilde{a}_k^\dagger\tilde{a}_k + \hbar\tilde{\gamma}\int_0 \mathrm{d}k\, \left(\sigma_+\tilde{a}_k + \tilde{a}_k^\dagger\sigma_-\right), \tag{3.7}$$

where $\omega(k)$ gives the waveguide dispersion relation and the operator $\tilde{a}_k$ destroys a photon of wavenumber k while obeying $[\tilde{a}_k, \tilde{a}_{k'}^\dagger] = \delta(k - k')$. We have assumed the fixed coupling rate $\tilde{\gamma}$ between optical modes of wavenumber k and the atomic transition and adopted the convention

that unspecified lower and upper integration limits imply negative and positive infinity respectively.

It is shown by e.g, Maier [67] that the dispersion relation for waveguide confined optical modes is surface-plasmonic. We linearise this about some central wavenumber k_0 so that, when the photon group velocity is v_g, $\tilde{\omega}(k) \approx \omega_0 + v_g(k - k_0)$. This means that

$$H = \frac{1}{2}\hbar\Omega\sigma_z + \int \mathrm{d}k\, \hbar\omega_0 \tilde{a}_k^\dagger \tilde{a}_k + \hbar v_g(k - k_0)\tilde{a}_k^\dagger \tilde{a}_k + \hbar\tilde{\gamma}\int \mathrm{d}k\, \left(\sigma_+ \tilde{a}_k + \tilde{a}_k^\dagger \sigma_-\right), \tag{3.8}$$

where we have also extended the limits of integration to cover the entirety of reciprocal space—an appropriate approximation when the band of populated modes is narrow. We next introduce the variable: $\epsilon \equiv v_g(k - k_0)$, which we use to re-write the Hamiltonian

$$H = \frac{1}{2}\hbar\Omega\sigma_z + \int \mathrm{d}\epsilon\, \hbar(\omega_0 + \epsilon)a_\epsilon^\dagger a_\epsilon + \hbar\gamma\int \mathrm{d}\epsilon\, \left(\sigma_+ a_\epsilon + \sigma_- a_\epsilon^\dagger\right) \tag{3.9}$$

where we have defined $\gamma \equiv 1/\sqrt{v_g}\tilde{\gamma}$ and $a_\epsilon \equiv 1/\sqrt{v_g}\tilde{a}_{k_0 + v_g^{-1}\epsilon}$. It can be easily shown that the commutation relation $[a_\epsilon, a_{\epsilon'}^\dagger] = \delta(\epsilon - \epsilon')$ is preserved.

At this point we can simply use the definition of the interaction Hamiltonian (see Sec. 2.3) and equation (3.9) to deduce that

$$H_\mathrm{I}(t) = \hbar\gamma\int \mathrm{d}\epsilon\, (e^{-i\Delta_\epsilon t}\sigma_+ a_\epsilon + e^{i\Delta_\epsilon t}\sigma_- a_\epsilon^\dagger), \tag{3.10}$$

which is the desired result, with the detuning defined by $\Delta_\epsilon \equiv \omega_0 + \epsilon - \Omega$. Eq. (3.10) has the expected structure of an interaction Hamiltonian, with phases on the operators given by the energy mis-match between photons and emitter.

3.2 Master Equations

We saw in Sec. 2.6 that a pure quantum state can become mixed if it is coupled to a second system that we cannot monitor. This has consequences for the evolution of quantum systems in non-ideal or 'real-world' conditions, as the system of interest will almost inevitably be coupled to a large, noisy environment. Suppose we have the state $|\psi(t_0)\rangle$, which evolves under the unitary transformation $U(t, t_0)$ to $|\psi(t)\rangle$. The associated density matrix evolves to $\rho(t) = |\psi(t)\rangle\langle\psi(t)|$ and continues, for all t, to describe a quantum system in a pure state. This means that quantum systems coupled to unmonitored environments or 'open quantum systems' cannot have their dynamics described by unitary transformations.

Formally, the density matrix associated with the system of interest, $\rho(t)$ can be found by unitarily evolving the combined system-environment density matrix $\rho_\mathrm{tot}(t_0)$ from the initial time, t_0 to t and then tracing out the environmental degrees of freedom [68]. This is in general too complicated to be feasible however and instead we want to find a 'dynamical map,' which will necessarily be non-unitary but act only on the system sub-space. This map should describe both the isolated evolution of the system and the dissipative dynamics associated with the system-environment coupling. Furthermore, we must take care to map valid density matrices to new valid density matrices, which obey the conditions:

I The density matrix is Hermitian, $\rho(t) = \rho^\dagger(t)$.

II All probabilities sum to unity, $\mathrm{Tr}[\rho(t)] = 1$.

III The density matrix is positive, $\langle x|\,\rho(t)\,|x\rangle \geq 0\ \forall x$.

A general map, constrained only by these conditions, does not especially simplify our calculations and additional approximations are therefore required. We now discuss how, with two additional approximations, the map can be re-cast into a particular form of 'master equation' for the density matrix $\rho(t)$.

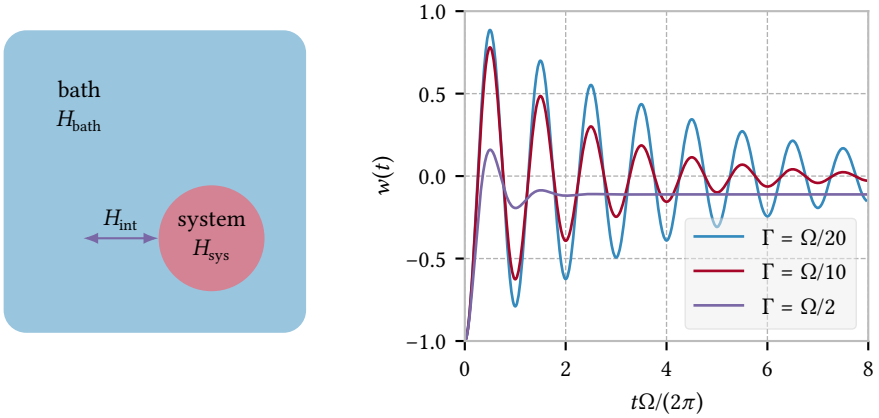

(a) System-bath interaction.

(b) Damped Rabi oscillations.

Figure 3.1: (a) Some quantum system, which we can measure, exchanges energy with an unmonitored environment. The system-bath entanglement means that the evolution of the system is no longer unitary. (b) Time dynamics of the population inversion of a classically, resonantly driven two-level-system with Rabi frequency Ω for a variety of radiative damping rates Γ.

3.2.1 The Lindblad Form

It was determined by Lindblad in 1976 that, with two additional approximations, the form of the dynamical map can be reduced to the master equation [69]

$$\dot{\rho}(t) = \mathscr{L}\rho(t), \tag{3.11}$$

where $\mathscr{L}$ is the Liouvillian super-operator, which acts on the density operator as

$$\mathscr{L}\rho(t) \equiv -\frac{i}{\hbar}[H, \rho(t)] + \sum_k L_k \rho(t) L_k^\dagger - \frac{1}{2}\left(L_k^\dagger L_k \rho(t) + \rho(t) L_k^\dagger L_k\right). \tag{3.12}$$

In Eq. (3.12) the Hamiltonian H is the system Hamiltonian and, like the Lindblad operators L_k, acts only on the system sub-space. The Lindblad operators corresponding to a given system-environment interaction process can be deduced from microscopic models [70] but it is often preferable to judiciously choose these operators by requiring that the solution to the resulting master equation (3.11) reproduces the expected behaviour.

We do not explicitly derive Eq. (3.12) in this thesis, instead discussing some illustrative examples, and refer to e.g. Ref. [71] for mathematical details. It is however important to understand the approximations underlying the form of the Liouvillian super-operator and subsequent limitations to the validity of the Lindblad form of the master equation. The approximations we make about the evolution of the system are:

IV. Linearity; that elements of the density matrix for the system at some time $t > t_0$ can be written as a linear combination of elements in the matrix at an earlier time t_0

$$\rho_{ij}(t) = \sum_{k,l} c_{ij;kl}\rho_{kl}(t_0). \tag{3.13}$$

V. Markovian evolution; that the density matrix at time t depends only on the values of the density matrix at some earlier time t_0 and not the set of earlier times $\{t_0, t_1, t_2 \ldots t_N\}$. This is sometimes referred to as the 'memoryless' approximation.

The Lindblad form is the most general master equation assuming that the evolution of the system is well approximated as linear and Markovian. We will go on to see in the next section that, under these approximations, many interesting phenomena can be predicted but this is not to say that these approximations hold generally. In particular the observation of non-Markovian dynamics has been reported in a wide variety of systems such as in Ref. [72], where the bath of phonons comprising the environment of a semiconductor quantum dot cannot be thought of as memoryless. Alternative techniques, which dispense with the Markovian approximation are available [73].

3.2.2 Examples

Radiative and Non-Radiative Damping

One canonical example of a situation in which we can employ a Lindblad-type master equation is that of a simple, two-level atom coupled to free space [74]. When the system of interest is the isolated atom, with ground state $|g\rangle$ and excited state $|e\rangle$, we already understand the unitary dynamics and so set the Hamiltonian $H = 0$ for simplicity. It is only through the environment that the states can couple and we postulate that the Lindblad operator associated with decay of the atom (though e.g. photon emission) is $L = \sqrt{\Gamma}\,|g\rangle\langle e|$. Assuming this is the sole dissipation channel, the Lindblad equation reads

$$\begin{pmatrix} \dot{\rho}_{11}(t) & \dot{\rho}_{12}(t) \\ \dot{\rho}_{21}(t) & \dot{\rho}_{22}(t) \end{pmatrix} = \Gamma \begin{pmatrix} -\rho_{11}(t) & -\rho_{12}(t)/2 \\ -\rho_{21}(t)/2 & \rho_{11}(t) \end{pmatrix}, \tag{3.14}$$

which can be solved to give

$$\begin{pmatrix} \rho_{11}(t) & \rho_{12}(t) \\ \rho_{21}(t) & \rho_{22}(t) \end{pmatrix} = \begin{pmatrix} \rho_{11}(0)e^{-\Gamma t} & \rho_{12}(0)e^{-\Gamma t/2} \\ \rho_{21}(0)e^{-\Gamma t/2} & 1 - \rho_{11}(0)e^{-\Gamma t} \end{pmatrix}. \tag{3.15}$$

Note that we have explicitly written the density matrix according to the convention of Eq. (2.10), such that $\rho_{11}(t)$ represents the excited state population and $\rho_{22}(t)$ the ground. This is the expected form of the density matrix as we see that a system starting in the excited state $|e\rangle$ such that $\rho_{11}(0) = 1$ will decay to the ground state at a rate Γ. In the infinite time limit, the system will have entirely relaxed to the ground state $|g\rangle$.

It should be noted that in Eq. (3.15) the off-diagonal matrix elements decay in addition to the diagonal ones. These off-diagonal matrix elements are often called the 'coherences' of the system and here they indicate whether the density matrix ρ represents a quantum or classical superposition of the $|g\rangle$ and $|e\rangle$ states. The off-diagonal elements decay to zero when the state can be described by a purely classical probability distribution and it is intuitive that as the system decays into the environment, the quantum mechanical correlations should vanish. Processes where both energy and correlations are lost to the environment are referred to as 'radiative damping' but there are also processes that can occur where quantum correlations are lost in a system without a corresponding loss of energy. 'Non-radiative damping' is sometimes referred to as 'pure dephasing' and can for example occur when systems couple to an environment through 'virtual' transitions, in which the uncertainty in a system's energy due to Heisenberg's Uncertainty Principle causes the coherent phase relationship between quantum states to break down [75]. Pure dephasing processes can also be modelled using a Lindblad type master equation with the Lindblad operator $L = \sqrt{\Gamma_d/2}\sigma_z$. In this case the master equation becomes

$$\begin{pmatrix} \dot{\rho}_{11}(t) & \dot{\rho}_{12}(t) \\ \dot{\rho}_{21}(t) & \dot{\rho}_{22}(t) \end{pmatrix} = \Gamma_d \begin{pmatrix} 0 & -\rho_{12}(t) \\ -\rho_{21}(t) & 0 \end{pmatrix} \tag{3.16}$$

and can be solved to give

$$\begin{pmatrix} \rho_{11}(t) & \rho_{12}(t) \\ \rho_{21}(t) & \rho_{22}(t) \end{pmatrix} = \begin{pmatrix} \rho_{11}(0) & \rho_{12}(0)e^{-\Gamma_d t} \\ \rho_{21}(0)e^{-\Gamma_d t} & \rho_{22}(0) \end{pmatrix} \tag{3.17}$$

as expected. Radiative and non-radiative dephasing processes become important when we model experimental systems in Chapter 5.

A Coherently Driven Atom

We can also find Lindblad equations for systems where the evolution of even the isolated system is non-trivial, i.e. where $H \neq 0$. A particular example of this is the coherently driven, radiatively damped, two-level atom. In the interaction frame with respect to $H_0 = \hbar\omega_l\sigma_z/2$, the Hamiltonian for the atom coupled to a monochromatic, classical laser field with amplitude α and frequency ω_l is

$$H = \frac{1}{2}\hbar\Delta\sigma_z - \hbar g\alpha\left(\sigma_+ + \sigma_-\right), \tag{3.18}$$

with $\Delta \equiv \omega_a - \omega_l$ giving the atom-laser detuning and g the light-matter coupling strength. Assuming a single decoherence process, of spontaneous emission from the excited atomic level, we can employ the Lindblad operator of the previous section to describe the dissipative dynamics and determine a master equation for the density operator. Following convention we rearrange this equation to describe the evolution of the *Bloch vector*, defined by

$$\begin{pmatrix} u(t) \\ v(t) \\ w(t) \end{pmatrix} \equiv \begin{pmatrix} \rho_{12}(t) + \rho_{21}(t) \\ i(\rho_{12}(t) - \rho_{21}(t)) \\ \rho_{11}(t) - \rho_{22}(t) \end{pmatrix}. \tag{3.19}$$

Using the Hamiltonian in Eq. (3.18) and radiative damping Lindblad operator, we can find the master equation for the density matrix and subsequently the coupled differential equations for elements of the Bloch vector

$$\dot{u}(t) = -\Delta v(t) - \frac{\Gamma}{2}u(t) \tag{3.20a}$$

$$\dot{v}(t) = \Delta u(t) + \Omega w(t) - \frac{\Gamma}{2}v(t) \tag{3.20b}$$

$$\dot{w}(t) = -\Omega v(t) - \Gamma w(t) - \Gamma \tag{3.20c}$$

where $\Omega \equiv 2g\alpha$. Assuming an initially de-excited atom, the boundary conditions can also be easily determined as

$$w(0) = -1, \qquad u(0) = 0 \qquad \text{and} \qquad v(0) = 0. \tag{3.21}$$

These equations are sometimes referred to as the 'Optical Bloch Equations' [76].

In general the optical Bloch equations are not analytically solvable and, as with the vast majority of master equations we might derive, we would implement a numerical solution. There are a number of dedicated software packages for just this purpose, notable among which is 'QuTiP' for the Python programming language [77]. For illustrative purposes we can however restrict ourselves to a parameter range in which the equations are tractable and use a Laplace transformation technique (App. A.1) as in Ref. [78] to determine the exact solution. One such soluble case exists when the laser is resonant with the atomic transition, $\Delta = 0$, and we Laplace transform Eqs. (3.20a)-(3.20c) to yield

$$\begin{pmatrix} s + \Gamma/2 & 0 & 0 \\ 0 & s + \Gamma/2 & -\Omega \\ 0 & \Omega & s + \Gamma \end{pmatrix} \begin{pmatrix} \bar{u}(s) \\ \bar{v}(s) \\ \bar{w}(s) \end{pmatrix} = \begin{pmatrix} 0 \\ 0 \\ -\Gamma/s - 1 \end{pmatrix}, \tag{3.22}$$

which we can solve via a standard matrix inversion method. We then implement an inverse Laplace transformation in the Mathematica software package [79] and arrive upon

$$w(t) = -\frac{\Gamma^2 + 2\Omega^2 e^{-\frac{3\Gamma t}{4}}\left(\frac{3\Gamma \sinh\left(\frac{1}{4}t\sqrt{\Gamma^2 - 16\Omega^2}\right)}{\sqrt{\Gamma^2 - 16\Omega^2}} + \cosh\left(\frac{1}{4}t\sqrt{\Gamma^2 - 16\Omega^2}\right)\right)}{\Gamma^2 + 2\Omega^2}. \tag{3.23}$$

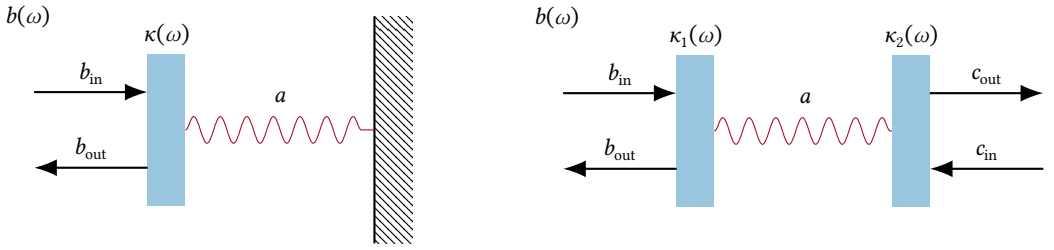

(a) One-sided optical cavity.

(b) Two-sided optical cavity.

Figure 3.2: (a) A one-sided optical cavity, with mode operator a coupled to an external continuum of bosonic modes $b(\omega)$ through a leaky mirror at a rate $\kappa(\omega)$. (b) Two-sided optical cavity as in (a), with the perfect mirror to the right replaced with a second partially reflecting element.

Now, via definition (3.19), we see that $w(t)$ represents the probability of finding an excited atom, minus that of measuring the ground state and this is sometimes called the 'inversion.' We plot this quantity in Figure 3.1b and observe a pattern of damped oscillations at the 'Rabi frequency' Ω, tending towards a mixed steady state.

3.3 Input-Output Formalism

Another important technique in the quantum optics toolbox is the so-called "Input-Output Formalism," developed by Collett and Gardiner in the 1980s [80, 81]. Originally devised to find the response of an optical cavity to a driving field, the formalism is particularly applicable when the input field to a system is coherent and a detailed description of the local system dynamics are not required. For these reasons, it is often employed in the modelling of experimental systems and in Chapter 5 we deploy the formalism for just such a purpose. To begin with however we follow the approach of Walls and Milburn [82] and derive the equations of motion for the mode operator of an optical cavity in an external bosonic bath. This allows us to identify input and output field operators, from which we construct the formalism.

3.3.1 Derivation

Consider the system of Figure 3.2a; a one-sided, single-mode, optical cavity with annihilation operator a, is coupled through a leaky mirror to a bath of oscillators $b(\omega)$ at a rate $\kappa(\omega)$. The mode a couples only through the left-hand interface, as the cavity is defined by a perfect mirror to the right. The Hamiltonian for this system is

$$\begin{aligned} H &= H_{\text{cavity}} + H_{\text{bath}} + H_{\text{cav-bath}} \\ &= \hbar\omega_0 a^\dagger a + \int \mathrm{d}\omega\, \hbar\omega b^\dagger(\omega) b(\omega) + i\hbar \int \mathrm{d}\omega\, \kappa(\omega) \left[b(\omega) a^\dagger - b^\dagger(\omega) a \right], \end{aligned} \tag{3.24}$$

where we have assumed that the cavity supports only a single mode of angular frequency ω_0 and couples to the external bath via a dipole interaction in the rotating wave approximation, as discussed in Sec. 3.1.1. It is of course an approximation to extend the integration over all of frequency-space but this is justified when the band of populated modes is narrow[1].

[1]The logic here is discussed by Collett and Gardiner and is similar to the justification for the rotating-wave-approximation. Essentially we can move to a frame rotating at a drive frequency Ω and this shifts the lower limit of integration from 0 to $-\Omega$. Provided that this is large compared to the bandwidth of populated modes, it is justified to approximate $\Omega \longrightarrow -\infty$.

From the Hamiltonian of Eq. (3.24) we can find Heisenberg equations for mode operators and first determine that the bath operator $b(\omega)$ obeys

$$\dot{b}(\omega) = \frac{i}{\hbar}[H, b(\omega)] = -i\omega b(\omega) - \kappa(\omega)a. \tag{3.25}$$

Suppose now that we know the state of the bath at some initial time t_0 and we label this $b_0(\omega)$. We can then re-cast Eq. (3.25) as

$$b(\omega) = e^{-i\omega(t-t_0)}b_0(\omega) - \kappa(\omega)\int_{t_0}^{t} \mathrm{d}t'\ e^{-i\omega(t-t')}a \tag{3.26}$$

and this procedure could be similarly applied to the case where we instead know the field operator $b_1(\omega)$ at some final time $t = t_1$. We have then integral equations for the bosonic bath operator in terms of either its value at some initial or final time and the cavity mode operator. This operator also obeys a Heisenberg equation

$$\dot{a} = \frac{i}{\hbar}[H, a] = -i\omega_0 a + \int \mathrm{d}\omega\ b(\omega)\kappa(\omega) \tag{3.27}$$

and, in theory, the dynamics of the system are now fully specified. It is somewhat unclear however how we should interpret these equations. If we were to drive the cavity mirror with a laser for example, it is not obvious how this would correspond to a state for the bath of oscillators $b(\omega)$.

At this point we make the simplifying approximation that the coupling between bosonic and cavity modes is frequency independent, $\kappa(\omega) = \sqrt{\gamma/2\pi}$, which is again justified when the bandwidth of populated bosonic modes is narrow compared with the cavity linewidth.[2] We then substitute Eq. (3.26) into Eq. (3.27) and use a resolution of the Dirac delta function [83] to determine

$$\dot{a} = -i\omega_0 a - \frac{\gamma}{2}a + \frac{\sqrt{\gamma}}{\sqrt{2\pi}}\int \mathrm{d}\omega\ e^{-i\omega(t-t_0)}b_0(\omega). \tag{3.28}$$

It is the form of Eq. (3.28) that guides us here and motivates our definition of the input operator

$$b_{\mathrm{in}} \equiv \frac{1}{\sqrt{2\pi}}\int \mathrm{d}\omega\ e^{-i\omega(t-t_0)}b_0(\omega), \tag{3.29}$$

so that

$$\dot{a} = -i\omega_0 a - \frac{\gamma}{2}a + \sqrt{\gamma}b_{\mathrm{in}}. \tag{3.30}$$

It is then clear why we identified the input operator as in Eq. (3.29), as we can draw analogy between the form of Eq. (3.30) and the driven, damped harmonic oscillator. We see that Eq. (3.30) consists of three terms representing; a harmonic oscillation at frequency ω_0, damping of this oscillation at a rate γ and driving of the oscillation with a field b_{in} respectively. Thinking about the system sketched in Fig. 3.2a, this is exactly the form of equation we would expect to describe the dynamics and we have identified clearly the operator describing the input to the system.

We have then an equation relating the evolution of the cavity mode operator a to the operator for an input optical mode and all that remains is to determine how this subsequently relates to a similar output operator. There are several ways to arrive at this equation, we could for instance repeat the procedure outlined above but use the final time, t_1 boundary conditions to rewrite

[2] In fact this also turns out to be a necessary condition for the system to evolve in a Markovian manner, as in the Lindblad master equation.

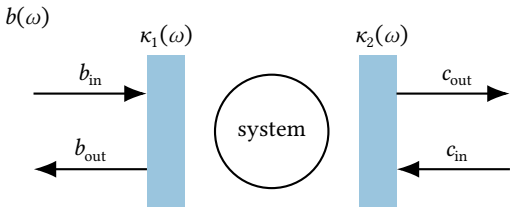

Figure 3.3: Some local system coupled through two partially transmissive elements to a bath of bosonic modes.

Eq. (3.26) and substitute this into Eq. (3.27) for the cavity mode operator. A more elegant solution exists however and we can argue that, by time reversal of Eq. (3.30), we logically arrive upon

$$\dot{a} = -i\omega_0 a + \frac{\gamma}{2} a - \sqrt{\gamma} b_{\text{out}}. \tag{3.31}$$

This is because the time reversal transformation acts to reverse the direction of the coherent evolution, turns input operators to outputs and sets $t \longrightarrow -t$. Damping is an irreversible process and this is the origin for the change of sign on the damping term compared with Eq. (3.30). Combining equations for the input and output optical fields we finally arrive upon the input-output relation

$$b_{\text{in}} + b_{\text{out}} = \sqrt{\gamma} a, \tag{3.32}$$

which we might choose to interpret as a boundary condition on the optical field at the mirror surface. This is because we have a condition relating field amplitudes at a surface and we can draw analogy between this and the procedure for finding how the classical electromagnetic field behaves at e.g. a dielectric boundary.

In some senses the one-sided optical cavity is the quintessential illustration of the Input-Output Formalism, with one of the most simple systems we could imagine, coupled to single input and output bosonic modes. Fortunately the formalism is not limited to such idealised systems and can readily be extended to describe a wider range of local systems, coupled to multiple input and output modes. Consider first the two-sided optical cavity shown in Fig. 3.2b. It is relatively simple to see how we extend the formalism to account for the second set of input modes and we have now

$$\dot{a} = -i\omega_0 a - \left(\frac{\gamma_1}{2} + \frac{\gamma_2}{2}\right) a + \sqrt{\gamma_1} b_{\text{in}} + \sqrt{\gamma_2} c_{\text{in}}, \tag{3.33}$$

where $\kappa_2(\omega) = \sqrt{\gamma_2(\omega)/2\pi}$. We arrived at Eq. (3.33) by allowing the mode operator to now decay via an additional channel at the right-hand mirror and adding a coupling to a second driving field at this interface. The input-output relations now read

$$b_{\text{in}} + b_{\text{out}} = \sqrt{\gamma_1} a \qquad \text{and} \qquad c_{\text{in}} + c_{\text{out}} = \sqrt{\gamma_2} a, \tag{3.34}$$

which we argue are the obvious generalisations of the boundary condition given in Eq. (3.32). This procedure can be continued for the case of multiple input and output optical modes but the two interface example most commonly occurs in real-world systems.

As well as generalising the formalism to account for more input and output optical modes we can replace the simple single mode cavity with more complex local systems. The key assumption here is that the coupling between bosonic modes and this system retains the form given in the Hamiltonian of Eq. (3.24), i.e. that the only allowed transformation is $H_{\text{cavity}} \longrightarrow H_{\text{system}}$, where H_{system} describes some new local setup. The form of $H_{\text{cav-bath}}$ must be preserved and the new

local system must have an excitation operator that couples linearly to the bath modes, $b(\omega)$ in the same way as a does in the cavity system. In this case it is clear that all of the logic employed previously continues to hold, as the only term in e.g. Eq. (3.30) that originates from this Hamiltonian is the coherent oscillation, $-i\omega_0 a$. We therefore transform Eq. (3.33) to

$$\dot{d} = \frac{i}{\hbar}\left[H_{\text{system}}, d\right] - \left(\frac{\gamma_1}{2} + \frac{\gamma_2}{2}\right) d + \sqrt{\gamma_1} b_{\text{in}} + \sqrt{\gamma_2} c_{\text{in}}, \tag{3.35}$$

where d represents the local system operator now coupled to the driving fields. For example, suppose that we take the two-sided optical cavity of Fig. 3.2b but couple to it a two-level atom with a single optical transition of frequency Ω. In this case $d \longrightarrow a$ and

$$\begin{aligned} H_{\text{system}} &= H_{\text{atom}} + H_{\text{cavity}} + H_{\text{coupling}} \\ &= \frac{\hbar\Omega}{2}\sigma_z + \hbar\omega_0 a^\dagger a + ig\hbar\left(a\sigma_+ - a^\dagger\sigma_-\right) \end{aligned} \tag{3.36}$$

where the Pauli operators are defined as in Chapter 2 and we have assumed a Jaynes-Cummings type coupling with an amplitude g. This is one of the two systems we analyse in the following section.

3.3.2 Examples

Two-Sided Optical Cavity

We now employ the Input-Output formalism to treat two prototypical examples; the two-sided optical cavity shown in Fig. 3.2b and the same cavity coupled to a two-level-system, as discussed previously. It may seem something of a trivial exercise to examine the two-sided optical cavity in any great detail, after all the classical description of such a system is extremely well-known, with Maxwell's equations predicting the emergence of 'Fabry-Pérot' interference fringes [84]. It turns out however that a quantum description of this phenomenon, where the cavity fully reflects an incoming monochromatic laser except at sharp points corresponding to resonance frequencies, is challenging. This is because a cavity is usually characterised by a set of standing-wave modes, which once excited have no reason to preferentially decay into one direction or the other. The problem is explained in detail by Barlow *et al.* [85] and they develop a master equation approach to the problem, which complements the plethora of existing techniques based on e.g. photon quasi-mode decompositions [86], modes of the universe theories [87] and the input-output description presented here.

We first suppose that the optical cavity is driven from the left such that $c_{\text{in}} = 0$ and also that the mirrors are equally lossy so that $\gamma_1 = \gamma_2 \equiv \gamma$. If we have a coherent laser driving field then we can replace the remaining input operator with a complex number $b_{\text{in}} \longrightarrow \alpha e^{-i\omega_l t}$, where ω_l is the laser frequency and α its amplitude. The resulting differential equation is readily solved and at steady-state we find that the expectation value of the cavity mode operator obeys

$$\langle a \rangle = \frac{\sqrt{\gamma}}{i(\omega_0 - \omega_l) + \gamma}\alpha e^{-i\omega_l t} \tag{3.37}$$

and this leads immediately to an equation for the transmissivity of the cavity

$$T \equiv \frac{|\langle c_{\text{out}}\rangle|^2}{|\alpha|^2} = \frac{\gamma^2}{\gamma^2 + (\omega_0 - \omega_l)^2}. \tag{3.38}$$

We plot this this quantity in Fig. 3.4a for a variety of mirror reflectivities and find that the expected behaviour, where the bandwidth of filtered modes becomes more limited with increased mirror reflectivity, is reproduced.

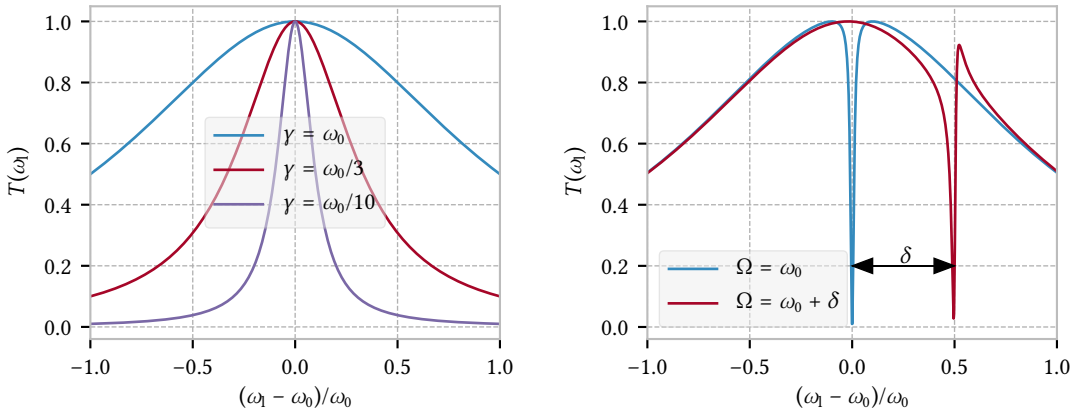

(a) Transmissivity of a two-sided cavity.

(b) Transmissivity of a two-sided cavity with emitter.

Figure 3.4: (a) Transmissivity of the two-sided optical cavity, with resonance frequency ω_0 and coupled to an external laser at a rate γ, as a function of the laser driving frequency ω_l. (b) Plot as in (a), with $\gamma = \omega_0$ but with an atom coupled to the cavity at a rate $g = \gamma/10$. The atomic transition energy is either degenerate with the cavity resonance or offset by $\delta = \gamma/2$.

Two-Sided Optical Cavity and Emitter

Let's now consider the case where this same cavity is coupled via a Jaynes-Cummings type Hamiltonian to a two-level atom. Retaining all previous assumptions, the equation for the cavity mode operator reads

$$\dot{a} = -i\omega_0 a - \gamma a + \sqrt{\gamma}\alpha e^{-i\omega_l t} - g\sigma_-, \tag{3.39}$$

where g is the cavity-atom coupling rate. We take the 'bad-cavity' limit where the cavity is much more strongly coupled to the incoming laser than the atom, $\gamma \gg g$, and this means that $\dot{a} = -i\omega_l a$ [3] and therefore

$$a = \frac{\sqrt{\gamma} b_{\text{in}} - g\sigma_-}{\gamma - i(\omega_l - \omega_0)}. \tag{3.40}$$

We can substitute Eq. (3.40) into the Heisenberg equation for the σ_- Pauli operator, which under the 'weak-excitation' approximation that $\langle \sigma_z \rangle \approx -1$, is

$$\dot{\sigma}_- = -i\Omega\sigma_- + ga. \tag{3.41}$$

We substitute Eq. (3.40), into Eq. (3.41), make the approximation that $\dot{\sigma}_- = -i\omega_l\sigma_-$ and substitute the result into the input-output relation Eq. (3.34) to find the transmissivity of the cavity

$$T = \left| \frac{\gamma}{\gamma - i(\omega_l - \omega_0)} \left[1 - \frac{g^2}{g^2 - i(\omega_l - \Omega)(\gamma - i(\omega_l - \omega_0))} \right] \right|^2. \tag{3.42}$$

In Fig. 3.4b we plot the transmissivity under these approximations for both the case where the emitter is resonant with the cavity and detuned by some finite frequency δ. We see that in both cases that the presence of the atom drastically changes the behaviour of the cavity, even in this weak-coupling limit. The total loss of transmissivity on resonance with the emitter is

[3] At steady-state, in the Heisenberg picture, we would expect the cavity mode operator to evolve coherently at the laser frequency so that $a(t) \approx e^{-i\omega_l t} C$, where C is a time-independent operator.

an extremely interesting phenomenon, which we will go on to explain thoroughly in Chapter 5 and here we simply note that, working in the bad cavity regime, this effect persists under the addition of leaky mirrors. When the atomic transition energy is offset from the cavity resonance frequency, the convolution of the transmission drop with the Fabry-Pérot background leads to an asymmetric line-shape or a 'Fano-resonance' [88].

3.4 The Scattering Matrix

In both the master equation and input-output approaches studied in the previous sections, we considered classical, coherent optical input states. Both formalisms are highly suited to this scenario and they are therefore widely employed in the modelling of experimental systems, where the most convenient optical input is generally a continuous wave laser. It is clear however that to optically manipulate qubits on short time-scales, continuous driving and measurement of a system is not ideal and we need instead to move to a regime where we inject and detect discrete optical states. This implies the transition to a new formalism and we borrow the 'S-matrix' object from relativistic quantum field theory, which is well suited to analysing exactly these situations.

3.4.1 Definition

We use the S-matrix to describe the results of scattering-type experiments, where two or more quantum systems start spatially separated, interact for a time and then become spatially separated once more. In particular the object tells us how some quantum 'in' state, $|\Psi_{\text{in}}\rangle$ at time $t_0 \longrightarrow -\infty$ evolves to an 'out' state, $|\Psi_{\text{out}}\rangle$ at $t_1 \longrightarrow +\infty$. There are several good reasons to adopt this description and one motivating factor is that, in an experiment, the asymptotic input and output states are the ones we have control of and access to respectively. Secondly, from a theoretical point of view, the input and output states are easy to describe as they are eigenstates of the free Hamiltonian H_0, which governs the dynamics of the systems in the absence of interactions. This is in contrast to the general case where the total Hamiltonian for the system is given by the sum of free and interacting parts, $H = H_0 + H_{\text{int}}$ and the eigenstates are complex to determine.

The scattering matrix is implicitly defined by [89]

$$\mathscr{A} = \langle \Psi_{\text{out}} | \, S \, | \Psi_{\text{in}} \rangle \,, \tag{3.43}$$

where $\mathscr{A}$ is the probability amplitude for the process where $|\Psi_{\text{in}}\rangle$ scatters to $|\Psi_{\text{out}}\rangle$. Now, we can use the facts that: a) at $t = 0$ all the dynamical pictures of quantum mechanics align and b) that the input and output states are stationary in the interaction picture at $t \longrightarrow \pm\infty$ to deduce

$$\mathscr{A} = \langle \Psi_{\text{out}}(t=0) | \Psi_{\text{in}}(t=0) \rangle = \lim_{t \to \infty} \langle \Psi_{\text{out}} | \, U_{\text{I}}(t,0) U_{\text{I}}(0,-t) \, | \Psi_{\text{in}} \rangle \,, \tag{3.44}$$

where $U_{\text{I}}(t', t)$ is the time evolution operator evaluated in the interaction picture. This gives us the useful fact that

$$S = \lim_{t \to \infty} U_{\text{I}}(t,0) U_{\text{I}}(0,-t) \tag{3.45}$$

and subsequently a method to calculate the S-matrix. It turns out that our task is not complete however because the time evolution operator in the interaction picture does not have as simple a form as its equivalent in the Schrödinger picture and this is the subject for the following section.

3.4.2 Dyson Series

We want to find the time translation operator in the interaction picture, $U_{\text{I}}(t', t)$, which evolves the interaction picture state $|\psi_{\text{I}}(t)\rangle$ from time t to the later time t'. From the definition of an interaction picture state we deduce that

$$U_{\text{I}}(t', t) = e^{iH_0 t'/\hbar} e^{-iH(t'-t)/\hbar} e^{-iH_0 t/\hbar}, \tag{3.46}$$

where H is the total system Hamiltonian in the Schrödinger picture and H_0 the free Hamiltonian, with respect to which we defined the interaction picture. This means that, working now in units where $\hbar = 1$, the operator obeys the differential equation

$$\frac{\mathrm{d}}{\mathrm{d}t'} U_{\mathrm{I}}(t', t) = -iH_{\mathrm{I}}(t')U_{\mathrm{I}}(t', t), \tag{3.47}$$

where $H_{\mathrm{I}}(t')$ is the interaction picture Hamiltonian as before. We do not derive the solution to Eq. (3.47) here specifically and refer to e.g. Ref. [90] for a thorough explanation but we do note that it is non-trivial. The problem occurs because the commutator $[H_{\mathrm{I}}(t'), H_{\mathrm{I}}(t)]$ is in general non-zero for $t \neq t'$ and this means that solution via the usual exponentiation method is not possible.

It was deduced by Dyson that time evolution in the interaction picture is generated by the operator [91]

$$U_{\mathrm{I}}(t', t) = \mathscr{T} e^{-i\int_t^{t'} \mathrm{d}s\, H_{\mathrm{I}}(s)} = 1 - i\int_t^{t'} \mathrm{d}s_1\, H_{\mathrm{I}}(s_1) + (-i)^2 \int_t^{t'} \mathrm{d}s_1 \int_t^{s_1} \mathrm{d}s_2\, H_{\mathrm{I}}(s_1)H_{\mathrm{I}}(s_2) + \dots, \tag{3.48}$$

where $H_{\mathrm{I}}(t)$ is the interaction Hamiltonian and $\mathscr{T}$ the 'time-ordering' operator, which acts on a string of time-dependent operators and rearranges their order so those at earlier times act before those at later ones. Although infinite, the series representation of the time evolution operator and hence the S-matrix is used extensively in modern high-energy physics for the evaluation of e.g. cross-sections in particle collisions [92]. There is a close relationship between terms in the expansion of the S-matrix and the famous 'Feynman diagrams,' which give a more intuitive understanding of sub-atomic particle dynamics.

3.4.3 Connection to the Input-Output Formalism

In general the S-matrix is calculated numerically via the perturbation expansion of Eq. (3.48) but Fan *et al.* derived an important connection between the S-matrix and the Input-Output formalism discussed in Sec. 3.3 [93]. They derive the S-matrices that describe the scattering of one and two photon optical states from a single, two-level-system embedded inside an optical waveguide. This is an extremely important result, as it connects the well-studied Input-Output Formalism to the object which describes how discrete photon states are scattered and we therefore summarise their results for the single photon case. These results will also be important when we come to describe some experimental implementations of quantum optical systems in Chapter 5.

The situation is as follows; at time $t = t_0$ we have a single, monochromatic photon described by the energy eigenstate $|k\rangle$, which impinges on a two-level-system and interacts before leaving the system in the $|p\rangle$ eigenstate at time $t = t_1$. We assume that the waveguide is unidirectional such that the only supported mode, with annihilation operator a_k, travels from left-to-right and we want to find the continuum of S-matrix elements S_{pk}. We first find the Hamiltonian for the system

$$H = H_0 + H_{\mathrm{int}} = \int \mathrm{d}\omega\, \omega a_\omega^\dagger a_\omega + \frac{1}{2}\Omega\sigma_z + g\int \mathrm{d}\omega\, \left(\sigma_+ a_\omega + a_\omega^\dagger \sigma_-\right), \tag{3.49}$$

as explained in Sec. 3.1, and this allows us to derive Heisenberg equations and an input-output relation (by analogy with the one-sided cavity of Sec. 3.3). The system dynamics are fully specified by

$$a_{\mathrm{out}} = a_{\mathrm{in}} - i\sqrt{\frac{2}{\tau}}\sigma_-, \tag{3.50}$$

$$\frac{\mathrm{d}N}{\mathrm{d}t} = -i\sqrt{\frac{2}{\tau}}\left[\sigma_+ a_{\mathrm{in}} - a_{\mathrm{in}}^\dagger \sigma_-\right] - \frac{2}{\tau}N \qquad \text{and} \qquad \frac{\mathrm{d}\sigma_-}{\mathrm{d}t} = -i\Omega\sigma_- + i\sqrt{\frac{2}{\tau}}\sigma_z a_{\mathrm{in}} - \frac{1}{\tau}\sigma_-, \tag{3.51}$$

where $N \equiv (\sigma_z + 1)/2$ and the lifetime of the emitter is given by $\tau/2 = (2\pi g^2)^{-1}$. It is key to remember how the input and output operators are defined

$$a_{\text{in}} = \frac{1}{\sqrt{2\pi}} \int \mathrm{d}k \; e^{-ik(t-t_0)} a_k(t_0) \qquad \text{and} \qquad a_{\text{out}} = \frac{1}{\sqrt{2\pi}} \int \mathrm{d}k \; e^{-ik(t_1-t)} a_k(t_1) \tag{3.52}$$

and it is these which Fan *et al.* connect to the system's S-matrix.

Note first that by definition

$$S_{pk} \equiv \langle p| \, S \, |k\rangle = \langle p^0 | k^0 \rangle = \langle 0| \, a_{\text{out}}(p) a_{\text{in}}^\dagger(k) \, |0\rangle \tag{3.53}$$

where $|p^0\rangle$ and $|k^0\rangle$ are the photon energy eigenstates evaluated at time $t = 0$ and $|0\rangle$ is the multi-mode vacuum. We have defined the operator $a_{\text{in}}^\dagger(k)$ such that it creates a photon with energy k at time $t = 0$ and $a_{\text{out}}^\dagger(p)$ does the same but with energy p. Fan *et al.* show that in the limits: $t_0 \longrightarrow -\infty$ and $t_1 \longrightarrow +\infty$, the operators $a_{\text{out}}(p)$ and $a_{\text{in}}(k)$ are nothing more than the spectral representations of the input and output operators in Eq. (3.52), i.e. that

$$a_{\text{out}} = \frac{1}{\sqrt{2\pi}} \int \mathrm{d}p \; e^{-ipt} a_{\text{out}}(p). \tag{3.54}$$

In order for this result to hold, we have to integrate over the whole of frequency-space, p and in the strictest sense the Hamiltonian Eq. (4.2) should only be valid for positive values of p. We are making the approximation here that the band of populated modes is sufficiently narrow so that the extension of this Hamiltonian over negative values is allowed. The infinite time limit is well justified and simply a restatement of the fact that the initial and final photonic states are free. This means that, in order to calculate the single photon scattering amplitudes, we simply need to compute the output operator expectation values using input-output theory and perform an inverse Fourier transformation on the results. Explicitly we have that

$$S_{pk} = \langle 0| \, a_{\text{out}}(p) a_{\text{in}}^\dagger(k) \, |0\rangle = \frac{1}{\sqrt{2\pi}} \int \mathrm{d}p \; e^{ipt} \, \langle 0| \, a_{\text{out}} \, |k^0\rangle \tag{3.55}$$

and $\langle 0| \, a_{\text{out}} \, |k^0\rangle$ can be determined by converting the operator differential equations in Eq. (3.51) to those for an expectation value. After performing the inverse Fourier transform, the result is that

$$S_{pk} = \frac{\tau(k-\Omega) - i}{\tau(k-\Omega) + i} \delta(p-k) \equiv t_k \delta(p-k), \tag{3.56}$$

which conserves energy as we would expect. We will return to this formula multiple times in this thesis and here simply note here that $|t_k| = 1$, meaning that t_k represents a phase shift on the scattered photon. Furthermore we see that when the incident photon is resonant with the emitter, this phase shift is maximised and equal to π radians.

3.5 Summary

We have seen that, in the dipole and rotating-wave-approximations, light-matter coupling can be described by a simple Hamiltonian, which preserves the excitation number of the combined system. We went on to study dissipative behaviour and showed that, when a quantum system is coupled to an unmonitored environment, a Lindblad-type master equation for the density matrix can capture a variety of decoherence processes. We then studied the famous Input-Output formalism and used it to predict the transmission spectra for both empty and atom-containing coherently driven cavities. The input-output relations are useful in and of themselves but we further showed how one can relate these to the S-matrix describing a few-photon scattering event.

Chapter 4

Analytic Few-Photon Scattering

In this chapter, based on Ref. [94], we develop a technique for calculating scattering amplitudes in waveguide QED via diagrammatic representation of the Dyson series. In Sec. 4.1 we review the relevant literature and set this project in the context of previous work. We go on to explain a general procedure for calculating the global dynamics of a waveguide QED system and in Sec. 4.3 we perform this procedure explicitly for a two-level-system scatterer. In Sec. 4.6 we repeat the calculation for a Λ-system emitter and this allows us, in Sec. 4.7, to compare the pole structures of the two scattering matrices. We discuss the rich relationship between the pole structure of the scattering matrix and the underlying physics of the system. Our technique complements the array of existing techniques for calculating S-matrices in waveguide QED and, in particular, gives us new insight into the connection between the standard waveguide QED Hamiltonian and virtual processes occurring during the light-matter interaction. Furthermore, the technique should be possible to scale to higher photon number input states, as the technique makes explicit the link between the photon combinatorics and S-matrix elements.

4.1 Background

The set-up analysed in this chapter consists of some general local system, coupled to the right-propagating modes a_ω of an optical waveguide, as shown in Fig. 4.1a. The details of unidirectional transport in quantum optics are discussed in detail in Sec. 5.1 and here we simply assume that the waveguide supports only optical modes with positive group velocity. The local system is in general complex and composed of multiple sub-systems; therefore the coupling is characterised by the set of rates $\{\Gamma_i\}$. This is the prototypical waveguide QED system and it is no surprise that it has been studied in great detail, with notable developments including the single and multi-photon scattering matrices [95] and generalisations of the input-output formalism [96] and master equation [97] to similar systems. There has also been a substantial body of work focussed on applying techniques from relativistic quantum field theory to the problem, with the LSZ reduction formula [98], cluster decomposition principle [99] and diagrammatic evaluation of Green's functions [100] all having also been studied. Theoretical tools have been developed for the extension of these formalisms into the strong-coupling regime [101] and to multi-mode optical inputs [102].

Schemes for engineering entanglement between matter qubits as in e.g. Refs. [103] require the stationary qubit state conditional on that of the optical field. This is not a universal feature of previously derived techniques, with e.g. the master equation description only specifying the local system state and input-output treatments being often limited to emitters with degenerate ground states [104]. Furthermore, those tools that do specify the total light-matter state, such as those derived from relativistic field theories or stochastic calculus [105, 106], while extremely powerful, often rely on advanced or computationally expensive mathematics. The aim of this project therefore is to develop a technique that captures the combined emitter-optical state nec-

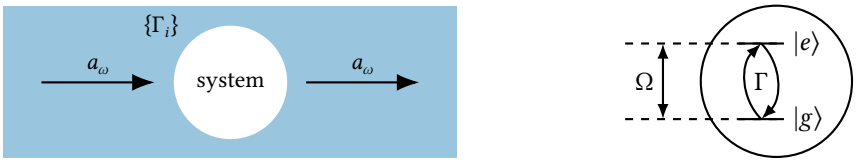

(a) Waveguide and chirally-coupled system.

(b) Two level system.

Figure 4.1: (a) Some unspecified local system interacting with the continuum of optical bosonic modes a_ω. The system may be composed of several sub-systems and thus the coupling is characterised in general by the set of rates $\{\Gamma_i\}$. (b) Two-level-system with an excited level $|e\rangle$, coupled to the ground state $|g\rangle$ at a rate Γ.

essary for the analysis of entanglement generation schemes, which remains transparent to the user, with the maths and physics clearly and intimately connected.

4.2 Transition Amplitude

At some time $t_i \longrightarrow -\infty$ the state of the system shown in Fig. 4.1a is given by $|\phi_{\text{in}}; \psi_{\text{in}}\rangle$, where ψ_{in} represents the input optical wavefunction and $|\phi_{\text{in}}\rangle$ is the state in which the emitter is prepared. A scattering event then occurs, and the global system dynamics are in general complicated to describe until a time $t_f \longrightarrow +\infty$, when the emitter has relaxed to some ground or meta-stable level and the optical state $|\psi_{\text{out}}\rangle$ is coupled out of the waveguide. Working in the interaction picture, the input and output states are eigenstates of the free Hamiltonian H_0 that describes the dynamics of an uncoupled waveguide-emitter system. This allows us to construct input and output optical states from the usual creation and annihilation operators for photons. The transition amplitude $\mathscr{A} \equiv \langle \phi_{\text{out}}; \psi_{\text{out}}| \mathscr{U} |\phi_{\text{in}}; \psi_{\text{in}}\rangle$ gives the overlap between an output state $|\phi_{\text{out}}; \psi_{\text{out}}\rangle$ and an input state evolved from $t \longrightarrow -\infty$ to $t \longrightarrow +\infty$ by the operator $\mathscr{U}$. With $\mathscr{U}$ representing the time evolution operator in the interaction picture, the transition amplitude $\mathscr{A}$ completely specifies the global system dynamics.

We expand the transition amplitude $\mathscr{A} \equiv \mathscr{A}^{(0)} + \mathscr{A}^{(1)} + \mathscr{A}^{(2)} + \ldots$ in terms of the Dyson series representation of $\mathscr{U} = \sum_{n=0}^{\infty} \mathscr{U}^{(n)}$ (see Sec. 3.4.2), so that $\mathscr{A}^{(n)} \equiv \langle \phi_{\text{out}}; \psi_{\text{out}}| \mathscr{U}^{(n)} |\phi_{\text{in}}; \psi_{\text{in}}\rangle$. We then use

$$\mathscr{U}^{(n)} = (-i)^n \int \mathrm{d}t_1 \int^{t_1} \mathrm{d}t_2 \ldots \int^{t_{n-1}} \mathrm{d}t_n \, H_{\text{I}}(t_1) H_{\text{I}}(t_2) \ldots H_{\text{I}}(t_n), \tag{4.1}$$

to determine that the n^{th} order term in the transition amplitude contains n copies of the interaction Hamiltonian. This is an important observation for cases where the interaction Hamiltonian is of Jaynes-Cummings form and conserves excitation number.

4.3 Two Level System Scattering Matrix

We now explicitly calculate the transition amplitude $\mathscr{A}$ for the scenario where the local system is a single two-level-emitter (TLS) with states $\{|g\rangle, |e\rangle\}$. We show a TLS schematically in Fig. 4.1b and define the transition frequency as Ω and the strength of the emitter-optical coupling as γ. In units where $\hbar = 1$ the interaction Hamiltonian for this system is given by (see Sec. 3.1)

$$H_{\text{I}}(t) = \gamma \int \mathrm{d}\epsilon \, (e^{-i\Delta_\epsilon t} \sigma_+ a_\epsilon + e^{i\Delta_\epsilon t} \sigma_- a_\epsilon^\dagger), \tag{4.2}$$

where we define the detuning $\Delta_\epsilon \equiv \omega_0 + \epsilon - \Omega$, with ω_0 representing the waveguide's central frequency. We assume that the TLS is prepared in the ground state $|g\rangle$ and, as $t_f \longrightarrow \infty$, it naturally relaxes so that $|\phi_{\text{out}}\rangle = |g\rangle$.

The form of Hamiltonian (4.2) and our assumption of an initially and finally relaxed emitter means that the only non-zero contributions to $\mathscr{A}^{(n)}$ are those where n is even and the Pauli matrices are ordered as $\sigma_-\sigma_+ \ldots \sigma_-\sigma_+$. The general expression for the n^{th} order term in the transition amplitude is then

$$\mathscr{A}^{(n)} = (-i\gamma)^n \int \mathrm{d}\tilde{t}^{(n)} \int \mathrm{d}\bar{\epsilon}^{(n)}\; e^{i(\Delta_{\epsilon_1} t_1 - \Delta_{\epsilon_2} t_2 + \ldots - \Delta_{\epsilon_n} t_n)} \langle \psi_{\text{out}}|\, a^\dagger_{\epsilon_1} a_{\epsilon_2} a^\dagger_{\epsilon_3} \ldots a_{\epsilon_n} |\psi_{\text{in}}\rangle\,, \tag{4.3}$$

where $\int \mathrm{d}\tilde{t}^{(n)} \equiv \int \mathrm{d}t_1 \int^{t_1} \mathrm{d}t_2 \ldots \int^{t_{n-1}} \mathrm{d}t_n$ and $\int \mathrm{d}\bar{\epsilon}^{(n)} \equiv \int \mathrm{d}\epsilon_1 \int \mathrm{d}\epsilon_2 \ldots \int \mathrm{d}\epsilon_n$.

4.3.1 Single Photon

We now demonstrate how to calculate the transition amplitude in Eq. (4.3) for the situation where a single incident photon with energy $\omega_0 + i$ scatters to an output photon of energy $\omega_0 + f$. It is simply a matter of applying the bosonic commutation relation to determine $\mathscr{A}^{(0)} = \delta(f - i)$. Consider now the n^{th} order term given by

$$\mathscr{A}^{(n)} = (-i\gamma)^n \int \mathrm{d}\tilde{t}^{(n)} \int \mathrm{d}\bar{\epsilon}^{(n)}\; e^{i\Delta_{\epsilon_1} t_1 - i\Delta_{\epsilon_2} t_2 \ldots - i\Delta_{\epsilon_n} t_n} \langle 0|\, a_f a^\dagger_{\epsilon_1} a_{\epsilon_2} \ldots a_{\epsilon_n} a^\dagger_i\, |0\rangle\,, \tag{4.4}$$

we can use the vacuum expectation value in Eq. (4.4) to eliminate the first, final and half of the remaining frequency integrals

$$\mathscr{A}^{(n)} = (-i\gamma)^n \int \mathrm{d}\tilde{t}^{(n)} \int \mathrm{d}\epsilon_3 \mathrm{d}\epsilon_5 \ldots \mathrm{d}\epsilon_{n-1} e^{i\left(\Delta_f t_1 - \Delta_{\epsilon_3} t_2 + \Delta_{\epsilon_3} t_3 + \ldots \Delta_i t_n\right)}. \tag{4.5}$$

The integrand in (4.5) can be further decomposed into its constituent Dirac delta functions and we have then

$$\mathscr{A}^{(n)} = (-i\gamma)^n (2\pi)^{\left(\frac{n}{2}-1\right)} \int \mathrm{d}t_1\; e^{i\Delta_f t_1} \int^{t_1} \mathrm{d}t_2 \int^{t_2} \mathrm{d}t_3\; \delta(t_3 - t_2) \ldots \int^{t_{n-1}} \mathrm{d}t_n\; e^{-i\Delta_i t_n}. \tag{4.6}$$

Successively performing time integrals using the technique found in e.g. Ref. [107] and reproduced here in App. A.2 we arrive upon

$$\mathscr{A}^{(n)} = 2\,(-i\gamma)^n\, \delta(f - i)\, (\pi g(\Delta_i))^{\frac{n}{2}}\,, \tag{4.7}$$

where we defined $g(\Delta) \equiv \left[\pi\delta(\Delta) + i\Delta^{-1}\right]$ for brevity. Summing over even n and using the binomial theorem, we find

$$\mathscr{A} = \frac{1 - \gamma^2 \pi g(\Delta_i)}{1 + \gamma^2 \pi g(\Delta_i)}\, \delta(f - i) \equiv t(i)\, \delta(f - i), \tag{4.8}$$

Eq. (4.8) is valid under the condition $\left|\pi\gamma^2 g(\Delta_i)\right| < 1$, which is required for application of the binomial theorem. However in Sec. 4.4 we further use a Borel summation technique [108] to demonstrate the validity of the result for arbitrary values of $\left|\pi\gamma^2 g(\Delta_i)\right|$. Eq. (4.8) is the first key result of this work and demonstrates that our method yields analytic expressions for the single-photon transition amplitude.

Note that it is quite easy to understand the nature of the physical process described by Eq. (4.5) and we have sketched it explicitly in Fig. 4.2. We see that the atom absorbs the original incident photon and, before emitting the outgoing photon, emits and absorbs $\frac{n}{2} - 1$ photons of frequencies $\{\epsilon_{n-1}, \epsilon_{n-3} \ldots \epsilon_3\}$. The energies of these 'internal' photons are uncertain and we integrate over a continuum of possible values for each, which has the effect of reducing their duration to zero—a 'point-like' interaction.

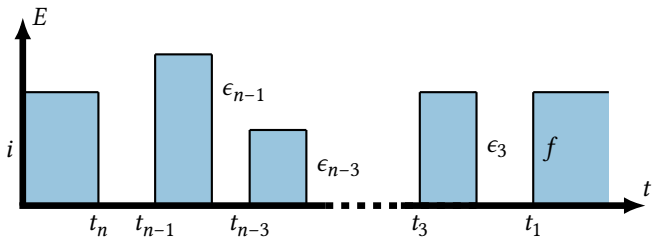

Figure 4.2: Diagram for the n^{th} order single photon scattering process. An incident photon of energy $\omega_0 + i$ is scattered to one of frequency $\omega_0 + f$. This occurs via the emission and absorption of $\frac{n}{2} - 1$ 'internal' photons.

4.3.2 Two Photon

We now calculate the transition amplitude $\mathscr{A}$ for the two-photon scattering case and note first that for input photons with energies $\omega_0 + i_0$ and $\omega_0 + i_1$ the n^{th} order term in the transition amplitude is

$$\mathscr{A}^{(n)} = (-i\gamma)^n \int \mathrm{d}\tilde{t}^{(n)} \int \mathrm{d}\bar{\epsilon}^{(n)}\, e^{i(\Delta_{\epsilon_1} t_1 - \Delta_{\epsilon_2} t_2 \ldots - \Delta_{\epsilon_n} t_n)} \langle 0|\, a_{f_0} a_{f_1} a^\dagger_{\epsilon_1} a_{\epsilon_2} \ldots a_{\epsilon_n} a^\dagger_{i_1} a^\dagger_{i_0}\, |0\rangle\,, \tag{4.9}$$

where f_0 and f_1 label the scattered photon frequencies. Evaluation of the vacuum expectation value in the integrand of Eq. (4.9) produces $2^{\frac{n}{2}+1}$ terms [109] and it is not feasible to mechanically calculate these. We instead use the physical interpretation of each term to provide further guidance.

As an example, consider one of the sixteen terms contributing to $\mathscr{A}^{(6)}$

$$\mathscr{A}^{(6)}_{(1)} = -\gamma^6 \int \mathrm{d}\tilde{t}^{(6)} \int \mathrm{d}\omega\, e^{i(\Delta_{f_1} t_1 - \Delta_\omega (t_2 - t_3) - \Delta_{i_1} t_4 + \Delta_{f_0} t_5 - \Delta_{i_0} t_6)}, \tag{4.10}$$

which, using exactly the same integration techniques as for the single-photon case, reduces to

$$\mathscr{A}^{(6)}_{(1)} = -2\pi^2 \gamma^6 \delta(f_0 + f_1 - i_0 - i_1) g(\Delta_{i_0}) g(\Delta_{i_0} - \Delta_{f_0}) g(\Delta_{i_0} + \Delta_{i_1} - \Delta_{f_0})^2. \tag{4.11}$$

By re-associating bosonic mode operators to their phases in the integrand of Eq. (4.10) we deduce that this term describes absorption by the atom of a photon with energy $\omega_0 + i_0$, prior to emission of a final $\omega_0 + f_0$ photon. Subsequently, the second incident photon is absorbed and emitted twice via an intermediate step of energy $\omega_0 + \omega$. Fig. 4.3a gives a pictorial representation of the process, with time evolving from left-to-right and energies of the two populated modes relative to ω_0 given by the distance from the horizontal axis.

We can derive amplitudes in general from diagrams such as Fig. 4.3a. By drawing the diagrams corresponding to the possible emission/absorption processes we can calculate the total transition amplitude. With each emission and absorption event in a diagram we associate a number Δ representing the difference between the total amount of absorbed radiation by the atom and the ground-excited energy gap. In Fig. 4.3a, the atom absorbs a photon of frequency $\omega_0 + i_0$ (yielding Δ_{i_0}), and emits a photon with energy $\omega_0 + f_0$ yielding $\Delta_{i_0} - \Delta_{f_0}$ corresponding to the residual energy between the two photons. Absorbing the second incident photon produces the factor $\Delta_{i_0} + \Delta_{i_1} - \Delta_{f_0}$. These terms appear as arguments of the frequency dependent function $g(x)$ in Eq. (4.11), which describes the amplitude of the process depicted in Fig. 4.3a. The 'loop' indicated by ω in Fig. 4.3a increases the power of $g(\Delta_{i_0} + \Delta_{i_1} - \Delta_{f_0})$ by one. Finally, we impose energy conservation via $\delta(f_0 + f_1 - i_0 - i_1)$.

Suppose that for a given n we have drawn all diagrams corresponding to $\frac{n}{2}$ light-matter interaction events. Four of these diagrams (the permutations over initial and final photon frequencies)

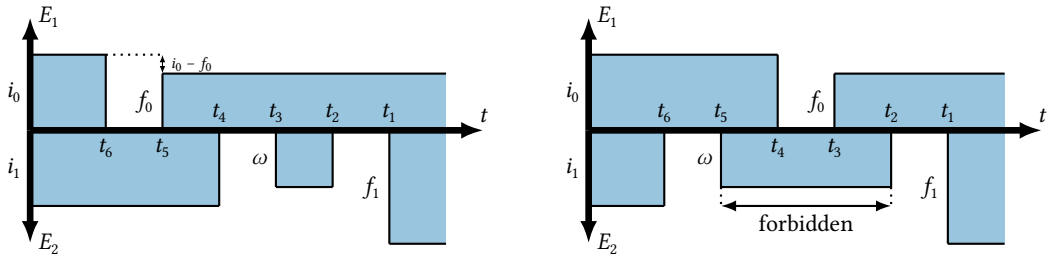

(a) Allowed $n = 6$ process.

(b) Forbidden $n = 6$ process.

Figure 4.3: Diagrams for one possible (a) and one impossible (b)) $n = 6$ processes. Incident photons of energy $\omega_0 + i_{0/1}$ are scattered to energies $\omega_0 + f_{0/1}$. An internal photon 'loop' of energy ω occurs, and ω is integrated over.

will always have one photon interacting with the emitter $\frac{n}{2}$ times, with the second photon passing through unperturbed (i.e., non-frequency mixing terms). These diagrams contribute amplitudes equivalent to the single photon case. Another class of diagrams we immediately discard is that in which an 'internal' photon (such as ω in Fig. 4.3a) is emitted at time t_m and *not* reabsorbed at $t = t_{m-1}$, since the interval $[t_m, t_{m-1}] \longrightarrow 0$. We rigorously demonstrate this in Sec. 4.5. The remaining diagrams are similar in structure to Fig. 4.3a, with initial absorption and final emission separated by a number of internal photon loops. The structure of the integrals corresponding to these diagrams is the same as in Eq. (4.10) with additional frequency and time integrals corresponding to these internal loops.

The procedure for converting diagrams into $\mathscr{A}^{(n)}$ is as follows:

(i) draw all possible diagrams with $\frac{n}{2}$ total interactions;

(ii) identify the single photon (non-frequency mixing) terms;

(iii) discard the terms in which internal photons are emitted and not immediately reabsorbed;

(iv) the remaining terms get the constant pre-factor $\frac{2}{\pi}(i\sqrt{\pi}\gamma)^n$;

(v) each absorption event gets a factor $g(\Delta)$, where Δ corresponds to the total absorbed radiation, and each emission event gets $g(\Delta_{\text{res}})$, where Δ_{res} is the amount of absorbed radiation not re-emitted;

(vi) for each loop, multiply by an additional factor of $g(\Delta)$ with the same Δ as at the previous absorption;

(vii) at the final emission, multiply by $\delta(f_0 + f_1 - i_0 - i_1)$.

The constant factor in step (iv) arises due to the $(i\gamma)^n$ that appears when we insert our interaction Hamiltonian into the Dyson series. We then convert $n/2 - 2$ frequency integrals into delta functions, which yields a factor of $(2\pi)^{n/2-2}$ but, when the time integrals are performed, these factors are halved. Multiplying by 2π then accounts for the final time integral, which produces the energy-conserving delta function and the correct factor is recovered. The four species of diagram for the $n = 8$ case are shown in Fig. 4.4 and we can explicitly perform this procedure to demonstrate equivalence between the diagrammatic and integral methods.

Firstly, the direct method; by definition we have that

$$\mathscr{A}^{(8)} = \gamma^8 \int \mathrm{d}\tilde{t}^{(8)} \int \mathrm{d}\tilde{\epsilon}^{(8)}\; e^{i(\Delta_{\epsilon_1} t_1 - \Delta_{\epsilon_2} t_2 + \Delta_{\epsilon_3} t_3 - \Delta_{\epsilon_4} t_4 + \Delta_{\epsilon_5} t_5 - \Delta_{\epsilon_6} t_6 + \Delta_{\epsilon_7} t_7 - \Delta_{\epsilon_8} t_8)} \times \langle 0 |\, a_{f_0} a_{f_1} a^\dagger_{\epsilon_1} a_{\epsilon_2} a^\dagger_{\epsilon_3} a_{\epsilon_4} a^\dagger_{\epsilon_5} a_{\epsilon_6} a^\dagger_{\epsilon_7} a_{\epsilon_8} a^\dagger_{i_1} a^\dagger_{i_0} \,| 0 \rangle. \tag{4.12}$$

The vacuum-expectation-value in this expression can be directly evaluated and we find expressions for a total of thirty-two terms

$$\begin{aligned}\mathscr{A}^{(8)} = \gamma^8 \int \mathrm{d}\tilde{t}^{(8)} \int \mathrm{d}\epsilon_1 \int \mathrm{d}\epsilon_2 \Big[& e^{i(\Delta_{f_0} t_1 - \Delta_{\epsilon_1} t_2 + \Delta_{f_1} t_3 - \Delta_{\epsilon_2} t_4 + \Delta_{\epsilon_1} t_5 - \Delta_{i_1} t_6 + \Delta_{\epsilon_2} t_7 - \Delta_{i_0} t_8)} \\ & + e^{i(\Delta_{f_1} t_1 - \Delta_{\epsilon_1} t_2 + \Delta_{f_0} t_3 - \Delta_{\epsilon_2} t_4 + \Delta_{\epsilon_1} t_5 - \Delta_{i_1} t_6 + \Delta_{\epsilon_2} t_7 - \Delta_{i_0} t_8)} \\ & + \ldots \\ & + e^{i(\Delta_{f_1} t_1 - \Delta_{i_0} t_2 + \Delta_{f_0} t_3 - \Delta_{\epsilon_2} t_4 + \Delta_{\epsilon_2} t_5 - \Delta_{\epsilon_1} t_6 + \Delta_{\epsilon_1} t_7 - \Delta_{i_1} t_8)} \Big] \end{aligned} \tag{4.13}$$

where we have used the delta functions from the decomposed vacuum-expectation-value to eliminate six of the eight frequency integrals. We can then use the definition of the Dirac delta function to transform the remaining frequency integrals and integrands into delta functions in time. Using the method outlined in App. 4.5, we can then eliminate any term with a delta function connecting non-adjacent times (e.g. $\delta(t_7 - t_4)$, $\delta(t_4 - t_1)$ etc.) and sixteen terms remain. There are however only four 'categories' of term—with each category containing four terms that are permutations over initial and final photon energies. We find that

$$\begin{aligned}\mathscr{A}^{(8)} = (2\pi)^2 \gamma^8 \sum_{s=0,1} \sum_{s'=0,1} \int \mathrm{d}\tilde{t}^{(8)} \Big[& 2\pi \delta(f_{s'} - i_s) \delta(t_7 - t_6) \delta(t_5 - t_4) \delta(t_3 - t_2)\, e^{i(\Delta_{f_{s'\oplus 1}} t_1 - \Delta_{i_{s\oplus 1}} t_8)} \\ & + \delta(t_7 - t_6) \delta(t_5 - t_4) e^{i(\Delta_{f_{s'}} t_1 - \Delta_{i_{s\oplus 1}} t_2 + \Delta_{f_{s'\oplus 1}} t_3 - \Delta_{i_s} t_8)} \\ & + \delta(t_3 - t_2) \delta(t_7 - t_6) e^{i(\Delta_{f_{s'}} t_1 - \Delta_{i_{s\oplus 1}} t_4 + \Delta_{f_{s'\oplus 1}} t_5 - \Delta_{i_s} t_8)} \\ & + \delta(t_5 - t_4) \delta(t_3 - t_2) e^{i(\Delta_{f_{s'}} t_1 - \Delta_{i_{s\oplus 1}} t_6 + \Delta_{f_{s'\oplus 1}} t_7 - \Delta_{i_s} t_8)} \Big]. \end{aligned} \tag{4.14}$$

The integrals in Eq. (4.14) can be evaluated directly, as in the main text for $n = 6$ and we find

$$\begin{aligned}\mathscr{A}^{(8)} = 2\pi^3 \gamma^8 \sum_{s=0,1} \sum_{s'=0,1} \Big[& \pi g^4(\Delta_{i_s}) \delta(f_{s'} - i_s) \delta(f_{s'\oplus 1} - i_{s\oplus 1}) \\ & + g^3(\Delta_{i_s}) g(\Delta_{i_s} - \Delta_{f_{s'}}) g(\Delta_{f_{s'\oplus 1}}) \delta(f_0 + f_1 - i_0 - i_1) \\ & + g^2(\Delta_{i_s}) g(\Delta_{i_s} - \Delta_{f_{s'}}) g^2(\Delta_{f_{s'\oplus 1}}) \delta(f_0 + f_1 - i_0 - i_1) \\ & + g(\Delta_{i_s}) g(\Delta_{i_s} - \Delta_{f_{s'}}) g^3(\Delta_{f_{s'\oplus 1}}) \delta(f_0 + f_1 - i_0 - i_1) \Big], \end{aligned} \tag{4.15}$$

which is the final result for the $n = 8$ term in the two-photon transition amplitude.

We now calculate $\mathscr{A}^{(8)}$ diagrammatically; the diagrams corresponding to the four species of term in Eqn. (4.14) are shown in Fig. 4.4. In the leftmost diagram a single photon is absorbed and emitted by the atom four times, in the next a photon is absorbed and emitted three times, before a second photon is absorbed and emitted once. The second from last diagram shows both photons being absorbed and emitted twice and the final diagram has a single absorption/emission for the first photon, followed by three for the second. The first diagram represents the non-frequency mixing component of the $n = 8$ term and therefore contributes a factor given by $2\pi^4 \gamma^8 g^4(\Delta_{i_s}) \delta(f_{s'} - i_s) \delta(f_{s'\oplus 1} - i_{s\oplus 1})$ to the amplitude—this being the single photon result multiplied by an additional delta function to impose conservation of energy for the second photon.

The three frequency mixing diagrams require application of the rules supplied in sec. 4.3. For example, consider the second from right diagram. We first associate the pre-factor $2\pi^3 \gamma^8$ to this diagram's term, substituting $n = 8$ into the expression $\frac{2}{\pi}(\sqrt{\pi}\gamma)^n$ for the n^{th} order case. The first absorption event then yields a factor of $g(\Delta_{i_s})$ as per the rules and we gain an additional factor of this term from the internal emission and absorption of the ϵ_1 photon. Emission of the photon with frequency $f_{s'}$ then yields the factor $g(\Delta_{i_s} - \Delta_{f_{s'}})$ before the next incident photon is absorbed, producing $g(\Delta_{i_{s\oplus 1}} + \Delta_{i_s} - \Delta_{f_{s'}})$. One additional copy of this factor is required, because of the second

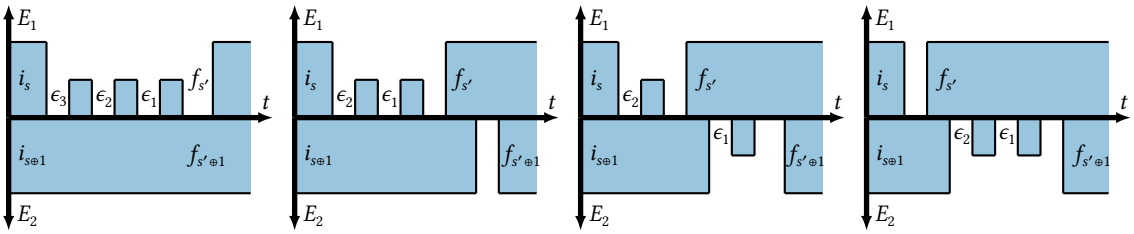

Figure 4.4: The four non-zero types of diagram for the $\mathscr{A}^{(8)}$ term in the expansion of the two photon amplitude. The leftmost diagram represents the non-frequency mixing term.

internal photon emission/absorption process but its argument can be simplified, as the final emission event yields the factor $\delta(f_0+f_1-i_0-i_1)$, meaning that $\Delta_{i_{s\oplus 1}}+\Delta_{i_s}-\Delta_{f_{s'}}=\Delta_{f_{s'\oplus 1}}$. Multiplying individual factors together yields the expression $2\pi^3\gamma^8 g^2(\Delta_{i_s})g(\Delta_{i_s}-\Delta_{f_{s'}})g^2(\Delta_{f_{s'\oplus 1}})\delta(f_0+f_1-i_0-i_1)$, exactly as found in Eq. (4.15).

We can now use these rules to calculate the total transition amplitude; let the frequency mixing term in $\mathscr{A}^{(n)}$ for the two-photon case be given by $\delta(f_0+f_1-i_0-i_1)\mathscr{M}^{(n)}$. From the above procedure we deduce that the total photon frequency mixing term in the two-photon transition amplitude is given by

$$\mathscr{M}^{(n)}=\sum_{s=0,1}\sum_{s'=0,1} g(\Delta_{i_s})g(\Delta_{i_s}-\Delta_{f_{s'}})g(\Delta_{f_{s'\oplus 1}})\frac{2}{\pi}(-\pi\gamma^2)^n\sum_{k=0}^{n-2} g(\Delta_{i_s})^k g(\Delta_{f_{s'\oplus 1}})^{n-2-k} \tag{4.16}$$

The sum over k can be evaluated using [110]

$$\sum_{k=0}^{n} x^k y^{n-k}=\frac{x^{(1+n)}-y^{(1+n)}}{x-y} \tag{4.17}$$

and we sum over all n to find $\mathscr{M}$. Adding this to the non-frequency mixing component yields a final expression for the two-photon transition amplitude

$$\begin{aligned}\mathscr{A}=&[t(i_0)+t(i_1)-1][\delta(f_0-i_0)\delta(f_1-i_1)+\delta(f_0-i_1)\delta(f_1-i_0)]\\&+2\pi\gamma^4\delta(f_0+f_1-i_0-i_1)\sum_{s=0,1}\sum_{s'=0,1}\frac{g(\Delta_{i_s})g(\Delta_{i_s}-\Delta_{f_{s'}})g(\Delta_{f_{s'\oplus 1}})}{[1+\pi\gamma^2 g(\Delta_{i_s})][1+\pi\gamma^2 g(\Delta_{f_{s'\oplus 1}})]},\end{aligned} \tag{4.18}$$

where $t(i)$ is defined in Eq. (4.8). Eq. (4.18) is the second main result of this work and demonstrates our formalism's power to produce non-perturbative amplitudes for multi-photon processes. It is in some ways quite pleasing that Eq. (4.18) has the form it does, with the sum of single photon transmission coefficients, but it is not conventionally expressed in this way. The factors of $g(\Delta)$ can be expanded out and algebra performed (App. B) to re-cast the expression into the more familiar form,

$$\begin{aligned}\mathscr{A}=&t(i_0)t(i_1)[\delta(f_0-i_0)\delta(f_1-i_1)+\delta(f_0-i_1)\delta(f_1-i_0)]\\&+\frac{4\pi i\gamma^4\delta(f_0+f_1-i_0-i_1)}{\left[\Delta_{f_0}+i\pi\gamma^2\right]\left[\Delta_{f_1}+i\pi\gamma^2\right]}\left(\frac{1}{\Delta_{i_0}+i\pi\gamma^2}+\frac{1}{\Delta_{i_1}+i\pi\gamma^2}\right).\end{aligned} \tag{4.19}$$

Other authors have previously found this quantity and Eq. (4.19) is precisely equivalent to the result found in e.g. Ref. [111]. It could be argued however that having the coefficient of the frequency preserving delta functions in the scattering matrix given by $(t(i_0)+t(i_1)-1)$ is more natural than the usual factor of $t(i_0)t(i_1)$. This comes down to a physical interpretation of the dynamics, with the amplitude for the process given by the amplitudes of each individual photon

scattering from the atom (minus unity to account for our double-counting of the process where no photon-atom interaction occurs).

An interesting observation here is that for $n \geq 6$ the particular form of Eq. (4.2) caused vanishing of the terms with internal photon emission not immediately followed by re-absorption (step (iii) of the above outlined rules). This behaviour is due to the Hamiltonian's instantaneous coupling between the emitter and continuum of waveguide modes (without cut-off) at a constant rate. It is interesting to note that this oft-employed model makes this prediction and still agrees well with experimental data. General Hamiltonians with discretised waveguide modes would not necessarily lead to these terms vanishing. We show one of these dis-allowed diagrams in Fig. 4.3b.

4.4 Borel Summation

In order to find the single photon transition amplitude it was necessary to evaluate the sum

$$\sigma = \sum_{n=0}^{\infty} \left(-\gamma^2 \pi g(\Delta_i)\right)^n, \tag{4.20}$$

which was rendered possible for the case of $\left|\pi\gamma^2 g(\Delta_i)\right| < 1$ via the binomial theorem. Terms in the series are divergent when this condition is not satisfied and we therefore need to take a more nuanced approach to assign a value to the sum outside of this regime. We first demand that $\Delta_i \neq 0$ and find

$$\sigma = \sum_{n=0}^{\infty} (-i\pi z)^n, \tag{4.21}$$

where $z \equiv \gamma^2/\Delta_i$. Naturally the series to be summed in Eq. (4.21) is still divergent for a large portion of the parameter space but there exists an often employed technique called "Borel summation," which can be used to interpret such sums. We discuss the mathematical details of Borel summation in App. A.3 and here simply state that the Borel summed form of Eq. (4.21) is

$$\mathscr{B}(\sigma) = \int_0^{\infty} \mathrm{d}t\; e^{-t} \sum_{n=0}^{\infty} \frac{(-i\pi z t)^n}{n!} = \int_0^{\infty} \mathrm{d}t\; e^{-t(1+i\pi z)} = \frac{1}{1 + i\pi z} \tag{4.22}$$

under the condition now that $\mathrm{Im}\left[\pi\gamma^2/\Delta_i\right] < 1$. We know however that γ^2 gives, up to some constant factor, the spontaneous emission rate of the emitter[1]. This means that $\pi\gamma^2/\Delta_i$ is a real quantity and thus the condition is always satisfied. The Borel-summed transition amplitude is then

$$\mathscr{A} = \delta(f - i)\frac{\Delta_i - i\pi\gamma^2}{\Delta_i + i\pi\gamma^2}, \tag{4.23}$$

valid for all coupling strengths.

4.5 Vanishing Diagrams

Before evaluating the transition amplitude for a different waveguide embedded emitter, we briefly digress and in this section show mathematically why diagrams with internal photon loops spanning multiple time integrals should be discarded. Consider the following; if we methodically

[1] This can be determined by deriving the Heisenberg equations for the number operator associated with the Hamiltonian in Eq. (4.2).

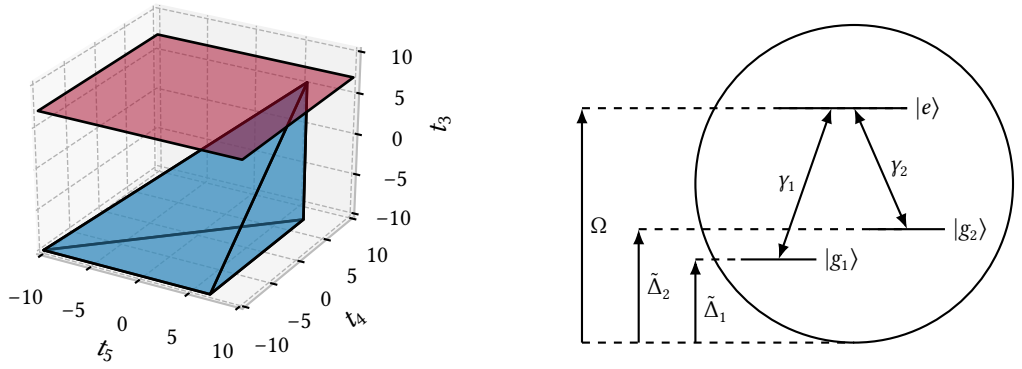

(a) Integration region.

(b) The Λ-system.

Figure 4.5: (a) Integration region defined by the enclosed volume. We see that it intersects the surface defined by $t_5 = t_2$ at only a single point. (b) A so-called Λ-system. Two ground levels $|g_1\rangle$ and $|g_2\rangle$ are coupled with amplitudes γ_1 and γ_2 respectively to an excited state $|e\rangle$. We define a zero-energy separated from $|e\rangle$ by Ω and denote the gap between $|g_1\rangle/|g_2\rangle$ and zero by $\tilde{\Delta}_1/\tilde{\Delta}_2$. Without loss of generality we assume $\Omega > \tilde{\Delta}_2 > \tilde{\Delta}_1$.

calculate $\mathscr{A}^{(6)}$ we arrive upon many terms, for example

$$\mathscr{A}^{(6)}_{\text{example}} = -\gamma^6 \int \mathrm{d}\tilde{t}^{(6)} \int \mathrm{d}\omega \; e^{i(\Delta_{f_1} t_1 - \Delta_\omega (t_2 - t_5) + \Delta_{f_0} t_3 - \Delta_{i_0} t_4 - \Delta_{i_1} t_6)}. \tag{4.24}$$

Evaluation of the frequency integral in this expression yields the Dirac delta function $\delta(t_5 - t_2)$ and so we are evaluating an integral of the form

$$\mathscr{A}^{(6)}_{\text{example}} \propto \int^{t_2} \mathrm{d}t_3 \int^{t_3} \mathrm{d}t_4 \int^{t_4} \mathrm{d}t_5 \; h(t_5, t_4, t_3)\delta(t_5 - t_2), \tag{4.25}$$

where $h(t_5, t_4, t_3)$ is some exponential function. The integral here is over a volume in time-space, bounded by the surfaces $t_5 = t_4$ and $t_4 = t_3$. The delta function has the effect of converting this volume integral into one over a surface—where the surface is defined by projection of the original volume onto $t_5 = t_2$. A representation of this is depicted in Figure 4.5a and we see that the resulting surface is given by a point. Therefore, under the assumption that the emitter starts in and returns to the ground state, this term does not contribute to the transition amplitude.

4.6 Λ-System Scattering Matrix

In many cases the perfect TLS is hard to realise, or some additional control is required over the system. This means that the emitter used in many light-matter interaction experiments has a more complex internal structure, e.g. in Refs. [112, 113, 114] This motivates the extension of our method to a second species of local system. Consider the Λ-system shown schematically in Fig. 4.5b. Neglecting polarisation, the interaction Hamiltonian describing the dynamics of this system is readily derived and given by

$$H_{\text{I}}(t) = \sum_{\lambda=1}^{2} \gamma_\lambda \int \mathrm{d}\epsilon \; e^{it\Delta_{\epsilon,\lambda}} a^\dagger_\epsilon \, |g_\lambda\rangle\langle e| + e^{-it\Delta_{\epsilon,\lambda}} a_\epsilon \, |e\rangle\langle g_\lambda| \tag{4.26}$$

where we have defined the detuning $\Delta_{\epsilon,\lambda} = \omega_0 + \epsilon - \Omega + \tilde{\Delta}_\lambda$, again linearising the waveguide dispersion relation about ω_0. In general, prior to and following a photon scattering event, a Λ-system will be in some state described by $|\phi\rangle = \alpha\,|g_1\rangle + \beta\,|g_2\rangle$, as radiative transitions to each

of the ground states are allowed but the $|g_1\rangle \leftrightarrow |g_2\rangle$ transitions are forbidden. In order to fully specify the dynamics, we need to evaluate matrix elements of the form

$$\mathscr{A}_{\mu\nu} = \langle \psi_{\text{out}}; g_\mu | \, \mathscr{U} \, | \psi_{\text{in}}; g_\nu \rangle \,, \tag{4.27}$$

where $\mu/\nu = 1, 2$. Inserting Hamiltonian (4.26) into this expression for the transition amplitude then yields

$$\begin{aligned} \mathscr{A}_{\mu\nu}^{(n)} = (-i)^n \sum_{\{\lambda_1,\lambda_2\ldots\lambda_n\}=1}^{2} \gamma_{\lambda_1}\gamma_{\lambda_2}\ldots\gamma_{\lambda_n} \int \mathrm{d}\tilde{t}^{(n)} \int \mathrm{d}\tilde{\epsilon}^{(n)} \; \langle \psi_{\text{out}}; g_\mu | \, e^{it_1\Delta_{\epsilon_1,\lambda_1}} a_{\epsilon_1}^\dagger \, |g_{\lambda_1}\rangle \\ \times \langle e | \, e^{-it_2\Delta_{\epsilon_2,\lambda_2}} a_{\epsilon_2} \, |e\rangle\langle g_{\lambda_2}| \ldots e^{-it_n\Delta_{\epsilon_n,\lambda_n}} a_{\epsilon_n} \, |e\rangle\langle g_{\lambda_n}| \psi_{\text{in}}; g_\nu \rangle \,, \end{aligned} \tag{4.28}$$

where, at each time step, we inserted only the two terms from the Hamiltonian which either raise a ground state or lower an excited one—the two terms corresponding to the opposite behaviour necessarily vanishing. This means that again, Eq. (4.28) is non-zero only when n is even. The final simplification Eq. (4.28) permits, before requiring knowledge about the input and output optical states, utilises the orthogonality of atomic states to eliminate $\frac{n}{2}+1$ of the sums over λ by replacing inner products between ground states with Kronecker Delta functions, e.g. $\langle g_{\lambda_2}|g_{\lambda_3}\rangle = \delta_{\lambda_2\lambda_3}$.

4.6.1 Single Photon

We can evaluate the amplitude of Eq. (4.28) for the case of single photon scattering as for the TLS. We denote the input and output optical states by $|\psi_{\text{in}}\rangle = |i\rangle$ and $|\psi_{\text{out}}\rangle = |f\rangle$ respectively. It is simple to deduce that

$$\langle 0 | \, a_f a_{\epsilon_1}^\dagger a_{\epsilon_2} \ldots a_{\epsilon_n} a_i^\dagger \, |0\rangle = \delta(f-\epsilon_1)\delta(\epsilon_2-\epsilon_3)\ldots\delta(\epsilon_{n-2}-\epsilon_{n-1})\delta(\epsilon_n - i) \tag{4.29}$$

and we can therefore eliminate $\frac{n}{2}+1$ of the integrals over ϵ in Eq. (4.28), leaving

$$\begin{aligned} \mathscr{A}_{\mu\nu}^{(n)} = (-i)^n \gamma_\mu\gamma_\nu \sum_{\{\lambda_2,\lambda_4\ldots\lambda_{n-2}\}=1}^{2} \gamma_{\lambda_2}^2\gamma_{\lambda_4}^2\ldots\gamma_{\lambda_{n-2}}^2 \int \mathrm{d}\tilde{t}^{(n)} \int \mathrm{d}\epsilon_2 \int \mathrm{d}\epsilon_4 \ldots \int \mathrm{d}\epsilon_{n-2} \\ e^{it_1\Delta_{f,\mu}} e^{-it_2\Delta_{\epsilon_2,\lambda_2}} e^{it_3\Delta_{\epsilon_2,\lambda_2}} \ldots e^{it_{n-1}\Delta_{\epsilon_{n-2},\lambda_{n-2}}} e^{-it_n\Delta_{i,\nu}}. \end{aligned} \tag{4.30}$$

Successively evaluating the frequency integrals in Eq. (4.30) in the same manner as for the TLS case, we find

$$\mathscr{A}_{\mu\nu}^{(n)} = 2(-i)^n [\pi(\gamma_1^2+\gamma_2^2) g(\Delta_{i,\nu})]^{\frac{n}{2}} \frac{\gamma_\mu\gamma_\nu}{\gamma_1^2+\gamma_2^2} \delta(\Delta_{f,\mu}-\Delta_{i,\nu}) \tag{4.31}$$

and again apply the binomial theorem/Borel summation to determine

$$\mathscr{A}_{\mu\nu} = \delta(\Delta_{f,\mu}-\Delta_{i,\nu}) \left(\delta_{\mu\nu} - \frac{2i\pi\gamma_\mu\gamma_\nu}{\Delta_{i,\nu} + i\pi(\gamma_1^2+\gamma_2^2)} \right) \equiv \delta(\Delta_{f,\mu}-\Delta_{i,\nu}) \left[\delta_{\mu\nu} + s_{\mu\nu}(\Delta_{i\nu}) \right]. \tag{4.32}$$

The predictions of Eq. (4.32) can be arrived upon via a variety of other methods, e.g. Refs. [115, 116, 117, 118]. Specifically we see that Eqs. (23) of Ref. [117] are recovered under the transformation $\pi\gamma_i^2 \longrightarrow \Gamma_i$. For a Λ-system with identical lifetimes into both ground states, i.e. $\gamma_1 = \gamma_2$, the prediction that a single resonant photon, incident upon an emitter prepared in the state $|g_1\rangle$ deterministically transfers the population to the state $|g_2\rangle$ is reproduced. It is interesting to note that this process is independent of any relative energy difference between the two ground states and that the transfer occurs for arbitrary values of the energy gap $\tilde{\Delta}_2 - \tilde{\Delta}_1$.

4.6.2 Two Photon

We now argue that is possible to extend the diagrammatic approach used to compute the two-photon transition amplitude for the TLS to the Λ-system. In order to do this we need to demonstrate that the rules enumerated in Sec. 4.3.2 continue to apply—with slight modifications specified by the added internal structure of the emitter. The first task therefore is to show that we can continue to discard terms in which internal photons are emitted and not immediately reabsorbed. These diagrams correspond to terms in the transition amplitude where an integral over the continuum of modes leads to a delta function connecting non-adjacent times. It is easy to determine that this continues to be the case by inspection of Eq. (4.28). We see that the structure of the time integral is not modified and so any delta function in the integrand of the form $\delta(t_i - t_j)$, where $|i - j| > 1$, will continue to integrate to zero by the logic of Sec. 4.5.

The non-frequency mixing diagrams for the Λ-system are again simple to analyse but yield a subtly different term to that found in the TLS case. This is expected and related to the breaking of photon exchange symmetry, introduced by the non-unique ground states of the atomic system [119]. Non-frequency mixing diagrams correspond to the four terms in the transition amplitude where, when the vacuum expectation value in Eq. (4.28) is evaluated, one of the creation operators for an initial photon state is commuted through one of the operators for a final state photon. This means that the structure of delta functions in the integrand of such terms is

$$\delta(f' - i')\delta(f - \epsilon_1)\delta(\epsilon_2 - \epsilon_3)\delta(\epsilon_4 - \epsilon_5)\dots\delta(\epsilon_n - i), \tag{4.33}$$

where f/f' and i/i' label the frequencies of final and initial state photons respectively. We can therefore construct the frequency-preserving portion of the transition amplitude

$$\begin{aligned}\mathcal{N}_{\mu\nu} =& \delta_{\mu\nu}\left[\delta(f_0 - i_0)\delta(f_1 - i_1) + \delta(f_0 - i_1)\delta(f_1 - i_0)\right] \\ &+ \sum_{s=0,1}\sum_{s'=0,1}\delta(f_{s'\oplus 1} - i_{s\oplus 1})\delta(\Delta_{f_{s'}\mu} - \Delta_{i_s\nu})s_{\mu\nu}(\Delta_{i_s\nu}).\end{aligned} \tag{4.34}$$

Having evaluated the non-frequency mixing terms and also those which do not contribute to the transition amplitude, the only species of terms remaining correspond to frequency mixing processes. Applying the constraint that internal photons must be immediately reabsorbed following emission, we find that the structure of the vacuum expectation value in the integrand of frequency mixing terms is

$$\delta(\epsilon_n - i)\delta(\epsilon_{n-1} - \epsilon_{n-2})\dots\delta(f - \epsilon_{m+1})\delta(i' - \epsilon_m)\delta(\epsilon_{m-1} - \epsilon_{m-2})\dots\delta(f' - \epsilon_1), \tag{4.35}$$

where m labels some point along the time evolution where one photon ceases its interaction with the emitter and the second one is absorbed. This completes our argument, as we see that again in order to calculate the n^{th} order term in the transition amplitude we have to sum all terms with $n/2$ total interactions, varying the number of times each of the initial photons interacts. Performing this procedure we calculate the n^{th} order frequency mixing term

$$\begin{aligned}\mathscr{M}^{(n)}_{\mu\nu} =& \frac{2}{\pi}(-\pi)^n\gamma_\mu\gamma_\nu(\gamma_1^2 + \gamma_2^2)^{n-2}\sum_{s=0,1}\sum_{s'=0,1}\sum_{\lambda=1,2}\gamma_\lambda^2 g(\Delta_{i_s\nu})g(\Delta_{i_s\nu} - \Delta_{f_{s'}\lambda})g(\Delta_{f_{s'\oplus 1}\mu}) \\ &\times\sum_{k=0}^{n-2} g(\Delta_{i_s\nu})^{n-2-m}g(\Delta_{f_{s'\oplus 1}\mu})^m\delta(\Delta_{f_{s'\oplus 1}\mu} + \Delta_{f_{s'}} - \Delta_{i_{s\oplus 1}} - \Delta_{i_s\nu}),\end{aligned} \tag{4.36}$$

which we see is similar in structure to Eq. (4.16) with an additional sum over the two possible mechanisms by which the two incident photons could now couple. After summing expression Eq. (4.36) over all n, adding this to the frequency preserving term and algebraic rearrangement

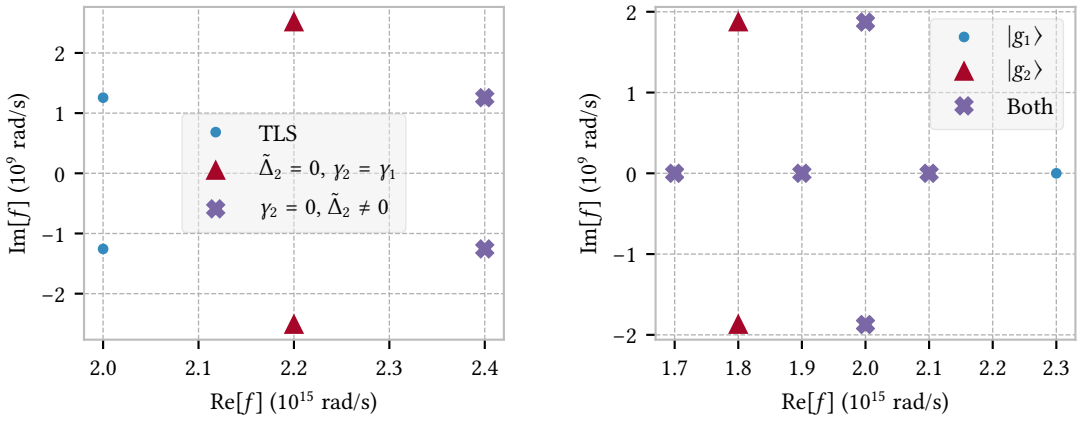

(a) TLS poles.

(b) Λ-system poles.

Figure 4.6: Location of poles in the photon mixing component of the total transition amplitude on the complex energy plane of f—the energy of one of the scattered photons. The coupling $\gamma_1 = 2 \times 10^4\ \sqrt{\text{rad/s}}$ corresponds to a lifetime of approximately 1 ns. In both cases we drive the system with two single-frequency photons, one positively detuned from Ω by $\delta = 1 \times 10^{14}$ rad/s and one negatively detuned by the same amount. (a) TLS and special Λ-system configurations. Central angular frequencies are $\Omega = 2{\times}10^{15}$, $2.2{\times}10^{15}$ and $2.4{\times}10^{15}$ rads^{-1} for systems represented by circles, triangles and crosses respectively. (b) Λ-system prepared initially in the state $|g_1\rangle$, with $\Omega = 2 \times 10^{15}$ rad/s, $\tilde{\Delta}_1 = 0$ and $\tilde{\Delta}_2 = \Omega/10$. We further set $\gamma_1 = 2 \times 10^4\ \sqrt{\text{rad/s}}$ and $\gamma_2 = \gamma_1/\sqrt{2}$. Some poles correspond specifically to the emitter scattering to a given state and others are present in both cases.

we find the total transition amplitude

$$\begin{aligned}\mathscr{A}_{\mu\nu} =& \mathscr{N}_{\mu\nu} + \frac{1}{2\gamma_\mu\gamma_\nu}\sum_{s,s',\lambda}\gamma_\lambda^2 s_{\mu\nu}(\Delta_{i_s\nu})s_{\mu\nu}(\Delta_{f_{s'\oplus 1}\mu})\delta(\Delta_{i_{s\oplus 1}\lambda} - \Delta_{f_{s'\oplus 1}\mu})\delta(\Delta_{i_s\nu} - \Delta_{f_{s'}\lambda}) \\ &+ \frac{i}{2\pi\gamma_\mu\gamma_\nu}\sum_{s,s',\lambda}\gamma_\lambda^2\frac{1}{\Delta_{i_s\nu} - \Delta_{f_{s'}\lambda}}s_{\mu\nu}(\Delta_{i_s\nu})s_{\mu\nu}(\Delta_{f_{s'\oplus 1}\mu})\delta(\Delta_{i_s\nu} - \Delta_{f_{s'\oplus 1}\mu} + \Delta_{i_{s\oplus 1}} - \Delta_{f_{s'}}).\end{aligned} \tag{4.37}$$

The transition amplitude of Eq. (4.37) exactly specifies the combined emitter-optical state following the scattering of two initial photons with frequencies i_0 and i_1 on the Λ-system depicted in Fig. 4.5b. We can use this to investigate the properties of light-matter scattering experiments and we do this in the following section.

Fewer reported techniques exist that capture the physics of Eq. (4.37), compared with the single-photon case. However, methods derived from those of relativistic quantum field theory do exist as in e.g. Ref. [120]. Here Pletyukhov and Gritsev derive an expression for the 'T-matrix,' $T^{(2)}(\omega)$ when two photons scatter from a Λ-system. It can be demonstrated that Eq. (4.37) of this thesis is equivalent to Eq. (46) of Ref. [120].

4.7 Pole Structure of the Scattering Matrices

In a scattering experiment it is known that many properties of the scattered state are determined by the pole structure of the transition amplitude [121]. In particular, poles in the complex plane of the scattered particle energy correspond to bound-states of the system [122]. Bound states of massive particles such as electrons, neutrons and protons are extremely familiar to us and a photonic bound state is the extension of this to massless particles. Two photons, which would

usually not interact strongly, become entangled in the frequency domain and travel through space as a single quasi-particle.

We might naively imagine that the pole structure of the amplitude is broadly similar whether the two-photons scatter from a TLS or a Λ-system, with the added internal structure of the emitter only slightly shifting their location for example. We can however demonstrate that this is not the case and that the addition of a second emitter ground-state introduces a great deal of richness to the system. In Fig. 4.6 we consider the frequency-mixing portion of the transition amplitude of Eq. (4.37) and plot poles in the complex plane of f, which gives the energy of one of the scattered photons. Note that given f, the energy of the second photon is completely specified by the energy conserving delta function. In both Figs. 4.6a and 4.6b we drive the system with two single-frequency photons, one detuned negatively from the transition energy Ω by $\delta = 1 \times 10^{14}$ rad/s and one positively by the same amount.

In Fig. 4.6a we plot the location of the poles for three different systems. Blue circles illustrate the locations of the poles for a simple TLS, with central frequency $\Omega = 2 \times 10^{15}$ rad/s and coupling $\gamma = 2 \times 10^4 \sqrt{\text{rad/s}}$. This coupling strength would correspond to a lifetime of ~ 1 ns, which is a reasonable estimate for a TLS formed by e.g. a semiconductor quantum dot. We note the two poles at $f = \Omega \pm i\pi\gamma^2$, this is the result found by many previous authors and corresponds to the formation of a frequency-entangled pair of photons. It is interesting to ask under which circumstances the photons scattered from a Λ-system appear indistinguishable from those scattered by a TLS. Obviously, we would expect that when $\gamma_2 = 0$, for arbitrary $\tilde{\Delta}_2$, the system should behave as the TLS—photons have no access to the state $|g_2\rangle$. As a validity check of Eq. (4.37) we plot the poles of such as a system (with $\Omega = 2.4 \times 10^{15}$ rad/s now) using purple crosses and find that this is indeed the predicted behaviour. A more surprising result is indicated by the red triangles of Fig. 4.6a. Here we set $\gamma_2 = \gamma_1$, with γ_1 the same as for the TLS. We find that, when $\tilde{\Delta}_2 = 0$, the pole structure of the Λ-system is again the same as that of the TLS—though the poles are now located at $f = \Omega \pm i\pi(\gamma_1^2 + \gamma_2^2)$. This is due to the degenerate ground states appearing indistinguishable to incoming photons and thus their only effect is a strengthening of the light-matter interaction, evidenced by shifting of the poles away from the real axis.

It is not generally true that the S-matrix associated with scattering from a Λ-system is well approximated by the TLS version. In Fig. 4.6b we consider a more general Λ-system, setting $\Omega = 2 \times 10^{15}$ rad/s, $\tilde{\Delta}_1 = 0$ and $\tilde{\Delta}_2 = \Omega/10$. We further assume the system is prepared initially in the lower ground state $|g_1\rangle$ and set the couplings asymmetrically so that $\gamma_1 = 2 \times 10^4 \sqrt{\text{rad/s}}$ and $\gamma_2 = \gamma_1/\sqrt{2}$. Now, it is important to note that the frequency mixing component of Eq. (4.37) corresponds to two distinct processes. In one the emitter returns to the state $|g_1\rangle$ following the scattering, while in the other it scatters to $|g_2\rangle$. We plot both species of poles in Fig. 4.6b, using blue circles and red triangles respectively and also use purple crosses to denote the location of poles common to both parts of the transition amplitude.

The most striking feature of Fig. 4.6b compared to 4.6a is the emergence of poles on the $\text{Im}[f] = 0$ axis of the complex plane. This means that there are now singularities in the transition amplitude corresponding to physical scattered photon energies—resonances. These occur at the frequencies of the photons input to the system and the input frequencies minus the energy gap $\tilde{\Delta}_2$. For the emitter state preserving portion of the amplitude there is an additional resonance at $\Omega + \tilde{\Delta}_2 + \delta$, stemming from a process where one of the photons scatters the system to $|g_2\rangle$, with the second photon then picking up this excess energy. The final point to note is the emergence of a second pair of imaginary poles at $\Omega - \tilde{\Delta}_2 \pm i\pi\left(\gamma_1^2 + \gamma_2^2\right)$ in the portion of the transition amplitude in which the emitter is scattered to the state $|g_2\rangle$. This has a simple physical interpretation; if we were to post-select onto this state, the bound state of entangled photons would have lower frequency in order to conserve overall energy.

4.8 Summary

We have developed an intuitive, diagrammatic approach to the problem of light-matter coupling in waveguide QED. In contrast to previously reported techniques, our method allows visualisation of the photon-atom dynamics. We have demonstrated analytical results for both single and two photon input optical states for both the TLS and Λ-systems. The diagrammatic approach is straight-forward to extend to higher photon number input states (though increasingly computationally expensive) and potentially more realistic Hamiltonians. Several open questions emerge from this work. For instance, how does the choice of Hamiltonian in Eq. (4.2) impact the transition amplitude? In particular, a waveguide will have a range of supported frequency modes defined largely by its dimensions. In theory this leads to observable consequences [123] and this would seem to suggest that some of the processes associated with forbidden diagrams actually contribute in physical systems. The limit on our method is ultimately a computational one, with an N-photon event requiring N permutations over both initial and final frequencies.

Chapter 5

Experimental Realisations

In this chapter we look at some experimental implementations of the prototypical waveguide system studied in Chapter 4. We begin by reviewing the topic of non-reciprocal transport in quantum optics and explain why this phenomenon arises naturally in the illustrative system of a QD coupled to a nanobeam waveguide. We go on, in Sec. 5.2, to make some predictions for the behaviour we would expect to observe in experimental systems and explain why these dynamics are not in fact reproduced in the laboratory. In Sec. 5.3 we perform a more detailed analysis and use the Input-Output Formalism to model some recent experiments on a nanobeam-coupled QD [124]. We perform a similar analysis on a related system [125] in Sec. 5.4 but pay particular attention to the emergence of the Fano-type dispersive lineshapes that are observed.

5.1 Unidirectional Transport in Quantum Optics

We first briefly review the field of 'unidirectional' or 'non-reciprocal' transport in quantum optics [126]. Suppose we have some nanostructure that supports optical modes propagating in two anti-parallel directions (conventionally $\pm z$) and an embedded emitter. We would expect, by symmetry, that the emitter will interact with photons travelling in either direction equally strongly. Non-reciprocal systems are those in which this propagation direction degeneracy is lifted and have been experimentally realised in e.g. photonic crystal coupled QDs [127] and micro-resonator coupled atoms [128]. We adopt the convention that points in a structure where an embedded emitter interacts unidirectionally are called 'c-points.' [1]

In order to understand the concept of non-reciprocal transport in quantum optics, we focus on the illustrative example of a QD coupled to a nanobeam waveguide. These structures of vacuum-clad, high refractive index semiconductor confine photons transversely to their propagation direction via total internal reflection. In order to recognise the origin of unidirectional coupling we need to scrutinise the nanobeam in greater detail than that presented in the simple model of e.g. Fig. 4.1a. We first note that quantum emitters have small physical dimensions and so, in order to make the light-matter interaction strong, the transverse optical confinement must be significant—on the order of a few nm. Consider next a general expression for the electric field amplitude of an electromagnetic wave, with angular frequency ω and wave-number k, propagating in a waveguide (Fig. 5.1a)

$$\mathbf{E}_{\pm}(z,t) = \mathbf{E}_0 e^{-i(\omega t \mp kz)}, \tag{5.1}$$

where positive and negative k values correspond to waves travelling in the positive and negative z-directions respectively. Assuming no free charges, Maxwell's equations tell us that the

[1] It is important to note that the phenomena described here are often labelled as belonging to the field of 'chiral' quantum optics. However, as there are no non-trivial topologies involved, this is somewhat misleading and for the avoidance of confusion we will endeavour to not use this terminology. It is however conventional to refer to emitters coupled to waveguides in a unidirectional manner as being located at c-points and, for want of clearer nomenclature, we do adopt this custom.

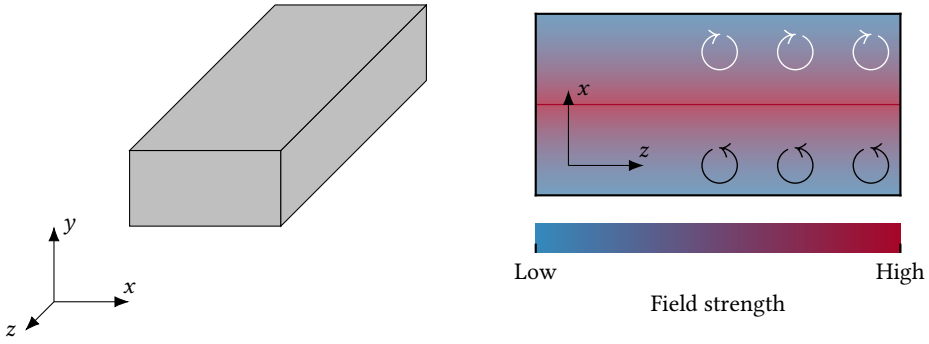

(a) Optical waveguide.

(b) Electric field distribution.

Figure 5.1: (a) Optical waveguide, which is effectively infinitely long in the propagation direction z but tightly confines light in the transverse xy-plane. (b) 2D slice through the $y = 0$ plane of the waveguide, showing the electric field intensity and assuming $E_y = 0$. Black and white arrows show that the sense of rotation of the field is reversed at either side of waveguide centre. This originates from the mirror symmetry of the system.

divergence of the electric field must vanish and in the limit where

$$\frac{\partial E_z}{\partial z} \ll \frac{\partial E_x}{\partial x}, \frac{\partial E_y}{\partial y} \tag{5.2}$$

this leads to an equation for the z-component of the electric field in terms of the transverse components

$$E_{\pm,z} = \mp \frac{i}{k}\left(\frac{\partial E_x}{\partial x} + \frac{\partial E_y}{\partial y}\right). \tag{5.3}$$

We see that, in clear contrast to the case of free space propagation, an electromagnetic wave propagating in a waveguide has a longitudinal component to its electric field vector. The size of this component is strongly dependent upon the gradient in the transverse fields and its direction is reversed for light propagating in opposite directions. Moreover we see, assuming some exponential decay function governing the behaviours of E_x and E_y, that E_z is $\pi/2$ radians out of phase with these transverse fields. This means that the electromagnetic field now carries orbital angular momentum, with the vector lying in the transverse plane. The direction of this vector is reversed when the propagation direction of the wave is reversed and this phenomenon is known as 'spin-momentum locking.' In the ideal case, at c-points in the waveguide, the magnitude of the longitudinal component of the electric field is sufficient to render the field circularly polarised, with the sense of rotation determined by the propagation direction, and we sketch this in Fig. 5.1b. The phenomenon of spin-momentum locking occurs spontaneously in nanobeam waveguides, as in Fig. 5.1, but can also be artificially engineered in photonic structures where the light-matter interaction is also enhanced [129].

At c-points in a waveguide structure, the spin of an electromagnetic wave is coupled to its propagation direction. For non-reciprocal transport it is then sufficient to have an emitter embedded at such a point, which couples preferentially to one of the two spin directions. Fortunately, this property is exhibited in one particular species of quantum emitter that is readily integrated into semiconductor waveguide structures; namely QDs formed via Stranski-Krastanov growth techniques. We do not discuss the details of epitaxial growth in this thesis but refer to e.g. the review of Ref. [130] and simply note that the QDs formed this way are hemispherical in shape but flattened in the growth axis, as illustrated in Fig. 5.2a. The strong confinement in all three

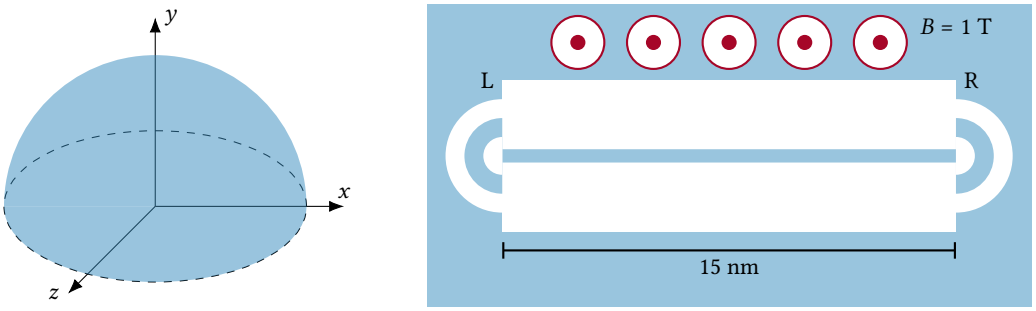

(a) Hemispherical QD.

(b) Nanobeam waveguide.

Figure 5.2: (a) An epitaxially grown QD typically has a hemispherical profile, symmetric in the growth axis y. Typical dimensions in this axis are of the order of 1 nm, while lateral confinement is usually closer to 10 nm. (b) Sketch of a nanobeam waveguide, which composed of GaAs (blue) and vacuum-clad (white). Left and right out-couplers are labelled and either scatter photons out of the sample to a detector or couple laser light into the nanobeam.

spatial dimensions leads to the emergence of discrete, atomic-like energy levels, which can be understood in basic terms as being related to those of the infinite potential well model [131].

There are many possible energy level configurations for a semiconductor QD, which may depend on its charge state. For example if a lone electron or hole is confined to the QD, then moving to the first excited state involves the formation of a negatively or positively charged 'trion.' For simplicity we consider the case where the QD is initially neutral, which means that the first excitation corresponds to the creation of a lone, bound electron-hole pair, a so called 'exciton.' A detailed description of the spin-properties of the neutral exciton can be found in e.g. Ref. [132] and we first note that the symmetry (growth) axis of the QD defines a fixed vector for one component of the total angular momentum. Furthermore, the lowest lying energy neutral exciton consists of a hole with total angular momentum $J = 3/2$ and electron with $J = 1/2$ and these combine to form 'bright' or 'dark' excitons with $J = 1$ and $J = 2$ respectively. The dark exciton is not optically active and we therefore neglect it, while the $J = 1$ exciton splits into the states with angular momentum projections $m_J = \pm 1$ onto the symmetry axis direction. In the case of a fully symmetric QD, these projections are degenerate but the degeneracy can be lifted via the application of a magnetic field along the growth axis—Zeeman splitting in the so-called 'Faraday' geometry. The splitting between these two states, which emit circularly polarised light with opposite senses of rotation, increases linearly as the strength of the magnetic field $\mathbf{B}$ is increased.

Supposing we have a QD located at a c-point in a waveguide and apply a Faraday geometry magnetic field to split the $m_J = \pm 1$ bright, neutral exciton states from one another, we have all the required ingredients to realise a unidirectional system. Imagine that we excite the QD from above, using a laser resonant with only one of the two spin states. The emitter will then be excited with definite spin and, due to the spin-momentum locking, can couple to an optical waveguide mode propagating only in one direction. Reversing the sign of the $\mathbf{B}$ field will change the spin state to which the laser couples and this in turn will reverse the direction of light propagation. This same experiment was realised by Coles et al. [133] and we go on to discuss an experimental implementation of a similar system in Sec. 5.3.

5.2 Elementary Model of Photon Scattering Experiments

Thinking in terms of the overall context of quantum information processing, it is not terribly useful to excite and collect the emission of a single QD from outside of the sample or 'off-chip.'

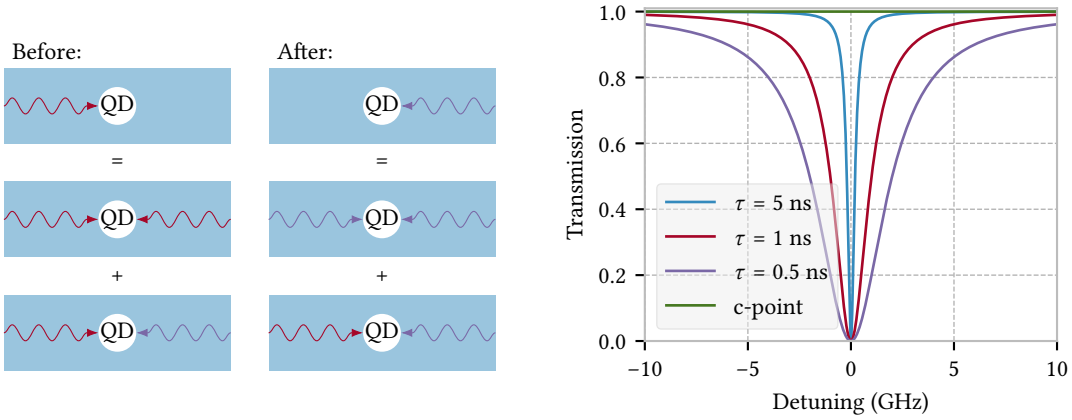

(a) Even-odd mode decomposition.

(b) Transmission spectra.

Figure 5.3: (a) Waves in phase are represented by red arrows and those in anti-phase are purple. The right-propagating mode is a sum of even and odd decompositions. The even mode picks up a π phase rotation, while the odd mode is unaffected and this means that, after scattering, the wave propagates to the left. (b) Transmission of a waveguide-coupled two-level-system as a function of single photon detuning from resonance. Spectra for various emitter lifetimes and for an emitter embedded at a c-point are shown.

We would ideally like a large network of sources, detectors and many QDs all connected within the sample or 'on-chip.' This motivates the set of experiments, which are based on the geometry of e.g. Fig. 4.1a, where a QD is probed indirectly by light injected into and detected from the mode of the waveguide to which it couples. It is important to understand, in the completely ideal case, what behaviour we would expect to observe in such a system. We can predict, using the tools detailed in Chapter 3, spectra for the light transmitted and reflected by waveguide-coupled QDs and departures from these overly-idealised predictions inform us about the dominant processes in real systems.

We already determined in Sec. 3.4.3 that if a single photon scatters from an emitter embedded in a waveguide at a c-point, the total intensity of the transmitted light is preserved. It is instructive to first understand why, even in a system free from experimental imperfection, a single photon may be totally reflected by a nanobeam-embedded QD. This occurs when the emitter is not embedded at a c-point in the waveguide and a very nice, intuitive explanation for this phenomenon can be found in the PhD thesis of Nysteen [134]. The right-propagating waveguide mode can be decomposed into a sum of 'odd' and 'even' bosonic modes. Consider the Hamiltonian of Eq. (3.49) that we used to derive the S-matrix for an emitter embedded at a c-point. In the case where the emitter couples to both left and right propagating modes at equal rates, this becomes

$$\begin{aligned} H &= \frac{1}{2}\Omega\sigma_z + \int \mathrm{d}\omega\ \omega(r_\omega^\dagger r_\omega + l_\omega^\dagger l_\omega) + g\int \mathrm{d}\omega\ \left(\sigma_+ r_\omega + r_\omega^\dagger\sigma_- + \sigma_+ l_\omega + l_\omega^\dagger\sigma_-\right) \\ &= \frac{1}{2}\Omega\sigma_z + \int \mathrm{d}\omega\ \omega(a_\omega^\dagger a_\omega + b_\omega^\dagger b_\omega) + \sqrt{2}g\int \mathrm{d}\omega\ (\sigma_+ a_\omega + a_\omega^\dagger\sigma_-), \end{aligned} \tag{5.4}$$

where l_ω and r_ω describe the left and right propagating modes respectively and we defined even, a_ω and odd, b_ω mode operators by

$$a_\omega \equiv \frac{r_\omega + l_\omega}{\sqrt{2}} \qquad \text{and} \qquad b_\omega \equiv \frac{r_\omega - l_\omega}{\sqrt{2}}. \tag{5.5}$$

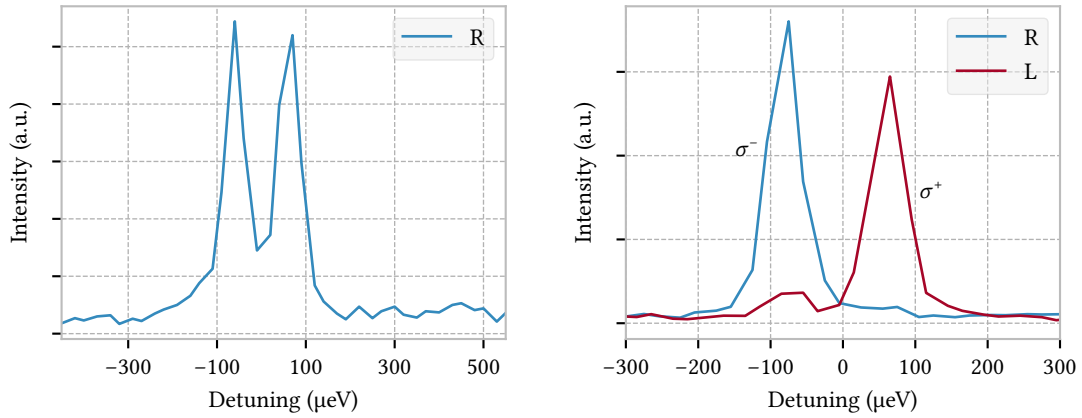

(a) Symmetric photoluminescence.

(b) Non-symmetric photoluminescence.

Figure 5.4: (a) Photoluminescence spectrum collected at the right out-coupler for a QD not located at a c-point in the nanobeam. Signals corresponding to both spin components are clearly visible, with comparable magnitude. (b) Photoluminescence spectra collected at both left and right out-couplers for a QD located at a c-point in the nanobeam. In both spectra we see a strong signal from one of the two spin components but not the other.

We see that the Hamiltonian of Eq. (5.4) can be decomposed into a sum of Hamiltonians for even and odd mode operators, with the odd operators not coupled to the emitter and the even operators coupled as in the c-point case (with an additional factor of $\sqrt{2}$ on the coupling-constant). We already determined that single photon states pick up a π phase rotation in the ideal c-point case and so the evolution of the mode operators under scattering is

$$r_\omega = \frac{a_\omega + b_\omega}{\sqrt{2}} \longrightarrow \frac{b_\omega - a_\omega}{\sqrt{2}} = -l_\omega, \tag{5.6}$$

meaning that the emitter behaves as a mirror. We sketch this process schematically in Fig. 5.3a and show some expected transmission spectra for ideal emitters in Fig. 5.3b.

5.3 Non-Reciprocal Transport of a Nanobeam-Coupled Quantum Dot

5.3.1 The Experiment

Armed with the expectations described in the previous section, we can begin to consider some real data and a number of experiments have been performed in Sheffield University laboratories on nanobeam-coupled QDs by C. Bentham, M.N. Makhonin and D.M. Price. Specifics regarding the sample used can be found in Ref. [135] and we only briefly outline the experimental details in this thesis. We sketch the sample in Fig. 5.2b and note that InGaAs QDs were grown via the Stranski-Krastanov method onto a GaAs substrate. A nanobeam waveguide, with two in/out-couplers, was etched onto this sample and it is through these that laser light was coupled into and out of the nanobeam. A magnetic field of 1 T was applied over the sample in the Faraday geometry, as discussed in Sec. 5.1, and additionally the sample was held in a bath cryostat at 4 K to minimise thermal noise.

A number of experiments were performed on several QDs coupled to the nanobeam and first it was necessary to locate a QD coupled at a c-point. This was done by exciting a QD from above with laser light and collecting the emission from one of the two out-couplers—a 'photoluminescence' experiment. As discussed in Sec. 5.1, if the QD was at a c-point then only the emission

from one of the spin components would arrive at each out-coupler. In the symmetric case, the spin and momentum of the electromagnetic field are not coupled and both components of the QD emission would be detected at both out-couplers. In Fig. 5.4a we show the photoluminescence signal at the right out-coupler for a typical QD not at a c-point and we see clear signals from both spin components, σ_+ and σ_-, which are split in energy by the applied **B**-field. This is in strong contrast with the photoluminescence spectra of Fig. 5.4b, where at each out-coupler we see signal for a different QD spin transition. The 'contrast' is defined by

$$C \equiv \frac{I^{\sigma_+} - I^{\sigma_-}}{I^{\sigma_+} + I^{\sigma_-}}, \tag{5.7}$$

where I^{σ} represents the intensity of photoluminescence signal for a given spin component, measures how strong the unidirectionality of a given QD is. The contrast $C_{\mathrm{R}} = -0.91$ at the right-hand out-coupler and $C_{\mathrm{L}} = 0.84$ at the left observed for the QD probed in Fig. 5.4b indicated it was located extremely close to a c-point in the nanobeam.

A weak laser was focussed onto one of the two out-couplers and the laser light collected from either the same or opposite coupler. A 're-pump' laser could be used to activate or deactivate the QD and hence the changes in transmission and reflection that the presence of the QD introduced could be measured. The 'differential' transmissions and reflections are defined by

$$\Delta T \equiv \frac{I^T_{\mathrm{on}} - I^T_{\mathrm{off}}}{I^T_{\mathrm{off}}} \qquad \text{and} \qquad \Delta R \equiv \frac{I^R_{\mathrm{on}} - I^R_{\mathrm{off}}}{I^T_{\mathrm{off}}}, \tag{5.8}$$

where e.g. I^T_{on} represents the transmitted laser intensity with the QD activated. We show the results of these measurements in Fig. 5.5 and this is the data that we aim to understand using a theoretical model of the system.

5.3.2 Analysis

Several contradictions between the predictions of the ideal model of Sec. 5.2 and the experimental data in Fig. 5.5 are immediately apparent. Firstly, in the transmission geometry experiments, we observe changes in the transmitted intensity of between 2% and 3% and not 0% as expected. We might be tempted to attribute this to the location of the QD slightly away from a c-point because, after all, 3% isn't terribly different from 0%. Another problem becomes apparent however and we see that the linewidths of the spectra are ~ 10 μeV, which corresponds to a QD lifetime of ~ 30 ps. This is two orders of magnitude below the expected value and we can only attribute this to broadening mechanisms not captured by our simple model.

Maybe more troubling than the transmission results however is the data collected in the reflection geometry. Consider a laser input to the right out-coupler and detected from the left (R⟶L) and suppose it couples with relative efficiency of ~95% to the σ^+ dipole, which is in turn coupled with ~5% efficiency to the L⟶R mode. By contrast, the σ^- dipole couples with relative efficiency of 5% to the R⟶L mode but 95% efficiency to the L⟶R mode. As a first-order approximation, the fraction of the laser reflected into the L⟶R mode is then ~ $(95\% \times 5\%)^2 \approx 0.2\%$ in *both* cases. We therefore expect parity between the signals observed in reflection geometry experiments for both spin components. This is also not the observed behaviour and motivates our construction of a more sophisticated model.

Input-Output Relations

Our calculation starts from the Hamiltonian describing a two-level system coupled to the right and left propagating modes of the waveguide

$$H = \int \mathrm{d}\epsilon\, \Delta_\epsilon \left(r^\dagger_\epsilon r_\epsilon + l^\dagger_\epsilon l_\epsilon \right) + \frac{1}{2}\Delta_\Omega \sigma_z + \int \mathrm{d}\epsilon \left(g_r r_\epsilon \sigma_+ + g_l l_\epsilon \sigma_+ + g_r r^\dagger_\epsilon \sigma_- + g_l l^\dagger_\epsilon \sigma_- \right). \tag{5.9}$$

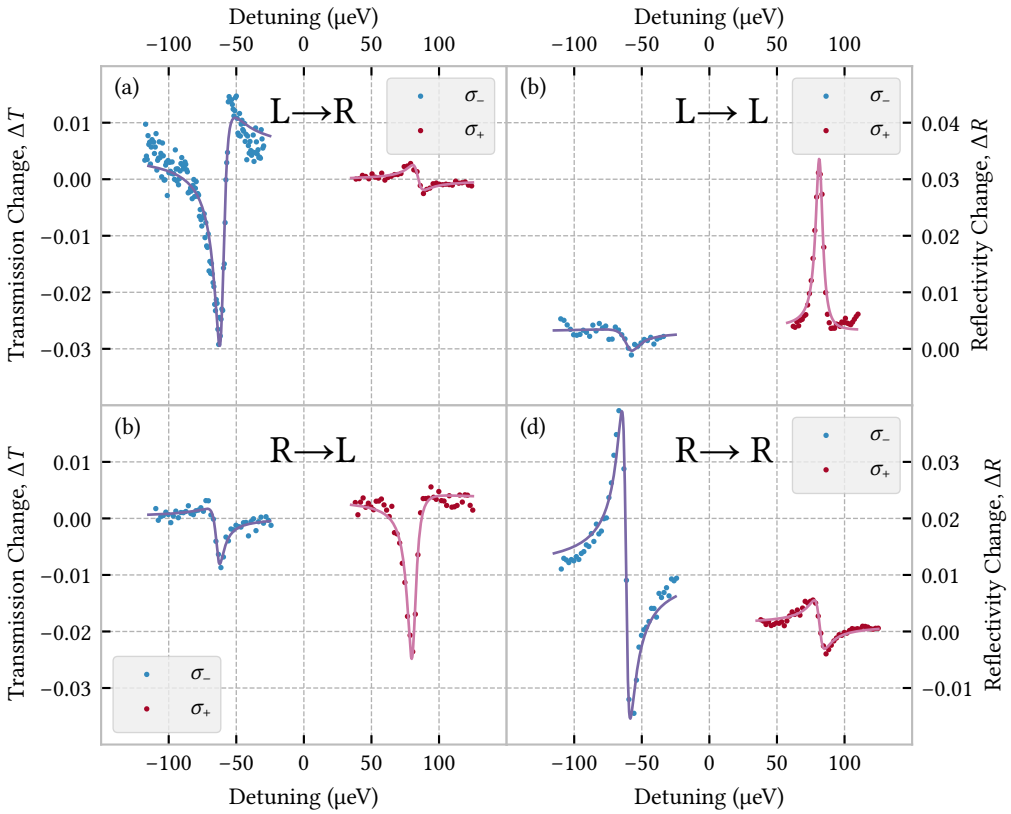

Figure 5.5: Differential transmission and reflection spectra for the QD with photoluminescence profile shown in Fig. 5.4b. Text on the plots refers to the propagation of the measured light and so e.g. (a) represents the experiment where the laser couples to the left out-coupler and is measured at the right and (b) gives the corresponding reflection experiment.

This is exactly the Hamiltonian described in Sec. 3.1 but we now take into account coupling at different rates to the left and right propagating waveguide modes, $g_l \neq g_r$. We also used the excitation number conserving property of the Hamiltonian, namely that $[H, N] = 0$, where $N \equiv \sigma_z/2 + \int \mathrm{d}\omega\, r_\omega^\dagger r_\omega + l_\omega^\dagger l_\omega$ to shift the zero energy by ω_0. The photon-drive detuning is given by Δ_ϵ and the emitter-drive detuning by Δ_Ω. From this Hamiltonian we can derive the coupled Heisenberg-Langevin equations for the system, e.g.

$$\dot{\sigma}_- = -i\Delta_\Omega \sigma_- + i\sigma_z \int \mathrm{d}\epsilon\ (g_r r_\epsilon + g_l l_\epsilon) \qquad \text{and} \qquad \dot{r}_\epsilon = -i\Delta_\epsilon r_\epsilon - i g_r \sigma_-, \tag{5.10}$$

which we approach using the Input-Output formalism in the same manner as in Chapter 3 so that

$$\dot{\sigma}_- = \left(-i\Delta_\Omega + \pi g_r^2 + \pi g_l^2\right)\sigma_- + i\sqrt{2\pi}\sigma_z\,(g_r r_{\mathrm{in}} + g_l l_{\mathrm{in}})\,, \tag{5.11}$$

where r_{in} (l_{in}) is the annihilation operator corresponding to the field propagating from the right (left) out-coupler.

We now follow the method of Ref. [136] and include a finite pure dephasing rate γ_d in our description and also emission into unguided modes at a rate γ. We note that this method produces the expected effect on our lowering operator, as we could have deduced from our discussion of radiative and non-radiative dephasing in Chapter 3,

$$\dot{\sigma}_- = \left(-i\Delta_\Omega + \pi g_r^2 + \pi g_l^2 + \gamma_\mathrm{d} + \frac{\gamma}{2}\right)\sigma_- + i\sqrt{2\pi}\sigma_z\,(g_r r_{\mathrm{in}} + g_l l_{\mathrm{in}})\,. \tag{5.12}$$

Making the notational contraction that $\tilde{\gamma} \equiv \gamma_\mathrm{d} + \gamma/2 + \pi g_r^2 + \pi g_l^2$, we can write down the full set of input-output relations for the system:

$$r_\mathrm{out} = r_\mathrm{in} - i\sqrt{\frac{\beta_\mathrm{d}\beta}{\tau}}\sigma_-, \qquad l_\mathrm{out} = l_\mathrm{in} - i\sqrt{\frac{(1-\beta_\mathrm{d})\beta}{\tau}}\sigma_-, \tag{5.13}$$

$$\dot{\sigma}_- = -(i\Delta_\Omega + \tilde{\gamma})\,\sigma_- + i\sigma_z\left(\sqrt{\frac{\beta_\mathrm{d}\beta}{\tau}}r_\mathrm{in} + \sqrt{\frac{(1-\beta_\mathrm{d})\beta}{\tau}}l_\mathrm{in}\right), \tag{5.14}$$

$$\dot{N} = -\frac{1}{\tau}N + i\left[\sqrt{\frac{\beta_\mathrm{d}\beta}{\tau}}\left(r_\mathrm{in}^\dagger\sigma_- - r_\mathrm{in}\sigma_+\right) + \sqrt{\frac{(1-\beta_\mathrm{d})\beta}{\tau}}\left(l_\mathrm{in}^\dagger\sigma_- - l_\mathrm{in}\sigma_+\right)\right], \tag{5.15}$$

where τ is the emitter lifetime. We characterised emission into unguided modes by the β-factor, which is defined by the rate of emission into the waveguide divided by the total emission rate, such that $\gamma = (1-\beta)/\tau$. We additionally defined the directional factor β_d, which captures the strength of non-reciprocal coupling in our system and is defined as the ratio of emission into the right photon modes to the total emission into all guided modes, $\beta_\mathrm{d} \equiv g_r^2/(g_r^2 + g_l^2)$.

In the steady state we can neglect time derivatives in the Heisenberg equations and therefore, by simple algebraic substitution, we arrive upon

$$r_\mathrm{out} = r_\mathrm{in} + \frac{\beta}{\tau\,(i\Delta_\Omega + \tilde{\gamma})}\left(\beta_\mathrm{d}r_\mathrm{in} + \sqrt{\beta_\mathrm{d}\,(1-\beta_\mathrm{d})}l_\mathrm{in}\right)\sigma_z \tag{5.16}$$

$$l_\mathrm{out} = l_\mathrm{in} + \frac{\beta}{\tau\,(i\Delta_\Omega + \tilde{\gamma})}\left(\sqrt{\beta_\mathrm{d}(1-\beta_\mathrm{d})}r_\mathrm{in} + (1-\beta_\mathrm{d})\,l_\mathrm{in}\right)\sigma_z, \tag{5.17}$$

meaning that the field output from the system is fully specified by the input field and the emitter population $N = (\sigma_z + 1)/2$. At this point we adopt the semi-classical hypothesis [137] and assume that the operators in the HL Eqs. (5.13)-(5.15) can be replaced by their expectation values. This yields

$$z = -1 + 2i\tau\sqrt{\frac{\beta_\mathrm{d}\beta}{\tau}}\,(\alpha^* s_- - \alpha s_-^*), \tag{5.18}$$

where we assumed that the emitter is driven from the right such that $l_\mathrm{in} = 0$ and we have substituted in the amplitude of the right input field α. We furthermore defined $s_- \equiv \langle\sigma_-\rangle$ and $z \equiv \langle\sigma_z\rangle$. Eliminating s_- from Eq. (5.18) we obtain

$$z = -\left(1 + \frac{4\beta\beta_\mathrm{d}\tilde{\gamma}|\alpha|^2}{\Delta_\Omega^2 + \tilde{\gamma}^2}\right)^{-1}, \tag{5.19}$$

and we can substitute this into Eqs. (5.16) and (5.17) to determine the left and right output field amplitudes in terms of the incident power. We then arrive upon an expression for e.g. the field transmitted by the system

$$\langle r_\mathrm{out}\rangle = \alpha\left[1 - \frac{\beta\beta_\mathrm{d}}{\tau\,(i\Delta_\Omega + \tilde{\gamma})\left(1 + \frac{4\beta\beta_\mathrm{d}\tilde{\gamma}|\alpha|^2}{\Delta_\Omega^2+\tilde{\gamma}^2}\right)}\right], \tag{5.20}$$

and define the transmission spectrum—highlighting its dependence on Ω, the QD central frequency—by

$$T(\Omega) \equiv \frac{|\langle r_\mathrm{out}\rangle|^2}{|\alpha|^2} = \left|1 - \frac{\beta\beta_\mathrm{d}}{\tau\,(i\Delta_\Omega + \tilde{\gamma})\left(1 + \frac{4\beta\beta_\mathrm{d}\tilde{\gamma}|\alpha|^2}{\Delta_\Omega^2+\tilde{\gamma}^2}\right)}\right|^2. \tag{5.21}$$

Of course, the same procedure can be carried out to find the reflected intensity by solving for l_out instead and defining $R(\Omega) \equiv |\langle l_\mathrm{out}\rangle|^2/|\langle\alpha\rangle|^2$.

Incoherent Emission

It is important to note that this description of the system is incomplete, as has been noted previously in e.g. Ref. [138]. This is a consequence of the increase in incoherent emission by the QD that accompanies an increase in its excitation. This incoherently emitted power is not captured by the Input-Output formalism and has to be added to the description via a conservation of energy argument

$$\mathscr{P}_{\text{incoh}} = \mathscr{P}_{\text{in}} - \mathscr{P}_{\text{trans}} - \mathscr{P}_{\text{refl}} - \mathscr{P}_{\text{scat}}. \tag{5.22}$$

The incoherently emitted power is the remainder, having subtracted the transmitted, reflected and scattered powers from the input power. There are then additional photons contributing to both the transmission and reflection spectra, with fluxes of $\beta\beta_{\text{d}}\mathscr{P}_{\text{incoh}}$ and $\beta(1-\beta_{\text{d}})\mathscr{P}_{\text{incoh}}$ respectively.

Spectral Wandering and Blinking

It turns out however that even this description of the system is not sufficient to capture all the dynamics and, in particular, the observed linewidths cannot be accounted for by coupling of the QD to external bosonic modes and pure dephasing alone, the rate of which can be measured [139]. In fact another broadening mechanism contributes extensively to the spectrum of a QD. Termed 'spectral wandering,' this is the process where charge fluctuations in the environment cause the central energy of the QD exciton to shift and is characterised by the long time-scales, relative to the exciton lifetime, on which it occurs [140].

In order to find the true spectrum then, as measured in experiment, we need to convolve Eq. (5.21) with a function characterising the charge noise around the QD and hence the spectral wandering. This procedure has been described previously in e.g. Ref. [141]. Note that we perform this procedure on the expression we derive for the transmitted *intensity* and not the amplitude. As, by definition, spectral wandering occurs over time-scales longer than the emitter lifetime. If we assume the charge noise profile causes the central frequency of the QD to fluctuate according to a Gaussian distribution with variance σ we have that

$$T(\Omega,\sigma) = \frac{1}{\sqrt{2\pi\sigma^2}}\int \mathrm{d}\varepsilon\, \exp\left(-\frac{\varepsilon^2}{2\sigma^2}\right) T(\Omega+\epsilon) \tag{5.23}$$

and also an analogous expression for the reflected intensity.

Finally, we need to account for so-called 'spectral blinking'. The semiconductor QDs we analyse here are well-approximated as a two-level-system but this does not capture entirely their relevant energy level structure. A photon arriving at the location of the QD therefore has a finite probability P_{dark} of finding the system in some optically inactive 'dark state.' This naturally implies that

$$T(\Omega,\sigma) \longrightarrow P_{\text{dark}} + (1-P_{\text{dark}})T(\Omega,\sigma). \tag{5.24}$$

Note that an optically inactive QD would lead to zero reflected intensity and so we include blinking instead via

$$R(\Omega,\sigma) \longrightarrow (1-P_{\text{dark}})R(\Omega,\sigma). \tag{5.25}$$

In order to model our system, we then simply have to integrate Eq. (5.21) according to Eq. (5.23) and account for blinking via the prescription of Eq. (5.24).

Parameter	Symbol	Value
β-factor	β	0.7
Directionality	β_{d}	0.95
Radiative lifetime	τ	1 ns
Dephasing time	τ_{d}	0.8 ns
Spectral wandering variance	σ	4 μeV
Dark probability	P_{dark}	0.25

Table 5.1: Parameters used in the theoretical model.

5.3.3 Experimental Parameters

Our task is not complete however because we notice that our model has many free parameters and we do not have a good way to extract them individually from the data. For example, the widths of the observed spectra are determined by: the QD lifetime, the pure dephasing rate and the spectral wandering variance. It is in theory possible to measure these quantities individually but this was not done and therefore a first-principles fitting of the model to experiment is not possible. Furthermore, for reasons that we will discuss in Sec. 5.4.2, even though we know the origin of the asymmetric lineshapes observed (Sec. 3.3), it is difficult to model these quantitatively for this system. Therefore we deduce any parameters we can from the available data and turn to the extensive background literature for those that remain. This gives us an understanding for the order of magnitude of the effects we should expect to observe and will allow us to explain e.g. the asymmetric reflection profiles for anti-parallel dipoles.

We summarise the parameters that we arrive upon in Table. 5.1. The coupling between the QD and a nanobeam waveguide is deduced from FDTD simulations [142] and the directionality, β_{d}, from the contrast ratio, C, defined in Eq. (5.7). The radiative lifetime of 1 ns is typical for InGaAs self-assembled QDs [143], as is the 800 ps pure dephasing time [144, 145][2]. The spectral wandering is characterised by the parameter σ, the variance of the distribution, with σ = 4 μeV giving a good fit to the measured 8 μeV QD linewidth. It is not possible to obtain a direct experimental estimate of P_{dark} but previously reported values (see Sec. 5.4.2) fall within the range $0 \leq P_{\mathrm{dark}} \leq 0.5$ and so we use $P_{\mathrm{dark}} = 0.25$ as a reasonable estimate. A key final parameter, which may appear pre-determined but is in fact not, is the amplitude of the optical field, α. This is because α is the power within the waveguide after unknown coupling losses and is therefore some unknown fraction of the laser power set experimentally. We will see that understanding the power dependence of the system is crucial for understanding the asymmetric reflection geometry results and therefore model the system for a range of input powers.

5.3.4 Results

The transmission spectra, calculated using the parameters of Table 5.1 are shown in Fig. 5.6a. The central energy of the QD is set at 1.3 eV, and the splitting between the low and high energy Zeeman components is 0.16 meV (as in the experimental data in Figs 5.4b), with the higher frequency component having the stronger coupling. This is equivalent to the experimental L⟶R and L⟶L geometries shown in Figs. 5.5(c) and 5.5(d). The transmission dips are asymmetric, with a stronger dip for the component preferentially coupled to the QD, in agreement with the experimental data. The depth of the dips are close to those observed in Fig. 5.5, a maximum of 4% experimentally and 5% in the model, showing that the parameters used in the model are a reasonable approximation to the real system. We furthermore note that the size of the stronger

[2]The pure dephasing time is highly variable and dependent on many factors. It may be as low as ~10 ps or as high as ~5 ns. Our value is expected to be on the upper end of this range, due to the resonant excitation employed in the experiment. Specifically τ_{d} = 800 ps was measured exactly on a QD in a similar sample.

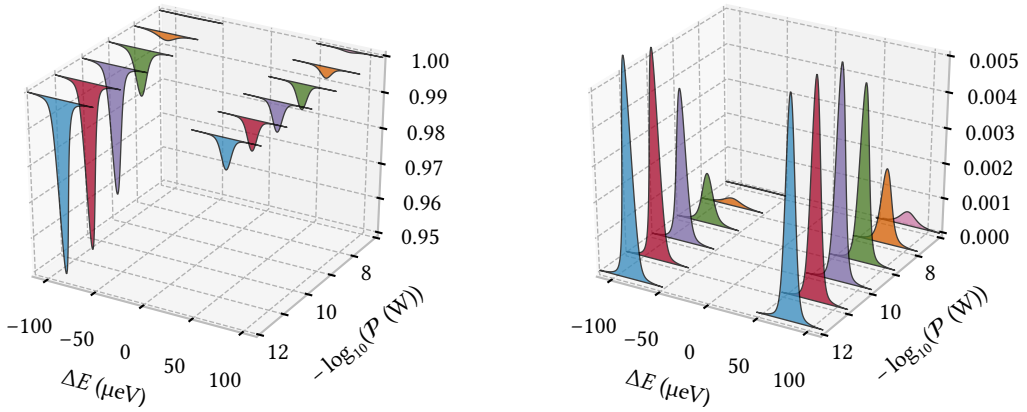

(a) Transmission geometry.

(b) Reflection geometry.

Figure 5.6: (a) Calculated transmission and (b) reflection of the system for incident L⟶R laser driving. Powers of 1, 10 and 100 pW are represented by blue, red and purple curves respectively, with 1, 10 and 100 nW shown in green, orange and pink. The saturation data in the inset of Fig. 5.7a indicates that the experimental conditions correspond to a power between 100 pW and 1 nW in the model.

dip is strongly dependent on the input power, which indicates that the system is saturated at powers of the order of 1 nW impinging on the QD.

In order to obtain a more thorough comparison of experiment and theory, we need to relate the power levels used in the model to those for the measured spectra. We can calibrate the external power relative to that within the waveguide by analysing the predicted power dependence of the stronger transmission dip and comparing with experiment. In the main part of Fig. 5.7a, we plot the power saturation dependence predicted by the model and show as an inset the experimentally determined power dependence. At low powers, below 10 pW, the main part of Fig. 5.7a confirms that the magnitude of the transmission dip is independent of incident laser power; fewer than one photon is interacting with the QD within its lifetime. As the power is increased up to 10 nW, the magnitude of the dip decreases as the QD can only interact with a certain fraction of the input light. At powers above 10 nW, the QD scatters an insignificant fraction of the incident photon flux and the fully saturated regime is entered. Experimentally we see very little reduction in transmission dip between 5 and 20nW and a marked reduction in transmission dip thereafter. By comparing points with the same 30% reduction in transmission dip and cross-correlating, we are able to deduce that the power of 50 nW incident on the sample corresponds to a power of between 100 pW and 1 nW within the waveguide. Having semiquantitatively calibrated the power, and returning to the theory curves of Fig. 5.6a, we see that in this power range (represented by the purple and green curves), the low frequency component still dominates in transmission, but the reflectivity has developed an asymmetry, with the higher frequency component being the stronger.

What's happening here is that the high powers used in the experiment are causing the QD transition to saturate in a directionally dependent fashion. As an illustrative example, consider the case discussed previously, where the R⟶L mode couples with relative efficiency of ~95% to the σ^+ dipole and ~5% efficiency to the σ_- dipole. In the low power regime, we would expect the reflection signal from both spin components to be equally strong and this is the behaviour shown in Fig. 5.6b. However, as we increase the power incident on the QD, the well coupled transition saturates more quickly, cannot absorb more photons from the laser field and its reflection signal subsequently decays. By contrast, the σ_- dipole has its poor coupling to the laser

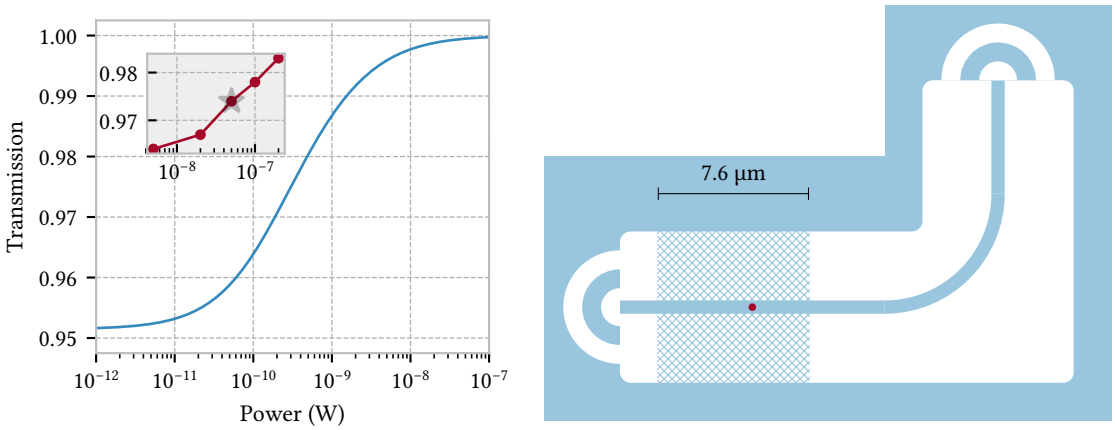

(a) Power dependence.

(b) Photonic crystal sample.

Figure 5.7: (a) Theoretical power dependence of the main transmission dip on resonance for the preferentially coupled component. Inset: the experimentally measured dependence. The power employed for the resonant transmission and reflection experiments shown in Fig. 5.5 is indicated by the grey star marker. (b) Sketch of the sample as in Fig. 5.2b but where the blue, hatched region indicates a photonic-crystal section. The red dot shows the approximate location of the QD.

field compensated for by the increasing photon flux and its relative signal increases in strength, again shown in Fig. 5.6b. This behaviour continues until, at higher powers still, the fraction of incident photons interacting with the QD becomes negligible.

5.4 A Photonic Crystal-Coupled Quantum Dot

In the previous experiment it was hard to obtain a good comparison between theory and experiment, with the model only qualitatively reproducing the experimental data. There are several reasons for this, including: a) the number of free parameters not known to us, b) the inability of our model to capture asymmetric lineshapes and c) the modest magnitudes of the transmission and reflection features. This motivates our analysis of a second experiment, in which some of these difficulties are overcome. In particular, we now analyse a similar system where the QD is coupled to a waveguide but not at a c-point. This means that the magnitude of the observed features is larger and lower powers are employed in performing the experiments. In turn, this means that we can treat the effect that the QD has on the input field as linear and we will show that this leads to a simple way to recover the asymmetric lineshapes.

5.4.1 The Experiment

The experiments were performed by A. Foster and D. Hallett on a sample not dissimilar to that of the nanobeam in the previous section, with the key difference being that the QD was located in a region of 'photonic crystal' [146]. In these structures, holes are etched around the waveguide, which have the effect of lowering the group velocity of light in the waveguide and increasing the effective light-matter interaction. We sketch the sample in Fig. 5.7b and note that, as the QD was not located at a c-point, no **B**-field was applied. The entire sample was embedded inside a diode structure, allowing a controllable electric field to be placed over the QD. This field was used to alter the energy of the QD, via the Stark effect [147] and this provided a convenient way to change the laser-emitter detuning, while keeping the laser frequency fixed.

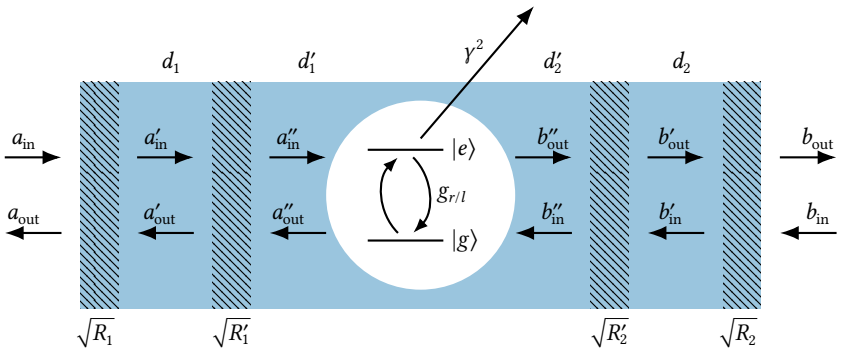

Figure 5.8: Dynamics of the combined waveguide, photonic crystal and QD system. Annihilation operators for the fields input to the left and right sides of the waveguide are given by a_{in} and b_{in} respectively and we have also indicated partially reflecting elements by their amplitude reflectivities $\sqrt{R}$.

5.4.2 Analysis

Our starting point is once again the input-output relations in Eqs. (5.13)-(5.15) but, as the powers used in the experiment are much smaller, we can make an approximation and solve them in a different way. Specifically, we know that no saturation of the QD transition was observed in experiment, with the magnitude of the measured features independent of laser power in the range of utilised powers. This means that we can make the 'weak-excitation' approximation and set $\sigma_z = -1$. In this case we find that

$$\sigma_- = -\frac{i}{(i\Delta_\Omega + \tilde{\gamma})}\left(\sqrt{\frac{\beta_{\text{d}}\beta}{\tau}}r_{\text{in}} + \sqrt{\frac{(1-\beta_{\text{d}})\beta}{\tau}}l_{\text{in}}\right) \tag{5.26}$$

and substitute this directly into the expressions for the output fields, finding

$$r_{\text{out}} = r_{\text{in}} - \frac{1}{(i\Delta_\Omega + \tilde{\gamma})}\left(\frac{\beta_{\text{d}}\beta}{\tau}r_{\text{in}} + \frac{\beta}{\tau}\sqrt{(1-\beta_{\text{d}})\beta_{\text{d}}}l_{\text{in}}\right). \tag{5.27}$$

The key observation here is that the output field in Eq. (5.27) depends only linearly upon the input fields and this means that we can apply the transfer matrix technique, developed in Ref. [148], to analyse the combined waveguide-QD system. Incorporating the reflections that take place at interfaces between surfaces of different refractive index, we would expect to reproduce the observed asymmetric lineshapes.

We sketch the system in Fig. 5.8 and have a section of nanobeam waveguide of length d_1 that takes light from an input coupler, with reflectivity R_1, to the boundary of a photonic crystal. A distance d_1' from this boundary resides the QD and a further section of crystal with length d_2' separates this from a second section of waveguide. This waveguide has length d_2 and joins an output coupler of reflectivity R_2. It is important to note that a refractive index mismatch means that reflections occur at the boundaries between the first section of nanobeam waveguide and photonic crystal and also where the crystal rejoins the waveguide, we denote these reflectivities by R_1' and R_2' respectively.

When the transformation between input and output fields is linear, we can describe it in terms of a transfer matrix. Specifically this matrix relates the fields on one side of an optical element to those on the other and is therefore often used for the purposes of imposing boundary conditions [149]. In the case of Fig. 5.8 we have for instance that

$$\begin{pmatrix} a_{\text{in}}' \\ a_{\text{out}}' \end{pmatrix} = T_{\text{refl}}(R_1)\begin{pmatrix} a_{\text{in}} \\ a_{\text{out}} \end{pmatrix}, \tag{5.28}$$

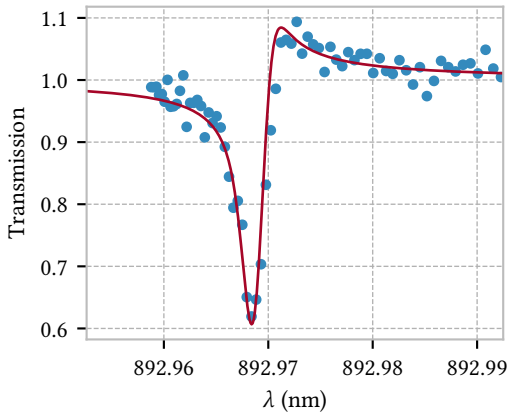

Figure 5.9: Transmission spectra for the photonic-crystal-coupled QD. Data is shown as blue points and the fitted model with a red line.

where $T_{\text{refl}}(R)$ is the transfer matrix associated with a partially reflecting mirror of reflectivity R. These matrices combine in sequence so that

$$\begin{pmatrix} b_{\text{out}} \\ b_{\text{in}} \end{pmatrix} = T_{\text{total}} \begin{pmatrix} a_{\text{in}} \\ a_{\text{out}} \end{pmatrix}, \tag{5.29}$$

$$T_{\text{total}} \equiv T_{\text{refl}}(R_2)T_{\text{phase}}(d_2)T_{\text{refl}}(R_2')T_{\text{phase}}(d_2')T_{\text{QD}}\,T_{\text{phase}}(d_1')T_{\text{refl}}(R_1')T_{\text{phase}}(d_1)T_{\text{refl}}(R_1), \tag{5.30}$$

with T_{QD} and $T_{\text{phase}}(d)$ representing transfer matrices associated with the QD and phase shifting elements of length d respectively. The matrices for reflecting and phase-shifting elements are well known

$$T_{\text{phase}} = \begin{pmatrix} e^{i\delta} & 0 \\ 0 & e^{-i\delta} \end{pmatrix}, \qquad T_{\text{refl}} = \frac{1}{i\sqrt{1-r^2}} \begin{pmatrix} -1 & -r \\ r & 1 \end{pmatrix} \tag{5.31}$$

and we can find T_{QD} from Eq. (5.27) and its reflected field counterpart. We then have, courtesy of Eq. (5.29), an expression relating the fields input to and output from the combined waveguide emitter system and we implement a solution in the Mathematica software package.

We account for spectral wandering and blinking of the QD in exactly the same manner as for the experiment in Sec. 5.3 but there is one additional factor to consider before our problem is totally solved. We find that including partially reflecting elements in the model causes it to predict a strong dependence of the transmission spectrum on the exact position of the QD within the photonic crystal. We therefore need to account for the fact that the specific position of the exciton within the QD is not well defined. We model this using a rectangular probability distribution, in which we might find the exciton responsible for the $|g\rangle \longrightarrow |e\rangle$ transition. The probability of finding the exciton at some position x is then described by the probability distribution function

$$p(x) = \begin{cases} \frac{1}{L} & x_{\text{cent}} - \frac{L}{2} \leq x \leq x_{\text{cent}} + \frac{L}{2} \\ 0 & \text{otherwise} \end{cases}, \tag{5.32}$$

where the length of the QD centered at position x_{cent} is given by L. We then simply average the field amplitude over the continuum of possible exciton locations before computing the transmitted intensity.

Parameter	Symbol	Value	Notes
β-factor	β	0.9	Typical value in literature, e.g. [150].
Directionality	β_d	0.5	C-points weak in photonic crystals [151].
Radiative lifetime	τ	440 ± 3 ps	Measured directly, pulsed excitation.
Dephasing time	τ_d	2.8 ± 0.7 ns	Measured using Michelson interferometry.
Spectral wandering	σ	1.2 ± 0.12 μeV	Inferred from spectral line width.
Dark probability	P_{dark}	0.09 ± 0.01	Fit parameter.
QD size	L	10 nm	Typical value, e.g. [152].
Reflectivity	R_1/R_2	20%	From FDTD simulation.
Reflectivity	R_1'/R_2'	10%	From FDTD simulation.
Nanobeam length	d_1 & d_2	5 & 17.9 μm	By sample design, electron lithography.
QD position	d_1'	5.11 ± 0.01 μm	Fit parameter. Note $d_1' + d_2' = 7.6$ μm.

Table 5.2: Parameters used in the theoretical model for the photonic-crystal-coupled QD.

5.4.3 Results

In this experiment, many more the parameters were measured and this made a fit of the model to the data possible. We summarise the parameters used in Table. 5.2 and note that the lifetimes and spectral wandering of the QD were directly measured. The beta factors and reflectivities of the boundaries were deduced via FDTD simulation and the lengths of nanobeam waveguide were found from scanning-electron-microscopy images of the sample. Andrew Foster then used a least-squares method to fit the Fano-lineshape of the model to that of the data by varying the location of the QD in the photonic crystal and the overall magnitude of the transmission dip by varying P_{dark}. The model with these parameters inserted is shown in Fig. 5.9 along with the experimental data.

This result is state-of-the-art and one of the highest magnitude transmission dips to have been observed experimentally but it is still many orders of magnitude away from ideal. Even employing error-correcting codes, a quantum computer still requires a physical qubit with an error-rate of ~ 1% or better [153]. We might note also that, even neglecting spectral wandering, the maximum phase shift we could hope to observe for a photon transported in the system described in Sec. 5.3 can be calculated and is ~ 0.4 rads, again far from the ideal case of π rads. The predominance of decoherence processes is characteristic of solid-state systems, where the qubit is embedded inside an environment that is hard to control. Alternative solid-state systems, such as SiV [154] or GeV [155] centres suffer from slightly weakened decoherence and this can be attributed, at least in part, to the lower number of nuclear spins in the environment of the qubit.

5.5 Summary

In summary we have explained the origin of non-reciprocal transport in one particular quantum optics system and applied the Input-Output Formalism in order to understand why the behaviour in experimental systems deviates from that in our idealised models. We have found that, even in state of the art experiments, the features we observe in real spectra are only half as strong as we would predict in the absence of noise processes. This means that current experimental implementations are dominated by imperfections and subsequent decoherence processes. At the present time, semiconductor QDs would appear to not be a good physical qubit candidate. In the next chapter we will start to probe this more deeply and look at how we might overcome one particular imperfection for the purposes of quantum information processing.

Chapter 6

Entangling Imperfect Emitters

In this final chapter we aim to relate the work of the previous two chapters to the grand goal of quantum technologies discussed at the outset of this thesis. We want to combine the theoretical understanding we have gained of on-chip light-matter interactions with what we now know about the realities of experimental systems. Entanglement, as a uniquely quantum phenomenon and resource for quantum technologies [156], forms an ideal platform for such an investigation. We want to determine the effect that imperfections in solid-state emitters have on our ability to entangle them. In particular we are going to derive strategies for overcoming spectral mismatch between emitters in an entanglement generation protocol.

6.1 Introduction

There are many potential architectures for quantum technologies but none are free from drawbacks. For example, superconducting circuit implementations enjoy excellent coherence properties but operate slowly [157], while trapped ion qubits can be prepared with almost unit fidelity but are difficult to scale [158]. In the previous chapter we saw that solid-state systems can operate quickly, at the GHz rate, but also suffer from charge-noise and phonon-induced dephasing processes. Another major drawback to solid-state emitters is that the central energies and lifetimes of their transitions are highly dependent on the fabrication process and vary significantly both across and within samples [159]. Known methods for deterministically entangling solid-state qubits require emitters with identical energies to facilitate path-erasure techniques [160]. This adds a practically insurmountable overhead to the process of matching multiple solid-state qubits for creating large entangled states. Stark shifting and strain tuning the emitter transitions has been employed to tune solid-state emitters onto resonance [161] but this adds a substantial technical difficulty and arbitrary emitters in a sample cannot in general be tuned onto resonance. We can overcome this difficulty if we are prepared to generate entanglement probabilistically [162, 163] and wait for a given detector signature. Here however, we propose a process for generating entanglement deterministically that is robust against spectral variations in the emitters' transition energies and line-widths.

Our setup is shown in Fig. 6.1a. Two solid-state emitters each have an L-type level structure with stable low-lying spin states, $|\uparrow\rangle$ and $|\downarrow\rangle$, and a dipole transition that couples one spin state (nominally $|\uparrow\rangle$) to an excited level $|e\rangle$[1]. The emitters are coupled to the waveguides at c-points

[1]Such a set-up can be realised using semiconductor QDs charged with single electrons. The spin of this electron forms the qubit states $|\uparrow\rangle$ and $|\downarrow\rangle$, with excited states corresponding to the trions $|\uparrow\downarrow\Uparrow\rangle$ and $|\downarrow\uparrow\Downarrow\rangle$ respectively. Single arrows represent electron spin directions, which we determined via the Pauli exclusion principle [164], and the double arrows represent hole spins, which carry 3/2 units of angular momentum as opposed to the 1/2 unit for electrons [165]. Each transition then involves the transfer of either +1 or −1 unit of angular momentum and therefore, provided the QDs are embedded at c-points as discussed in Chapter 5, light propagating in one direction will only interact with one of the two transitions.

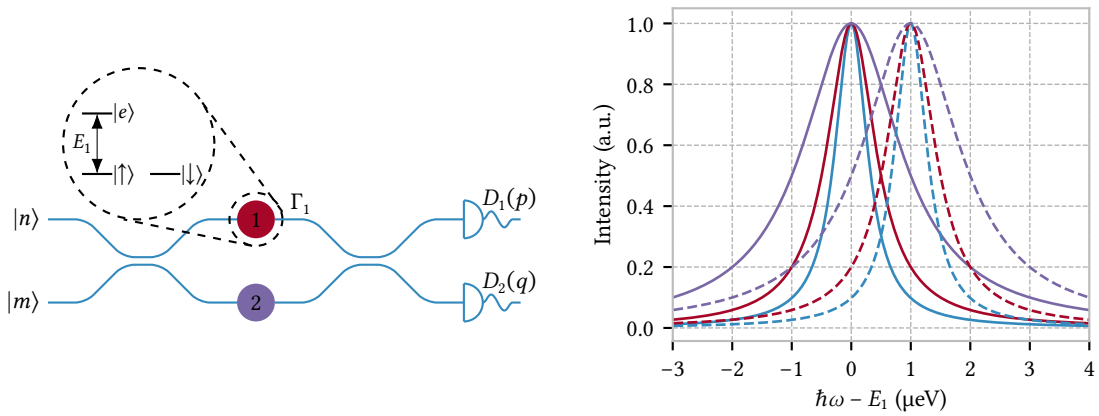

(a) Mach-Zehnder interferometer.

(b) Emitter spectra.

Figure 6.1: (a) Waveguide Mach-Zehnder interferometer with emitters embedded at positions 1 and 2, having L-type level structures. The excited state $|e\rangle$ is coupled to the spin qubit state $|\uparrow\rangle$ with transition energy E_α ($\alpha = 1, 2$) and line-width Γ_α. The emitters are placed off-axis in the waveguide at c-points, such that circularly polarised light scatters only in the forward direction. The loss rate from the guided mode is γ_α. Fock states $|n, m\rangle$ are injected into the interferometer, and photon number detectors D_1 and D_2 record the signature (p, q). (b) Lorentzian spectra for emitters with energies E_1 (solid), E_2 (dashed), and emitter line-widths 0.66 μeV (blue), 1.0 μeV (red), and 2.0 μeV (purple). $E_2 = E_1 + \delta$, where $\delta = 1$ μeV.

and initially prepared in the product state

$$|\phi_{\text{at}}^{\text{in}}\rangle = |\phi_1^{\text{in}}\rangle \otimes |\phi_2^{\text{in}}\rangle = \frac{1}{2}(|\uparrow\rangle + |\downarrow\rangle) \otimes (|\uparrow\rangle + |\downarrow\rangle) \equiv \frac{1}{2}\left(|\uparrow\uparrow\rangle + |\uparrow\downarrow\rangle + |\downarrow\uparrow\rangle + |\downarrow\downarrow\rangle\right). \tag{6.1}$$

The transition energies and linewidths for emitters $\alpha = 1, 2$ are labelled as E_α and Γ_α respectively. We input the two-mode Fock state $|n, m\rangle$ to the interferometer and the detectors D_1 and D_2 produce the classical signature (p, q), indicating the presence of p and q photons at each location.

It is relatively easy, in the ideal case, to understand how we might create entanglement in this system. Assuming the emitters are identical, a single monochromatic resonant photon can be injected into one of the input arms, $|n, m\rangle = |1, 0\rangle$, and will evolve through the first beam-splitter to [166]

$$|1, 0\rangle \longrightarrow \frac{1}{\sqrt{2}}(|1, 0\rangle + |0, 1\rangle) \equiv |\psi_{\text{opt}}\rangle, \tag{6.2}$$

where the state $|1, 0\rangle$ has one photon in the upper interferometer arm, vacuum in the lower and the $|0, 1\rangle$ state has the opposite. The photon then scatters from the embedded emitters, induces a π radian phase shift as discussed in Chapter 4, and the total system state evolves to become light-matter entangled

$$|\psi_{\text{opt}}\rangle|\phi_{\text{at}}^{\text{in}}\rangle \longrightarrow \frac{1}{2\sqrt{2}}\left[|1, 0\rangle\left(-|\uparrow\uparrow\rangle - |\uparrow\downarrow\rangle + |\downarrow\uparrow\rangle + |\downarrow\downarrow\rangle\right) + |0, 1\rangle\left(-|\uparrow\uparrow\rangle + |\uparrow\downarrow\rangle - |\downarrow\uparrow\rangle + |\downarrow\downarrow\rangle\right)\right]. \tag{6.3}$$

The second beam-splitter then erases the 'which-path' information for the photon and the state prior to detection is

$$|\Psi\rangle = \frac{1}{2}\left[|1, 0\rangle\left(|\downarrow\uparrow\rangle - |\uparrow\downarrow\rangle\right) + |0, 1\rangle\left(|\downarrow\downarrow\rangle - |\uparrow\uparrow\rangle\right)\right] \tag{6.4}$$

so that at a signal or 'click' at D_1 or D_2 projects the atomic state onto

$$|\Psi^-\rangle = \frac{1}{\sqrt{2}}\left(|\downarrow\uparrow\rangle - |\uparrow\downarrow\rangle\right) \qquad \text{or} \qquad |\Phi^-\rangle = \frac{1}{\sqrt{2}}\left(|\downarrow\downarrow\rangle - |\uparrow\uparrow\rangle\right) \tag{6.5}$$

respectively. Note that $|\Psi^-\rangle$ and $|\Phi^-\rangle$ are actually 'Bell States,' which are maximally entangled [167]. Mahmoodian *et al.* showed that, for sufficiently identical emitters, this procedure can be made robust to photon loss and potentially used to generate cluster states [168] for quantum information processing [169].

6.2 Single Photon Performance

In practice, both the line-widths and transition energies vary significantly between solid-state emitters and it is also hard to couple emitters perfectly to optical waveguides. In this case the single-photon transmission coefficient derived in Chapter 4 must be modified according to the prescription of Ref. [170] so that

$$t_\alpha(\omega) = \frac{\hbar\omega - E_\alpha - i\hbar(\Gamma_\alpha - \gamma_\alpha)/2}{\hbar\omega - E_\alpha + i\hbar(\Gamma_\alpha + \gamma_\alpha)/2}. \tag{6.6}$$

In Eq. (6.6) $\hbar\omega$ gives the single-photon energy, γ_α the coupling between emitter α and non-guided optical modes. We characterise this emitter loss by the beta-factor, $\beta_\alpha \equiv \Gamma_\alpha/(\Gamma_\alpha + \gamma_\alpha)$. For non-zero emitter detuning, $\delta \equiv E_2 - E_1$, a photon cannot be resonant with both emitters simultaneously and the phase shift induced is not π radians in both cases. The setup then does not create maximally entangled states deterministically.

In order to understand the impact of emitter detuning and loss on the protocol, we need to quantify the effect they have on the entanglement generated. To this end we use the concurrence, $\mathscr{C}(\rho)$ for a two-qubit state ρ as described in Chapter 2. Specifically we define the *average* concurrence as

$$\mathscr{C}_{\text{avg}} \equiv \sum_{(p,q)} \Pr(p,q)\,\mathscr{C}\left(\rho_{(p,q)}\right), \tag{6.7}$$

where each possible detector signature (p, q) occurs with probability $\Pr(p, q)$ and results in an emitter state $\rho_{(p,q)}$. This is an appropriate figure of merit, since it provides a lower bound for the amount of entanglement expected from a given experiment without post-selection. The entanglement in the two-qubit state can be increased by discarding measurement outcomes corresponding to below-average concurrences, which comes at the expense of entanglement generation rate.

6.2.1 Monochromatic

We first quantify the impact of finite emitter detuning δ on the monochromatic single photon protocol outlined in the previous section. In this case we replace the π phase shifts used to find the evolution in Eq. (6.3) with the transmission coefficients from Eq. (6.6) and this means that the pre-detector state becomes

$$\begin{aligned}|\Psi\rangle = \frac{1}{4}\Big[&|1,0\rangle\left((t_1(\omega) - t_2(\omega))\,|\uparrow\uparrow\rangle + (t_1(\omega) - 1)\,|\uparrow\downarrow\rangle + (1 - t_2(\omega))\,|\downarrow\uparrow\rangle\right) \\ &+ |0,1\rangle\left((t_1(\omega) + t_2(\omega))\,|\uparrow\uparrow\rangle + (t_1(\omega) + 1)\,|\uparrow\downarrow\rangle + (1 + t_2(\omega))\,|\downarrow\uparrow\rangle + 2\,|\downarrow\downarrow\rangle\right)\Big],\end{aligned} \tag{6.8}$$

where ω gives the frequency of the photon we inject. We note that the state in Eq. (6.8) is not normalised because some photons are lost to the environment. We can determine the probability of each detector clicking by projecting onto the relevant optical sub-state and finding the magnitude of the resulting atomic state. The corresponding concurrence is then determined by

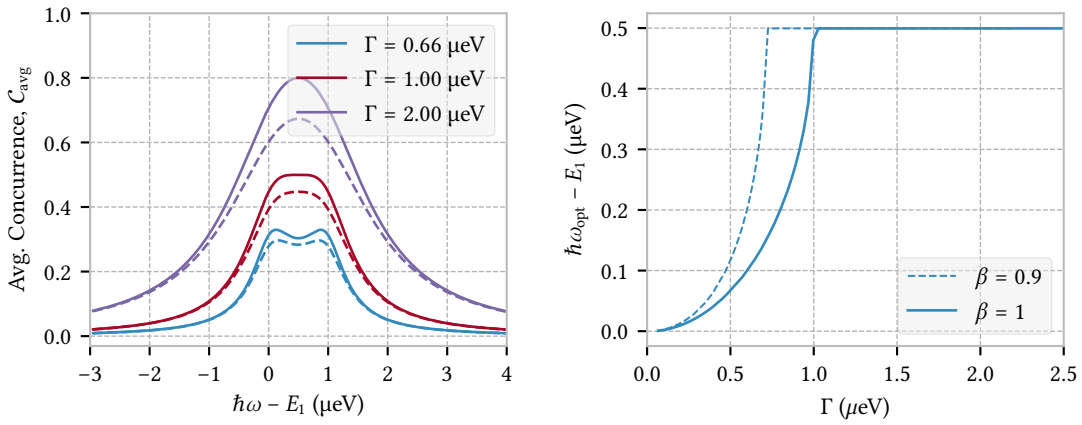

(a) Monochromatic photon input.

(b) Optimal energy.

Figure 6.2: Single-photon, $|n, m\rangle = |1, 0\rangle$, entanglement generation for a pair of detuned L-type emitters with equal linewidth Γ and energies E_1 and $E_2 = E_1 + \delta$, where $\delta = 1.0$ μeV. (a) $\mathscr{C}_{\text{avg}}$ versus monochromatic single-photon energy without loss ($\beta = \beta_1 = \beta_2 = 1$, solid) and with loss ($\beta = 0.9$, dashed). (b) Location of optimal input photon frequency for maximum $\mathscr{C}_{\text{avg}}$ as a function of emitter linewidth.

normalising the atomic state and using the formula of Eq. (2.59), where we have noted that the atomic state is in this case pure. As an illustrative example we take the two emitters with spectra shown in Fig. 6.1b and calculate the average amount of entanglement we generate using a single, monochromatic, probe photon of a given frequency. We plot this in Fig. 6.2a and, as expected, for spectrally distinct emitters the average concurrence does not reach its maximal value.

The amount of entanglement is determined by two competing processes. On the one hand, which-path information for the probe photon must be erased, while at the same time the phase shift induced by the photon scattering event must be maximised. Tuning closer to either emitter increases the relative phase shift but also imparts a degree of path information onto the probe, as the light-matter interaction is now stronger for one of the emitters. For emitters with finite detuning and line-width it is not obvious which photon energy maximises the average concurrence. Three emitter line-widths are shown in Fig. 6.1b, and Fig. 6.2a shows the corresponding $\mathscr{C}_{\text{avg}}$. The linewidths shown correspond to emitters with 1, 0.66 and 0.33 ns lifetimes, typical of semiconductor QDs benefiting from modest Purcell enhancements [171]. Increasing the line-width of the emitters leads to a larger spectral overlap, thereby erasing some of the which-path information and increasing $\mathscr{C}_{\text{avg}}$. For narrow line-widths it is preferable to tune the photon energy away from the mean emitter energy ($\hbar\omega - E_1 = 0.5$ μeV for $\delta = 1.0$ μeV), and towards resonance with one of the emitters (Fig. 6.2b). Though this reduces the concurrence in the state heralded by a click at detector D_2, it does increase the probability of a successful scattering event.

6.2.2 Broadband

One may expect that a photon with a wide frequency bandwidth that overlaps with both emitters will improve the entanglement generation and we therefore analyse a modified version of the protocol. Here we inject a single photon with a finite wavepacket, centred between the emitters at $\hbar\omega = (E_1 + E_2)/2$ and with a full-width-at-half-maximum (FWHM) of σ. The finite spectral width of the photon complicates our analysis somewhat and we proceed in the following manner [172].

The input optical state is now

$$|\psi_{\text{opt}}^{\text{in}}\rangle = \int \mathrm{d}\omega\, \xi(\omega) a^\dagger(\omega)\,|0\rangle\,, \tag{6.9}$$

where $a^\dagger(\omega)$ creates a photon of frequency ω in the upper interferometer arm, $|0\rangle$ represents the multi-mode vacuum and $\xi(\omega)$ gives the spectrum of the pulse. This evolves through the beam-splitter to

$$|\psi_{\text{opt}}^{\text{in}}\rangle \longrightarrow \frac{1}{\sqrt{2}} \int \mathrm{d}\omega\, \xi(\omega) \left(a^\dagger(\omega) + b^\dagger(\omega)\right)|0\rangle\,, \tag{6.10}$$

where $b^\dagger(\omega)$ creates a photon of frequency ω in the lower interferometer arm, and after scattering the combined light-matter state becomes

$$\begin{aligned}|\Phi\rangle = \frac{1}{2\sqrt{2}} \int \mathrm{d}\omega\, \xi(\omega) \Big[&\left(t_1(\omega)\,|\uparrow\uparrow\rangle + t_1(\omega)\,|\uparrow\downarrow\rangle + |\downarrow\uparrow\rangle + |\downarrow\downarrow\rangle\right) a^\dagger(\omega) \\ &+ \left(t_2(\omega)\,|\uparrow\uparrow\rangle + |\uparrow\downarrow\rangle + t_2(\omega)\,|\downarrow\uparrow\rangle + |\downarrow\downarrow\rangle\right) b^\dagger(\omega)\Big]\,|0\rangle\,,\end{aligned} \tag{6.11}$$

which evolves through the second beam-splitter to the pre-detector state

$$\begin{aligned}|\Psi\rangle = \frac{1}{4} \int \mathrm{d}\omega\, \xi(\omega) \Big[&\left((t_1(\omega) - t_2(\omega))\,|\uparrow\uparrow\rangle + (t_1(\omega) - 1)(\omega)\,|\uparrow\downarrow\rangle + (1 - t_2(\omega))\,|\downarrow\uparrow\rangle\right) a^\dagger(\omega) \\ &+ \left((t_1(\omega) + t_2(\omega))\,|\uparrow\uparrow\rangle + (t_1(\omega) + 1)\,|\uparrow\downarrow\rangle + (1 + t_2(\omega))\,|\downarrow\uparrow\rangle + 2\,|\downarrow\downarrow\rangle\right) b^\dagger(\omega)\Big]\,|0\rangle\,.\end{aligned} \tag{6.12}$$

For the sake of clarity we re-cast the state in Eq. (6.12) so as to clearly denote the optical and emitter portions

$$|\Psi\rangle = \frac{1}{\sqrt{2}} \int \mathrm{d}\omega\, \xi(\omega) \left(a^\dagger(\omega)\,|\psi_{\text{at}}^a(\omega)\rangle\,|0\rangle + b^\dagger(\omega)\,|\psi_{\text{at}}^b(\omega)\rangle\,|0\rangle\right), \tag{6.13}$$

where $|\psi_{\text{at}}^a\rangle$ and $|\psi_{\text{at}}^b\rangle$ are the atomic states heralded by clicks on detectors D_1 and D_2 respectively. Now, assuming our detectors are unable to resolve photon frequency, a click on the detector D_1 corresponds to the projective measurement

$$P_{D_1} = \int \mathrm{d}\omega\, a^\dagger(\omega)\,|0\rangle\langle 0|\,a(\omega). \tag{6.14}$$

so that the un-normalised, post-detection state is

$$|\Psi_{D_1}\rangle = \frac{1}{\sqrt{2}} \int \mathrm{d}\omega\, \xi(\omega) a^\dagger(\omega)\,|\psi_{\text{at}}^a(\omega)\rangle\,|0\rangle\,. \tag{6.15}$$

We can then deduce the probability of a D_1 detection event via

$$\Pr(D_1) = \frac{1}{2} \int \mathrm{d}\omega\, |\xi(\omega)|^2\, \langle \psi_{\text{at}}^a(\omega)|\psi_{\text{at}}^a(\omega)\rangle \tag{6.16}$$

and this allows us to construct the normalised atomic state, by tracing over photonic modes

$$\rho_{D_1} = \frac{1}{2\Pr(D_1)} \int \mathrm{d}\omega\, |\xi(\omega)|^2\, |\psi_{\text{at}}^a(\omega)\rangle\langle\psi_{\text{at}}^a(\omega)|\,. \tag{6.17}$$

We note that this is now a mixed state, meaning that we have to use the concurrence formula of Eq. (2.61), as opposed to the simple expression employed in the monochromatic case. The reason that the state is mixed is that we assume our detector is unable to resolve photon frequency and this means that we have lost information about the precise phase shifts that the emitters

underwent—classical uncertainty leads to mixing of quantum states. We can repeat the outlined procedure for a click at detector D_2 and the combined probabilities and density matrices for both events allow us to calculate $\mathscr{C}_{\text{avg}}$.

Fig. 6.3a shows the average concurrence for a single probe photon with Lorentzian, Gaussian and square spectral profiles as a function of the photon bandwidth. The spectral functions corresponding to these wavepackets are [173]

$$\xi_{\text{Lor}}(\omega) = \sqrt{\frac{2\sigma}{\pi}}\frac{1}{\sigma - 2i(\omega-\omega_0)}, \qquad \xi_{\text{Gau}}(\omega) = \left(\frac{4\ln(2)}{\pi\sigma^2}\right)^{\frac{1}{4}} e^{-2\ln(2)(\omega-\omega_0)^2/\sigma^2}$$
$$\text{and} \qquad \xi_{\text{squ}}(\omega) = \frac{1}{\sqrt{\sigma}}\theta(\sigma/2 - |\omega-\omega_0|), \tag{6.18}$$

where in all cases ω_0 gives the central frequency of the pulse and σ the full-width-half-maximum. We find that increasing the bandwidth of the input photon only degrades the average concurrence, and a narrow-band probe is preferable. We attribute this to the reduced temporal extent of the photon at larger bandwidths, which increases the probability of exciting the emitter, and thus the fraction of light emitted incoherently through spontaneous emission. This reduction is particularly noticeable for a Lorentzian wave-packet, where a close spectral match with the emitter increases the excitation probability.

6.3 Two Photon Performance

We have seen then that for a given pair of spectrally distinct emitters, the amount of entanglement we can generate between them using a single probe photon in the Mach-Zehnder geometry is fundamentally limited. In the monochromatic case it is clear that the fact a single photon cannot be resonant with both emitters limits the protocol and we demonstrated that the increase in spontaneous emission, which accompanies a broadening of the optical pulse, destroys any potential associated advantage. The most natural question to ask next is then whether an alternative optical input state can improve matters and we consider the case of two input photons so that $N \equiv n + m = 2$. We will go on to see that having access to an additional photon and subsequent emitter phase-shift can greatly improve our ability to entangle emitters that are not spectrally co-located. This is an important result as it means that it may not be necessary for future quantum technologies to have spectrally perfect emitters, provided we could instead engineer more complex N-photon Fock states.

6.3.1 Monochromatic

Consider an input state of two identical monochromatic photons $|n, m\rangle = |1, 1\rangle$ entering the interferometer. They will evolve into a two-photon NOON state [174] $(|2, 0\rangle - |0, 2\rangle)/\sqrt{2}$ via Hong-Ou-Mandel interference on the first beam splitter [175]. Assuming the system is lossless (we will discuss the effects of loss in Sec. 6.4), entanglement is heralded by three possible detector signatures: two photons at D_1, two photons at D_2, or a coincidence count. Before we detect the photons, they interact with the emitters and we saw in Chapter 4 that the two-photon S-matrix is given by a sum of two components, where one preserves individual photon frequency and one does not. This means that for an emitter α

$$\begin{aligned} S_\alpha(\nu_0, \nu_1, \omega_0, \omega_1) =& t_\alpha(\omega_0)t_\alpha(\omega_1)[\delta(\nu_0 - \omega_0)\delta(\nu_1 - \omega_1) + \delta(\nu_0 - \omega_1)\delta(\nu_1 - \omega_0)] \\ &+ iT(\nu_0, \nu_1, \omega_0, \omega_1)\delta(\nu_0 + \nu_1 - \omega_0 - \omega_1) \end{aligned} \tag{6.19}$$

where the incident photons have frequencies ω_0 and ω_1 and the scattered photons ν_0 and ν_1. Here $t_\alpha(\omega)$ is defined as in Eq. (6.6) and $T(\nu_0, \nu_1, \omega_0, \omega_1)$ describes the non-linear processes occurring during the scattering event. We derived the precise expression for $T(\nu_0, \nu_1, \omega_0, \omega_1)$ in Chapter 4

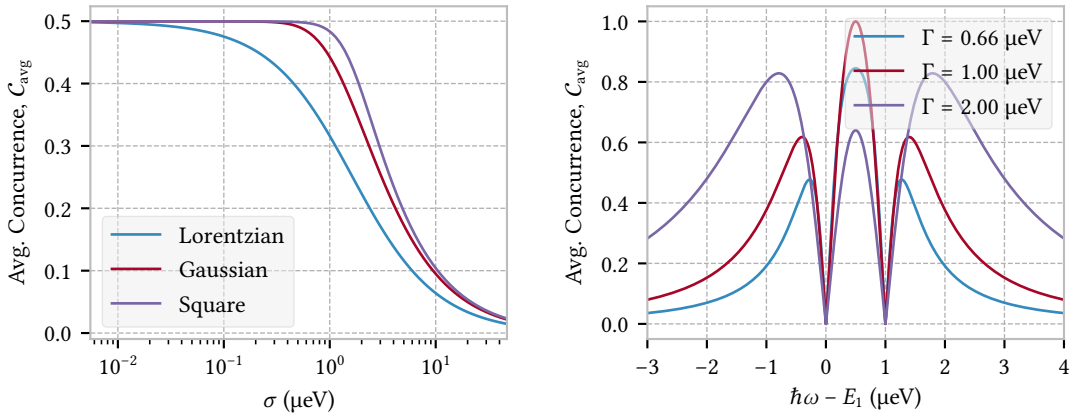

(a) Broadband photon input.

(b) Monochromatic two-photon input.

Figure 6.3: (a) $\mathscr{C}_{\text{avg}}$ for Lorentzian, Gaussian, and square single-photon envelopes as a function of FWHM pulse-width σ. Here, $\hbar\omega = (E_1 + E_2)/2$ and $\Gamma = 1.0$ μeV, with other parameters as in Fig. 6.2a. (b) Two-photon, $|n, m\rangle = |1, 1\rangle$, entanglement generation for a pair of detuned L-type emitters with equal linewidth Γ and energies E_1 and $E_2 = E_1 + \delta$, where $\delta = 1.0$ μeV. $\mathscr{C}_{\text{avg}}$ versus monochromatic single-photon energy without loss, $\beta = \beta_1 = \beta_2 = 1$.

of this thesis and specifically refer to Eq. 4.19 for the details. It turns out that, in the case of monochromatic photons we can neglect the non-linear term in the S-matrix [176]. This is because two photons which have infinitesimal width in frequency space have infinite extents in time-space and subsequently a vanishing probability of interacting with the emitter concurrently. Our ability to simplify the S-matrix in the monochromatic limit makes analysis of the protocol simple and we proceed in exactly the same manner as for the single-photon case, noting that light-matter interaction events now lead to coefficients of $t_\alpha^2(\omega)$, originating from the linear portion of Eq. (6.19). We find that the pre-detector state is

$$\begin{aligned}|\Psi\rangle = \frac{1}{4\sqrt{2}}\Big\{&\sqrt{2}\,|1,1\rangle\left[(t_1^2(\omega) - t_2^2(\omega))\,|\uparrow\uparrow\rangle + (t_1^2(\omega) - 1)\,|\uparrow\downarrow\rangle + (1 - t_2^2(\omega))\,|\downarrow\uparrow\rangle\right] \\ &+ |0,2\rangle\left[(t_1^2(\omega) + t_2^2(\omega))\,|\uparrow\uparrow\rangle + (t_1^2(\omega) + 1)\,|\uparrow\downarrow\rangle + (1 + t_2^2(\omega))\,|\downarrow\uparrow\rangle + 2\,|\downarrow\downarrow\rangle\right] \\ &+ |2,0\rangle\left[(t_1^2(\omega) + t_2^2(\omega))\,|\uparrow\uparrow\rangle + (t_1^2(\omega) + 1)\,|\uparrow\downarrow\rangle + (1 + t_2^2(\omega))\,|\downarrow\uparrow\rangle + 2\,|\downarrow\downarrow\rangle\right]\Big\}\end{aligned} \tag{6.20}$$

and we can calculate the probabilities and concurrences associated with each post-detection atomic state in the same manner as for the single photon case.

We plot the $\mathscr{C}_{\text{avg}}$ for the monochromatic two-photon protocol in Fig. 6.3b and see that using two probe photons leads to a rich structure in the average concurrence. It is now possible to reach deterministic maximal entanglement for spectrally distinct emitters with finite line-width. The reason for the two-photon advantage can be determined via inspection of Fig. 6.3b, where $\mathscr{C}_{\text{avg}}$ is shown as a function of the detuning between the photon energy and the transition energy of the first emitter. In the current example where $\delta = 1.0$ μeV, maximum entanglement fidelity occurs for emitters with line-widths of 1.0 μeV and input photons with energy $\hbar\omega = E_1 + \delta/2$. Comparing this value to Fig. 6.1b, this input energy corresponds to the point where the emitter spectra are at half of their maximum intensity. For monchromatic input states, the imparted phase shift is additive in photon number, i.e., for the two-photon case, each photon imparts a $\pi/2$ phase shift to the emitter and therefore achieves the required π phase shift.

6.3.2 Broadband

As in the single-photon case we consider the effect of finite pulse width on the two-photon protocol and note that we cannot any longer discard the non-linear component of the S-matrix in Eq. (6.19). We also expect the dependence of $\mathscr{C}_{\text{avg}}$ on pulse width, σ to be significantly different in the two-photon case. This is because there now exists the possibility that one photon can interact with an already excited emitter and induce stimulated emission. In this process the coherence of the emitted photon is maintained [177] and this effect could mitigate against the loss of coherence we observe due to spontaneous emission in the single-photon case.

Calculating $\mathscr{C}_{\text{avg}}$ in the broadband, two-photon case can be done in a broadly similar manner to that employed for either the monochromatic-two or broadband single-photon cases, though there are a number of subtleties to note. First we see that the input optical state

$$\begin{aligned}|\psi^{\text{in}}_{\text{opt}}\rangle &= \int \mathrm{d}\omega \int \mathrm{d}\omega'\ \xi(\omega,\omega')a^\dagger(\omega)b^\dagger(\omega')\,|0\rangle \\ &\longrightarrow \frac{1}{2}\int \mathrm{d}\omega \int \mathrm{d}\omega'\ \xi(\omega,\omega')\Big(b^\dagger(\omega)b^\dagger(\omega') + a^\dagger(\omega)b^\dagger(\omega') \\ &\qquad - a^\dagger(\omega)a^\dagger(\omega') - b^\dagger(\omega)a^\dagger(\omega')\Big)\,|0\rangle \end{aligned} \tag{6.21}$$

now does not evolve perfectly through the first beam-splitter to a pair of two-photon states. The size of the $|1,1\rangle$ contribution to the overall state is dependent on how closely the individual photon pulses match one another and its presence means we have to account for both single and two-photon scattering processes. This means that the post-scattering state

$$\begin{aligned}|\Phi\rangle =& \frac{1}{4}\int \mathrm{d}\omega \int \mathrm{d}\omega' \Big[b^\dagger(\omega)b^\dagger(\omega')\left(\tilde{\xi}_2(\omega,\omega')\,|\uparrow\uparrow\rangle + |\uparrow\downarrow\rangle + \tilde{\xi}_2(\omega,\omega')\,|\downarrow\uparrow\rangle + |\downarrow\downarrow\rangle\right) \\ &+ a^\dagger(\omega)b^\dagger(\omega')\left(t_1(\omega)t_2(\omega')\xi(\omega,\omega')\,|\uparrow\uparrow\rangle + t_1(\omega)\xi(\omega,\omega')\,|\uparrow\downarrow\rangle + t_2(\omega')\xi(\omega,\omega')\,|\downarrow\uparrow\rangle + |\downarrow\downarrow\rangle\right) \\ &- b^\dagger(\omega)a^\dagger(\omega')\left(t_2(\omega)t_1(\omega')\xi(\omega,\omega')\,|\uparrow\uparrow\rangle + t_1(\omega')\xi(\omega,\omega')\,|\uparrow\downarrow\rangle + t_2(\omega)\xi(\omega,\omega')\,|\downarrow\uparrow\rangle + |\downarrow\downarrow\rangle\right) \\ &- a^\dagger(\omega)a^\dagger(\omega')\left(\tilde{\xi}_1(\omega,\omega')\,|\uparrow\uparrow\rangle + \tilde{\xi}_1(\omega,\omega')\,|\uparrow\downarrow\rangle + |\downarrow\uparrow\rangle + |\downarrow\downarrow\rangle\right)\Big]\,|0\rangle \end{aligned} \tag{6.22}$$

contains both wavepackets that are simple phase shifts of the input packets and also the non-linear terms

$$\tilde{\xi}_\alpha(\omega,\omega') \equiv t_\alpha(\omega)t_\alpha(\omega')\left(\xi(\omega,\omega') + \xi(\omega',\omega)\right) + i\int \mathrm{d}\nu\ T(\nu,\omega+\omega'-\nu)\xi(\nu,\omega+\omega'-\nu), \tag{6.23}$$

which arise because of the frequency-mixing terms in the S-matrix.

We have to also take care in choosing projectors associated with given detection events. Projectors are constructed from normalised states and therefore the projector corresponding to a measurement of two photons at detector D_1 is

$$P_{D_1} = \frac{1}{2}\int \mathrm{d}\omega \int \mathrm{d}\omega'\ a^\dagger(\omega)a^\dagger(\omega')\,|0\rangle\langle 0|\,a(\omega)a(\omega'), \tag{6.24}$$

while

$$P_{\text{both}} = \int \mathrm{d}\omega \int \mathrm{d}\omega'\ a^\dagger(\omega)b^\dagger(\omega')\,|0\rangle\langle 0|\,a(\omega)b(\omega'), \tag{6.25}$$

which corresponds to a coincidence click, does not inherit the constant pre-factor. In order to calculate $\mathscr{C}_{\text{avg}}$ in the two-photon case we then simply have to evolve the state in Eq. (6.22) through the second beam-splitter, $|\Phi\rangle \longrightarrow |\Psi\rangle$, calculate the probabilities associated with each possible outcome, e.g.

$$\Pr(D_1) = \langle\Psi|\,P_{D_1}\,|\Psi\rangle \tag{6.26}$$

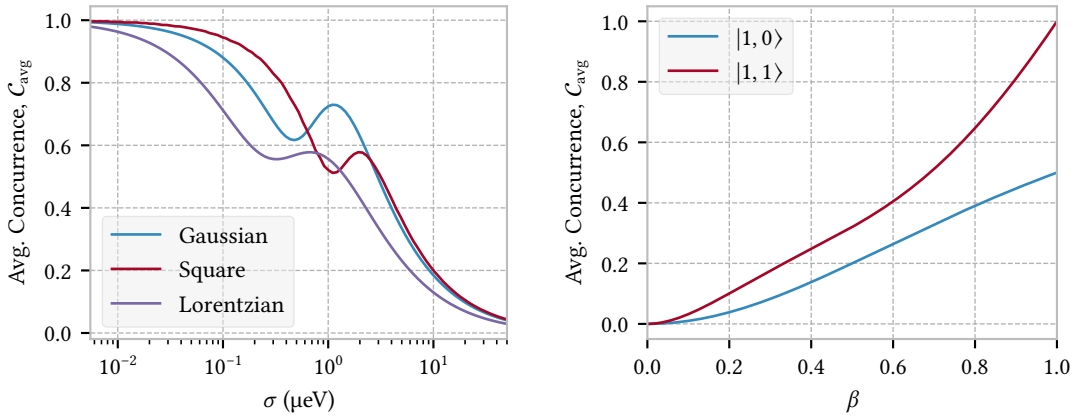

(a) Broadband two-photon input.

(b) Loss scaling.

Figure 6.4: (a) $\mathscr{C}_{\text{avg}}$ for Lorentzian, Gaussian, and square spectral envelopes as a function of FWHM pulse-width σ. Here, $\hbar\omega = (E_1 + E_2)/2$ and $\Gamma = 1.0$ μeV, with other parameters as in Fig. 6.3b. (b) Average concurrence as a function of $\beta = \beta_1 = \beta_2$ for a monochromatic two-photon pulse (red) and monochromatic single-photon pulse (blue); both emitters have line-widths of 1.0 μeV and $E_2 = E_1 + \delta$, where $\delta = 1.0$ μeV.

and use these to find the normalised atomic density matrices, e.g.

$$\rho_{D_1} = \frac{1}{\Pr(D_1)} \text{Tr}_{\text{optical}} \left[P_{D_1} |\Psi\rangle\langle\Psi| P_{D_1} \right]. \tag{6.27}$$

The average concurrence can then be readily determined as in the single-photon case, though with added computational complexity due to the non-linear scattering terms.

Competition between spontaneous and stimulated emission processes leads to non-monotonic behaviour of $\mathscr{C}_{\text{avg}}$ versus pulse width, which we plot in Fig. 6.4a. Although an increased bandwidth generally reduces $\mathscr{C}_{\text{avg}}$, a local maximum appears close to the emitter line-width. We can attribute this to the stimulated emission process, which is maximised for photons that are closely matched to the emitters' spectral profile. Further evidence for this conjecture is presented in e.g. Ref. [178], where it is noted that the two-photon interaction strength increases when the optical pulse width is broadened to the scale of the emitter line-width, where we observe our local maxima.

6.4 Loss and Detector Resolution

In the two-photon case loss is not as trivial to deal with as in the single-photon system. This is because, for single photons, loss implies no detection and simply acts to lower our success probability. In the two-photon protocol loss may not be heralded and therefore requires a more nuanced treatment. A key observation is that if the emitters are lossless, our protocol is the same regardless of the detectors' ability to resolve states of different photon number; if one detector clicks we can be sure that both photons arrived there. This logic does not apply when the emitters can scatter photons out of the waveguide because a simple 'on/off' click can now correspond to either two or single-photon states. Even with number-resolving detectors we remain ignorant of precisely where the photon was lost from and we need to account for this in our calculations.

We add two baths of optical modes, with annihilation operators $c(\omega)$ and $d(\omega)$, to our description of the system and couple emitters 1 and 2 to the $c(\omega)$ and $d(\omega)$ modes respectively. This

means that the pre-beam-splitter state in Eq. (6.22) is modified

$$\begin{aligned}|\Phi\rangle = \frac{1}{2}\int \mathrm{d}\omega \int \mathrm{d}\omega' \Big[& a^\dagger(\omega)a^\dagger(\omega')\,|\psi_{\mathrm{at}}^{aa}(\omega,\omega')\rangle + b^\dagger(\omega)b^\dagger(\omega')\,|\psi_{\mathrm{at}}^{bb}(\omega,\omega')\rangle \\ & + a^\dagger(\omega)b^\dagger(\omega')\,|\psi_{\mathrm{at}}^{ab}(\omega,\omega')\rangle + a^\dagger(\omega)c^\dagger(\omega')\,|\psi_{\mathrm{at}}^{ac}(\omega,\omega')\rangle \\ & + a^\dagger(\omega)d^\dagger(\omega')\,|\psi_{\mathrm{at}}^{ad}(\omega,\omega')\rangle + b^\dagger(\omega)c^\dagger(\omega')\,|\psi_{\mathrm{at}}^{bc}(\omega,\omega')\rangle \\ & + b^\dagger(\omega)d^\dagger(\omega')\,|\psi_{\mathrm{at}}^{bd}(\omega,\omega')\rangle + c^\dagger(\omega)c^\dagger(\omega')\,|\psi_{\mathrm{at}}^{cc}(\omega,\omega')\rangle \\ & + d^\dagger(\omega)d^\dagger(\omega')\,|\psi_{\mathrm{at}}^{dd}(\omega,\omega')\rangle + c^\dagger(\omega)d^\dagger(\omega')\,|\psi_{\mathrm{at}}^{cd}(\omega,\omega')\rangle \Big]\,|0\rangle\,, \end{aligned} \tag{6.28}$$

where e.g. the state $|\psi_{\mathrm{at}}^{bc}(\omega,\omega')\rangle$ is the atomic state that corresponds to the optical state with one photon in the lower interferometer arm and one lost to the environmental $c(\omega)$ mode. We calculate these states explicitly and find e.g.

$$|\psi_{\mathrm{at}}^{bc}(\omega,\omega')\rangle = t_1^{\mathrm{loss}}(\omega)t_2(\omega')\xi(\omega,\omega')\,|\uparrow\uparrow\rangle + t_1^{\mathrm{loss}}(\omega)\xi(\omega,\omega')\,|\uparrow\downarrow\rangle\,, \tag{6.29}$$

where

$$t_\alpha^{\mathrm{loss}}(\omega) \equiv \frac{-i\sqrt{\Gamma_\alpha\gamma_\alpha}}{\hbar\omega - E_\alpha + i\hbar(\Gamma_\alpha+\gamma_\alpha)/2} \tag{6.30}$$

is the probability amplitude for the process where emitter α scatters a photon of frequency ω into the environment. The second beam-splitter transforms the $a(\omega)$ and $b(\omega)$ mode operators as before and we can determine an expression for the final light-matter state $|\Psi\rangle$, which contains information about the whole system, including the lost photons.

In the case where our detectors resolve states of differing photon number, measurement corresponds to a set of projectors, which include those for the lossless case e.g. Eq. 6.24 and also

$$P_{D_1,\mathrm{loss}} = \int \mathrm{d}\omega \int \mathrm{d}\omega'\; a^\dagger(\omega)c^\dagger(\omega')\,|0\rangle\langle 0|\,a(\omega)c(\omega') + a^\dagger(\omega)d^\dagger(\omega')\,|0\rangle\langle 0|\,a(\omega)d(\omega') \tag{6.31}$$

$$P_{D_2,\mathrm{loss}} = \int \mathrm{d}\omega \int \mathrm{d}\omega'\; b^\dagger(\omega)c^\dagger(\omega')\,|0\rangle\langle 0|\,b(\omega)c(\omega') + b^\dagger(\omega)d^\dagger(\omega')\,|0\rangle\langle 0|\,b(\omega)d(\omega'). \tag{6.32}$$

We use these projectors to find the probabilities of given detection outcomes and corresponding atomic density matrices in the same manner as before. It is important to note that although we know whether we lost a photon or not we do not know specifically which emitter scattered it from the waveguide. In other words the modes $c(\omega)$ and $d(\omega)$ are unmonitored and the projectors do not differentiate between either of the two possible loss mechanisms. When the detectors do not differentiate between photon number states we do not have new projectors but must modify P_{D_1} from the version presented in Eq. (6.24) to

$$\begin{aligned} P_{D_1} = \int \mathrm{d}\omega \int \mathrm{d}\omega' \; & \frac{1}{2}a^\dagger(\omega)a^\dagger(\omega')\,|0\rangle\langle 0|\,a(\omega)a(\omega') + a^\dagger(\omega)c^\dagger(\omega')\,|0\rangle\langle 0|\,a(\omega)c(\omega') \\ & + a^\dagger(\omega)d^\dagger(\omega')\,|0\rangle\langle 0|\,a(\omega)d(\omega'), \end{aligned} \tag{6.33}$$

which we see projects onto any sub-state with photons in the $a(\omega)$ mode. The same logic can be used to construct P_{D_2}. We note at this juncture that in the presence of photon loss and non-number resolving detection schemes, it might be judicious to repeat our protocol until a coincidence count occurs. In this case the projector remains the same as in Eq. (6.25) and our final state is of high fidelity.

Fig. 6.4b shows the dependence of $\mathscr{C}_{\mathrm{avg}}$ on the loss rate β. We find in practice that the difference between number resolving and non-number resolving detectors is negligible. As expected, number-resolving detectors do offer a small advantage but this does not change the dependence of $\mathscr{C}_{\mathrm{avg}}$ on β in any noticeable way. This is because we find that the states where a single photon

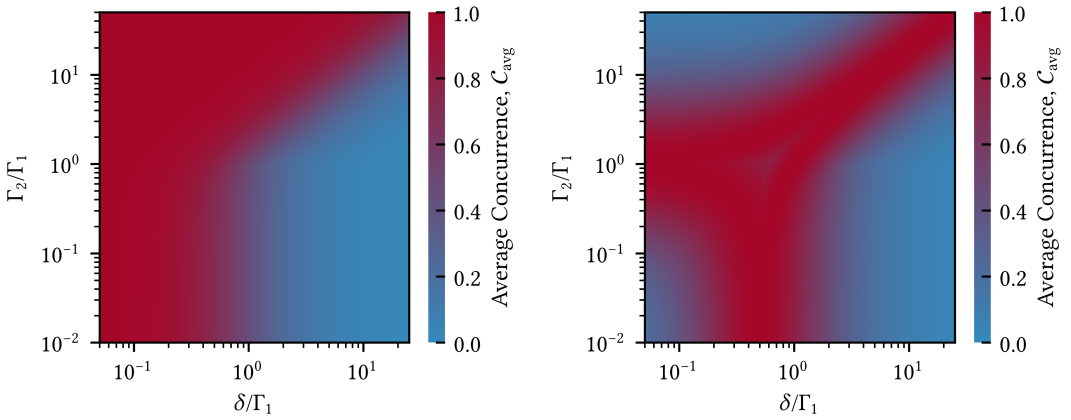

(a) One-photon, $|n, m\rangle = |1, 0\rangle$.

(b) Two-photons, $|n, m\rangle = |1, 1\rangle$.

Figure 6.5: Maximum average concurrence for different photon number input states injected into the interferometer. The emitter detuning δ and the line-width Γ_2 are both normalised to Γ_1 and we consider lossless waveguides, $\beta = 1$. The input photons are identical and monochromatic in the configurations (a) $|1, 0\rangle$ and (b) $|1, 1\rangle$.

loss is heralded are low in entanglement and so contribute very little to $\mathscr{C}_{\text{avg}}$. In the non-resolving case the average entanglement is lowered because the states heralded by detector clicks are mixed and of lower entanglement. It is of course preferable to have number-resolving detectors because in this case we can discard the lost-photon states and the fidelity of the atomic states that result from the protocol is thus higher. Finally, we note that for larger values of β the two-photon protocol does not scale as favourably with loss as the single-photon version. When we increase the number of photons input to the system the chance of loss increases.

6.5 General Behaviour

We have seen then that in certain regimes the two-photon protocol can be used to generate maximal entanglement deterministically between emitters where the single-photon protocol fails. It seems natural to ask whether this effect stems from some judicious choice of parameters that we made earlier, e.g. the 1 μeV detuning, or persists more generally. We answer this question in Figs. 6.5a and 6.5b, where we plot $\mathscr{C}_{\text{avg}}$ for both the single, $|n, m\rangle = |1, 0\rangle$ and two, $|n, m\rangle = |1, 1\rangle$ photon protocols over a segment of the total parameter space. We fix the linewidth of one of the emitters, Γ_1 and then vary the detuning between emitters, δ and lifetime of the second emitter, Γ_2. Regardless of linewidth, the single-photon protocol outperforms the two-photon version if the emitters are spectrally collocated. As expected, it can also be used to generate maximal entanglement deterministically if the linewidth of one emitter is sufficient to completely overlap the other. Crucially, however, by exploiting the multi-photon additivity of the phase shift, a two-photon process can efficiently generate entanglement for any finite detuning without requiring arbitrarily small emitter lifetimes. The reverse of this is also true and, for emitters with arbitrarily different lifetimes, there exists some finite detuning for which the two-photon protocol can maximally entangle the pair. In practice, this means a much greater freedom in matching solid-state emitters for entanglement generation in a Mach-Zehnder interferometer than previously thought.

We have then demonstrated that for a given pair of emitters it may be advantageous to utilise a two-photon input state in order to generate maximal entanglement deterministically. We note however that in moving from the single-photon protocol to the two-photon the complexity of

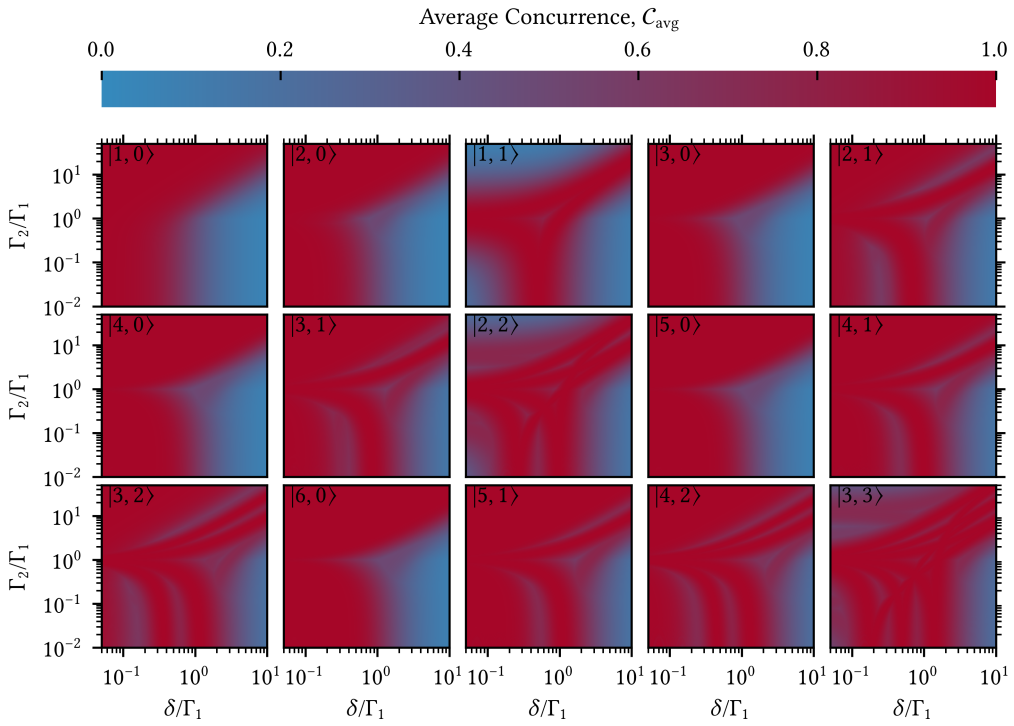

Figure 6.6: Plots of the average concurrence as a function of the coupling Γ_2 and emitter detuning δ for various input photon states $|n, m\rangle$.

the analysis massively increased. We had to track not only the combinatorics of the optical state evolving through the beam-splitter but also both linear and non-linear interactions, where photon frequencies were not preserved. If loss and non-number resolving detectors are included in the analysis then we also have to track all the possible loss mechanisms and this adds a further complexity, which scales as $N!$. Kristoffer Joanesarson noticed however that in the monochromatic, lossless case the combinatorics are in fact tractable and he extended the analysis presented here to the general $|n, m\rangle$ case. We don't reproduce this calculation here and refer instead to Ref. [179] for details but the essential point is that the input optical state evolves through the beam-splitter as

$$|\psi_{\text{opt}}^{\text{in}}\rangle = \frac{1}{\sqrt{n!m!}} \left(a^\dagger\right)^n \left(b^\dagger\right)^m |0\rangle \rightarrow \sum_{k=0}^{N} C_{k,N} \left(a^\dagger\right)^k \left(b^\dagger\right)^{N-k} |0\rangle, \tag{6.34}$$

where $C_{k,N}$ are the coefficients to be determined. The phase shift on each emitter is then proportional to the number of photons in the respective arm so, for the term with k photons in the upper arm and $N - k$ in the lower, the emitter in the upper arm accumulates a phase-shift given by $t^k(\omega)$ and the one in the lower gains $t^{N-k}(\omega)$. The state can then be evolved through the second beam-splitter and we determine the sub-states corresponding to p and q photons being detected by detectors D_1 and D_2 respectively.

In Fig. 6.5 we show $\mathscr{C}_{\text{avg}}$ as a function of the emitter detuning and the emitter line-width ratio for various optical input states $|n, m\rangle$. As we increase the total photon number, $N \equiv n + m$ we notice that there is a marked improvement in our entanglement generation ability. Larger areas of parameter space achieve a near-unity $\mathscr{C}_{\text{avg}}$ and this provides evidence for our contention that imperfections in the fabrication of two identical emitters can be overcome by optical state optimisation. We note also the interesting fact that e.g. the $|2, 1\rangle$ case inherits features from both the $|1, 1\rangle$ and $|1, 0\rangle$ processes and therefore performs well for both spectrally collocated emitters

and those with finite detuning. The complex structures emerging in all the plots are interesting to study and the result of multi-photon interference effects at the beam-splitters.

6.6 Summary

In conclusion, we have developed a method to entangle solid-state emitters embedded in a Mach-Zehnder interferometer, which is robust to spectral mismatch of the emitters. Entangling techniques that use solid-state emitters are well-known to place very stringent requirements on the spectral identity of the emitters and our approach overcomes these restrictions by tailoring multi-photon input states. Maximal, deterministic, entanglement between increasingly distinct emitters is possible using higher photon number input states and we have seen a rich structure emerge in the maps of $\mathscr{C}_{\text{avg}}$ over the potential emitter parameter space. This work indicates a possible new methodology for solid-state entanglement generation, where the requirement for perfectly matched emitters can be relaxed in favour of optical state optimisation.

There are of course practical challenges to be overcome before we can morph this entanglement generation protocol into a useful quantum technology. Firstly, a reduced coupling between the emitter and waveguide mode will reduce the phase shift imparted on the photons and therefore lower the average concurrence. Secondly, spectral wandering of the emitter may lead to classical uncertainty in the obtained phase shift, though the use of fast, high-efficiency detectors could mitigate against this [180]. Third, the photons must be created in identical quasi-monochromatic modes. This can be achieved using e.g., spontaneous parametric downconversion [181]. The higher-order photon pair generation in this process may also be beneficial to our entanglement generation process. Finally, dephasing will have an impact on the entanglement generation process. The dominant dephasing mechanisms for spin-doped solid-state emitters are nuclear spin interactions [182] and phonon scattering. While nuclear interactions naturally lead to random precession of the spin ground-state, there are a number of strategies based on dynamical decoupling that may be used to suppress its impact [183]. Phonon scattering leads to sidebands [184] that can be removed through frequency filtering or by placing the emitter in an optical cavity [185].

Chapter 7

Conclusions

7.1 Summary

In this thesis we broadly discussed the area of light-matter interactions, with a particular focus on integrated semiconductor nanostructure systems. We can loosely group the work into four areas:

1. The first two chapters of this thesis are concerned with foundations and outline the theories upon which the original work is based. In Chapter 2 we examine the mathematical formulation of quantum theory and thoroughly investigate the strange prediction of entanglement. We show how this uniquely quantum phenomenon can be used as a resource for communication protocols and discuss some of the methods used to overcome the inherent difficulties in quantifying its presence in a state.

   In Chapter 3 we discuss the area of quantum optics and the well-known treatments of light-matter interactions. We begin by justifying our use of the so-called Jaynes-Cummings Hamiltonian throughout this thesis and explain the rotating-wave-approximation from which it arises. The master equation approach is then discussed and we show how Lindblad-type super-operators can be used to model both elastic and inelastic dephasing processes in two-level-systems. We go on to derive the 'Input-Output' formalism from first-principles and demonstrate its great utility in the analysis of coherently driven quantum systems. To conclude, we explain why the more 'modern' scattering approach to the analysis of waveguide QED systems is appropriate and then show how the S-matrix may be connected to input-output theory.

2. Our first piece of original work is detailed in Chapter 4 and we develop a novel technique for calculation of S-matrices in waveguide QED systems. We explain generally how the dynamics can be calculated via summation of the Dyson series for the system, which is developed in terms of the interaction Hamiltonian. We calculate the S-matrices corresponding to four distinct situations:

   (a) Single-photon optical states scattering from single two-level-systems.

   (b) Two-photon optical states scattering from single two-level-systems.

   (c) Single-photon optical states scattering from single Λ-systems.

   (d) Two-photon optical states scattering from single Λ-systems.

   We are able to fully specify the evolutions of both the optical and emitter states in these scenarios. The series solutions we develop have closed forms only for some fraction of the total parameter space but we employ a summation technique, borrowed from relativistic quantum-field-theory, in order to extend the range of validity. It is interesting to note that the terms in the series we develop correspond to physical processes and that the choice of

Hamiltonian we made initially means that the majority of these terms are vanishing. We conclude by briefly studying the pole structures of the S-matrices we derive and map these onto the expected physical behaviour.

3. We move away from the idealised systems considered in Chapter 4 and, in Chapter 5, apply some of the quantum optics techniques discussed previously to real experimental systems. We begin by explaining the origins of non-reciprocal coupling in optical waveguides and show how QDs can be used to realise unidirectional transport. We go on to outline a recent experimental implementation of such a unidirectional system and demonstrate that it is not well described by a naive two-level-system model. In order to understand the system dynamics we adapt the input-output relations to include the effects of pure and radiative dephasing, as well as imperfect unidirectionality. We further consider the effects of charge noise on the system and show that, in the experimentally studied regime, power saturation effects play a major role in determining the measured spectra. It proves difficult to capture the observed asymmetric line-shapes in the high-power regime but we study a related experimental system and use a transfer matrix technique to predict these shapes. As expected, we determine that their origin lies in the convolution between the effects of a weak Fabry-Pérot cavity and the probed system.

4. Our final project is detailed in Chapter 6 and concerns the creation of matter-matter entanglement in a waveguide QED system. We note that entangling solid-state emitters is experimentally challenging, owing to the variation in spectra between emitters of even the same species. We show that, for a given pair of emitters, the single-photon entangling protocol is fundamentally limited and cannot necessarily be improved by modifying the pulse-width of the optical state. We go on to show that a two-photon protocol can, in certain regimes, massively out-perform the single-photon version and that the sensitivity to optical pulse-width is not, as in the single-photon case, monotonically decreasing. We explore a large parameter space of possible pairs of emitter spectra and determine the criteria for each protocol to be favourable. Finally, we study the results obtained for higher photon number input optical states and conjecture that an arbitrary degree of emitter mismatch can be overcome if we have the ability to engineer arbitrary $|n, m\rangle$ Fock states.

In summary, we study a prototypical waveguide QED system from a theoretical point of view and attempt to use this model to understand experimental results. We find that this fails and go on to quantify the dominant noise sources in two state-of-the-art experiments. We consider one specific imperfection, emitter spectral mismatch, and develop an entanglement generation protocol that is robust against this.

7.2 Conclusions

Each of the projects described in this thesis has associated conclusions and we say specifically that:

1. Analysis in general of photon scattering events in waveguide QED is difficult and, even in the case of a single coupled emitter, the dynamics are complex. There are both inherent difficulties of dealing with what are, in essence, interacting quantum field theories and also the intricacies associated with the combinatorics of N input and output photons. While the method we develop goes some way to addressing the first point, the combinatorics are essentially unavoidable and mean that the number of terms in a given S-matrix scales as $N!$ [186].

2. Full quantum control of semiconductor QDs is not yet possible and order of magnitude improvements in e.g. the lifetimes of these emitters are required before we can envisage their use as a stable, solid-state, qubit. We demonstrated that, even supposing we could

overcome charge noise limitations, a resonant photon would only acquire a 0.4 radian phase shift in scattering from the unidirectionally coupled QD sample studied. Given that the realisation of e.g. a single photon switch would require a π radian shift [187] and that proposals for fault-tolerant quantum computers require our qubit control accuracy to exceed 99%, we see that a lot of progress is required. We note though that this is an extremely active research area and new technologies are emerging on a regular basis [188].

3. Our ability to generate entanglement between solid-state emitters is limited for not only the reasons given in Chapter 5 but also because the spectra of two emitters in general do not perfectly overlap. We find however that various degrees of emitter mismatch can be overcome by engineering the optical state used to probe the system. We conclude that the inherent difficulties in fabrication of identical emitters could be surmounted by careful tailoring of the optical state. Of course, this is a difficult problem in itself but one which may ultimately prove more tractable [189].

These conclusions all have consequences in terms of the over-arching goal of on-chip quantum technologies. In particular they crystallise our understanding of where current limitations in both theoretical insight and experimental realisation lie.

7.3 Future Work

The work presented here is undoubtedly not definitive, not representing the last word on any one of the subjects discussed, and we therefore suggest some potential avenues for further investigation. We note that throughout this thesis we have only considered systems of single emitters coupled to optical waveguides. This assumption will have to be relaxed as experiments become more sophisticated and we are able to design more complex devices. Tools are being actively developed for the analysis of quantum networks where the input to one node is the output from another and notable among these is the 'SLH framework' [190]. However, it remains challenging to use such a formalism to describe systems suffering from experimental imperfections and this should be a key feature of any future theoretical techniques we develop.

We note also that the S-matrices we find in this thesis are, for the reasons discussed, limited to only single or two-photon input states. Previous authors have derived the N-photon generalisations of these for the two-level-system but finding expressions for the case where the emitter is arbitrary remains a difficult problem. A nice feature of the diagrammatic method we employ is that it is obvious how to extend the analysis to states of higher photon number, though the combinatorics will as ever render the task challenging. It would be interesting to perform this extension however, and to find the set of S-matrices for states of photon number up to, say, $N = 10$. This would make the analysis of systems where the optical input is squeezed light possible within the framework and these states have the benefit of being more experimentally accessible.

As far as experimental projects are concerned, the direction for future work is quite clear. We obviously require samples with fewer imperfections and either longer pure dephasing times or shorter radiative recombination times. It is not the magnitude of the pure dephasing rate that determines its effect on the spectrum but rather the ratio between this and the emitter lifetime. This is intuitive because an emitter only imparts phase uncertainty on a photon during their interaction time. In Fig. 7.1 we show the model used to produce the experimental fit in Fig. 5.9 with some adjusted parameters. Of all the noise processes, we find that spectral wandering is the dominant one but, even if we could eliminate this from our samples, we see that the waveguide-emitter coupling still has to be increased to see total extinction of the transmitted photon signal. Recently, experimentalists have focussed on reducing spectral wandering by increasing the size of the nanobeam waveguides. This has the effect of isolating the emitter from surfaces where charge noise can build up but at the expense of β-factor. We see that this approach is not going to be sustainable in the long-term.

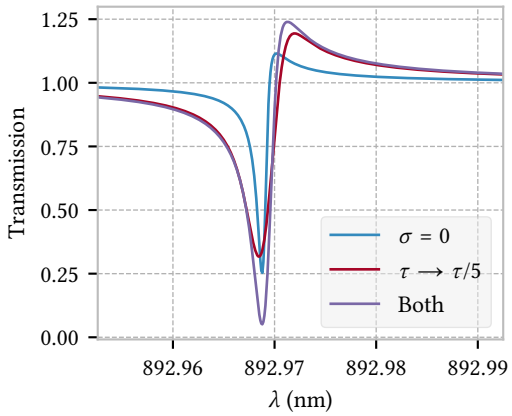

Figure 7.1: Calculated transmission spectra for the photonic crystal coupled QD experiment (Fig. 5.9) with modified parameters. The blue line shows the spectrum in the absence of spectral wandering, the red shows the version where the QD is Purcell enhanced by a factor of five and the purple shows the combined effect of both modifications.

We showed that the entanglement generation scheme discussed in Chapter 6 can be improved in certain parameter regimes when the number of input photons is increased. We did not however consider whether Fock states themselves are optimal for the protocol or whether e.g. a two-mode-squeezed input, which has the form [191]

$$|\zeta e^{i\theta}\rangle = \frac{1}{\cosh\zeta}\sum_{n=0}^{\infty} e^{in\theta}\tanh^n\zeta\,|n,n\rangle\,, \tag{7.1}$$

where ζ is the 'squeezing parameter,' could perform equally well. In fact a more thorough analysis of the range of possible optical inputs would seem prudent as arbitrary Fock states are generally more difficult to generate than squeezed states [192]. We could also consider the effects of not just photon number resolving or non-resolving detectors on the protocol but also imagine employing e.g. homodyne detectors. We would expect that, in the regime of non-negligible photon loss, these detectors could outperform the simple photon counters [193].

Appendix A

Useful Mathematics

A.1 The Laplace Transformation

We define the one-sided Laplace Transformation of a function $f(t)$ by [194]

$$L[f(t)] \equiv \bar{f}(s) \equiv \int_0 \mathrm{d}t\; e^{-st} f(t), \tag{A.1}$$

where $s = \sigma + i\omega$ is in general a complex number. The utility of the Laplace Transformation becomes clear when we consider

$$L\left[\frac{\mathrm{d}f(t)}{\mathrm{d}t}\right] = \int_0 \mathrm{d}t\; e^{-st}\frac{\mathrm{d}f(t)}{\mathrm{d}t} = s\bar{f}(s) - f(0), \tag{A.2}$$

which is the result of integration by parts and the assumption that $\lim_{t\to\infty} f(t)e^{-st} \to 0$. This means that a system of N linear differential equations in time-space can be transformed into N coupled algebraic expressions in Laplace space. Solution of this problem is generally possible analytically and we are then left having to invert N Laplace transformed functions $\bar{f}(s) \to f(t)$. In general such an inverse Laplace transformation is not well-defined but there exist many specific cases where inversion is possible.

A.2 An Integration Technique

For completeness we describe here the integration technique used to evaluate the explicit integral expressions for the single and two photon transition amplitudes. We define the integral $\mathcal{I}$ and begin by changing variables so as to shift the limits of integration

$$\mathcal{I} \equiv \int_{-\infty}^{t_1} \mathrm{d}t_2\; e^{-i\Delta_i t_2} = \int_0^{\infty} \mathrm{d}t_2\; e^{-i\Delta_i(t_1-t_2)}.$$

This can be decomposed and multiplied by unity to give

$$\mathcal{I} = e^{-i\Delta_i t_1} \lim_{\alpha\to 0} \int_0^{\infty} \mathrm{d}t_2\; e^{-\alpha t_2}\left[\cos(\Delta_i t_2) + i\sin(\Delta_i t_2)\right] \tag{A.3}$$

and we then make use of standard results [195], for example noting

$$\delta(x) = \frac{1}{\pi}\lim_{a\to 0}\frac{a}{a^2 + x^2} \tag{A.4}$$

to find that

$$\mathcal{I} = e^{-i\Delta_i t_1}\lim_{\alpha\to 0}\left(\frac{\alpha}{\alpha^2+\Delta_i^2} + i\frac{\Delta_i}{\alpha^2+\Delta_i^2}\right) = e^{-i\Delta_i t_1}\left(\pi\delta(\Delta_i) + \frac{i}{\Delta_i}\right), \tag{A.5}$$

which is the desired formula.

A.3 Borel Summation

In many areas of physics [196], notably quantum electrodynamics (QED) [197], calculations are performed via summation of terms in a perturbation expansion. It turns out however that these series are often divergent, meaning that terms grow larger and tend to infinity as higher order corrections are included. It is often possible to assign a finite value to these divergent sums and there are a number of potential techniques. Here we describe the Borel summation method, which can be used to interpret series with an n^{th} term divergent up to a factor of $n!$ [198].

To perform the Borel summation technique we take the divergent series

$$S = \sum_{n=0}^{\infty} a_n, \tag{A.6}$$

where the terms a_n do not vanish sufficiently quickly as $n \longrightarrow \infty$ and multiply each term by the identity

$$1 = \frac{\int_0^{\infty} \mathrm{d}t\ t^n e^{-t}}{n!}. \tag{A.7}$$

The Borel sum $\mathscr{B}$ is then defined as the quantity that results from interchanging the orders of summation and integration

$$\mathscr{B}(S) \equiv \int_0^{\infty} \mathrm{d}t\ e^{-t} \sum_{n=0}^{\infty} \frac{a_n t^n}{n!}. \tag{A.8}$$

We can use this technique to interpret an otherwise divergent series. Consider the sum of alternating positive and negative unity

$$S = 1 - 1 + 1 - 1 + \ldots = \sum_{n=0}^{\infty} (-1)^n. \tag{A.9}$$

The Borel sum of this series is given by

$$\mathscr{B}(S) = \int_0^{\infty} \mathrm{d}t\ e^{-t} \sum_{n=0}^{\infty} \frac{(-t)^n}{n!} = \int_0^{\infty} \mathrm{d}t\ e^{-2t} = \frac{1}{2}, \tag{A.10}$$

which is in some sense the only sensible answer.

It may seem false to claim the the Borel sum tells us anything about physical reality at all. We could argue that any theory we develop that leads to a divergent perturbation series is simply invalid. This is not the prevailing opinion in the scientific community however and infinities often arise and must be similarly interpreted in e.g. high energy QED perturbation series. The results of these calculations are among the most rigorously experimentally tested in all of physics [199]. We say instead that an infinite series forms some *representation* of the quantity we want to calculate but one that is only valid for some subset of our parameter space. We increase the range of validity by introducing a new representation of the quantity and deduce that it was our choice of representation and not the quantity itself, which presented the problem.

Appendix B

Transition Amplitude Rearrangement

In this appendix we demonstrate the equivalence between our results for the one and two-photon transition amplitudes for a TLS and those found by Fan *et al.* As our transition amplitudes are evaluated in the limit $t \longrightarrow \infty$ and the single final atomic state $|g\rangle$ is assumed, then the scattering matrix is in fact the quantity given by these amplitudes. For the single photon case we find that

$$\mathscr{A} = \frac{1 - \pi\gamma^2 g(\Delta_i)}{1 + \pi\gamma^2 g(\Delta_i)}\delta(f - i). \tag{B.1}$$

We can substitute our definition of $g(\Delta)$ into Eq. (B.1) to determine

$$\mathscr{A} = \frac{\Delta_i - i\pi\gamma^2 - \pi^2\gamma^2\Delta_i\delta(\Delta_i)}{\Delta_i + i\pi\gamma^2 + \pi^2\gamma^2\Delta_i\delta(\Delta_i)}\delta(f - i), \tag{B.2}$$

which is naturally equal to that found by Fan *et al.*

$$\mathscr{A} = \frac{\Delta_i - i\pi\gamma^2}{\Delta_i + i\pi\gamma^2}\delta(f - i) \tag{B.3}$$

as required.

The two-photon result requires a little more effort, our result is that

$$\begin{aligned}\mathscr{A} =& [t(i_0) + t(i_1) - 1][\delta(f_0 - i_0)\delta(f_1 - i_1) + \delta(f_0 - i_1)\delta(f_1 - i_0)] \\ &+ 2\pi\gamma^4\delta(f_0 + f_1 - i_0 - i_1)\sum_{s=0,1}\sum_{s'=0,1}\frac{g(\Delta_{i_s})g(\Delta_{i_s} - \Delta_{f_{s'}})g(\Delta_{f_{s'\oplus 1}})}{[1 + \pi\gamma^2 g(\Delta_{i_s})][1 + \pi\gamma^2 g(\Delta_{f_{s'\oplus 1}})]}.\end{aligned} \tag{B.4}$$

Now, if we expand out the factor $g(\Delta_{i_s} - \Delta_{f_{s'}})$ so that

$$\begin{aligned}\frac{g(\Delta_{i_s})g(\Delta_{i_s} - \Delta_{f_{s'}})g(\Delta_{f_{s'\oplus 1}})}{[1 + \pi\gamma^2 g(\Delta_{i_s})][1 + \pi\gamma^2 g(\Delta_{f_{s'\oplus 1}})]} =& \frac{\pi g(\Delta_{i_s})\delta(\Delta_{i_s} - \Delta_{f_{s'}})g(\Delta_{f_{s'\oplus 1}})}{[1 + \pi\gamma^2 g(\Delta_{i_s})][1 + \pi\gamma^2 g(\Delta_{f_{s'\oplus 1}})]} \\ &+ \frac{ig(\Delta_{i_s})g(\Delta_{f_{s'\oplus 1}})}{(\Delta_{i_s} - \Delta_{f_{s'}})[1 + \pi\gamma^2 g(\Delta_{i_s})][1 + \pi\gamma^2 g(\Delta_{f_{s'\oplus 1}})]},\end{aligned} \tag{B.5}$$

it is then true that

$$\begin{aligned}\mathscr{A} =&\left[t(i_0)+t(i_1)-1\right]\left[\delta(f_0-i_0)\delta(f_1-i_1)+\delta(f_0-i_1)\delta(f_1-i_0)\right]\\&+4\pi^2\gamma^4\left[\delta(f_0-i_0)\delta(f_1-i_1)+\delta(f_0-i_1)\delta(f_1-i_0)\right]\frac{g(\Delta_{i_0})g(\Delta_{i_1})}{\left[1+\pi\gamma^2 g(\Delta_{i_0})\right]\left[1+\pi\gamma^2 g(\Delta_{i_1})\right]}\\&+2\pi i\gamma^4\delta(f_0+f_1-i_0-i_1)\left[\frac{g(\Delta_{i_0})g(\Delta_{f_0})}{(\Delta_{i_0}-\Delta_{f_1})\left[1+\pi\gamma^2 g(\Delta_{i_0})\right]\left[1+\pi\gamma^2 g(\Delta_{f_0})\right]}\right.\\&+\frac{g(\Delta_{i_0})g(\Delta_{f_1})}{(\Delta_{i_0}-\Delta_{f_0})\left[1+\pi\gamma^2 g(\Delta_{i_0})\right]\left[1+\pi\gamma^2 g(\Delta_{f_1})\right]}+\frac{g(\Delta_{i_0})g(\Delta_{f_1})}{(\Delta_{i_1}-\Delta_{f_0})\left[1+\pi\gamma^2 g(\Delta_{i_1})\right]\left[1+\pi\gamma^2 g(\Delta_{f_1})\right]}\\&\left.+\frac{g(\Delta_{i_1})g(\Delta_{f_0})}{(\Delta_{i_1}-\Delta_{f_1})\left[1+\pi\gamma^2 g(\Delta_{i_1})\right]\left[1+\pi\gamma^2 g(\Delta_{f_0})\right]}\right].\end{aligned}\tag{B.6}$$

We can rearrange the frequency-conserving terms and again substitute the definition of $g(\Delta)$ into the frequency-mixing term to determine

$$\begin{aligned}\mathscr{A} =\ & t(i_0)t(i_1)\left[\delta(f_0-i_0)\delta(f_1-i_1)+\delta(f_0-i_1)\delta(f_1-i_0)\right]+\frac{2\pi i\gamma^4\delta(f_0+f_1-i_0-i_1)}{\left[\Delta_{f_0}+i\pi\gamma^2\right]\left[\Delta_{f_1}+i\pi\gamma^2\right]}\\&\times\left[\frac{\Delta_{f_1}+i\pi\gamma^2}{(\Delta_{f_1}-\Delta_{i_0})\left[\Delta_{i_0}+i\pi\gamma^2\right]}+\frac{\Delta_{f_0}+i\pi\gamma^2}{(\Delta_{f_0}-\Delta_{i_0})\left[\Delta_{i_0}+i\pi\gamma^2\right]}\right.\\&\left.+\frac{\Delta_{f_0}+i\pi\gamma^2}{(\Delta_{f_0}-\Delta_{i_1})\left[\Delta_{i_1}+i\pi\gamma^2\right]}+\frac{\Delta_{f_1}+i\pi\gamma^2}{(\Delta_{f_1}-\Delta_{i_1})\left[\Delta_{i_1}+i\pi\gamma^2\right]}\right].\end{aligned}\tag{B.7}$$

Straight-forward algebraic manipulation of Eq. (B.7) then leads us to

$$\begin{aligned}\mathscr{A} =&t(i_0)t(i_1)\left[\delta(f_0-i_0)\delta(f_1-i_1)+\delta(f_0-i_1)\delta(f_1-i_0)\right]\\&+\frac{4\pi i\gamma^4\delta(f_0+f_1-i_0-i_1)}{\left[\Delta_{f_0}+i\pi\gamma^2\right]\left[\Delta_{f_1}+i\pi\gamma^2\right]}\left(\frac{1}{\Delta_{i_0}+i\pi\gamma^2}+\frac{1}{\Delta_{i_1}+i\pi\gamma^2}\right),\end{aligned}\tag{B.8}$$

which is the result by Fan *et al.*

Bibliography

[1] G. E. Moore. "Cramming more components onto integrated circuits". In: *Proceedings of the IEEE* **86**.1 (1998), pp. 82–85.

[2] S. B. Desai et al. "MoS2 transistors with 1-nanometer gate lengths". In: *Science* **354**.6308 (2016), pp. 99–102.

[3] P. W. Shor. "Polynomial-time algorithms for prime factorization and discrete logarithms on a quantum computer". In: *SIAM Review* **41**.2 (1999), pp. 303–332.

[4] L. K. Grover. "A fast quantum mechanical algorithm for database search". In: *Proceedings of the twenty-eighth annual ACM symposium on Theory of computing*. ACM. 1996, pp. 212–219.

[5] I. M. Georgescu, S. Ashhab, and F. Nori. "Quantum simulation". In: *Reviews of Modern Physics* **86**.1 (2014), p. 153.

[6] A. M. Childs and W. Van Dam. "Quantum algorithms for algebraic problems". In: *Reviews of Modern Physics* **82**.1 (2010), p. 1.

[7] M. Roser and H. Ritchie. *Technological Progress*. 2018. URL: https://ourworldindata.org/technological-progress (visited on 01/07/2018).

[8] R. Van Meter, K. M. Itoh, and T. D. Ladd. "Architecture-dependent execution time of Shor's algorithm". In: *Controllable Quantum States: Mesoscopic Superconductivity and Spintronics (MS+ S2006)*. World Scientific, 2008, pp. 183–188.

[9] T. D. Ladd et al. "Quantum computers". In: *Nature* **464**.7285 (2010), p. 45.

[10] V. Giovannetti, S. Lloyd, and L. Maccone. "Advances in quantum metrology". In: *Nature Photonics* **5**.4 (2011), p. 222.

[11] N. Gisin et al. "Quantum cryptography". In: *Reviews of Modern Physics* **74**.1 (2002), p. 145.

[12] R. P. Feynman. "Simulating physics with computers". In: *International Journal of Theoretical Physics* **21**.6-7 (1982), pp. 467–488.

[13] A. Haque and S. Sumaiya. "An Overview on the Formation and Processing of Nitrogen-Vacancy Photonic Centers in Diamond by Ion Implantation". In: *Journal of Manufacturing and Materials Processing* **1**.1 (2017), p. 6.

[14] M. Eriksson, S. Coppersmith, and M. Lagally. "Semiconductor quantum dot qubits". In: *MRS Bulletin* **38**.10 (2013), pp. 794–801.

[15] R. Blatt and C. F. Roos. "Quantum simulations with trapped ions". In: *Nature Physics* **8**.4 (2012), p. 277.

[16] S. Barz. "Quantum computing with photons: introduction to the circuit model, the one-way quantum computer, and the fundamental principles of photonic experiments". In: *Journal of Physics B: Atomic, Molecular and Optical Physics* **48**.8 (2015), p. 083001.

[17] G. Wendin. "Quantum information processing with superconducting circuits: a review". In: *Reports on Progress in Physics* **80**.10 (2017), p. 106001.

[18] A. Einstein, B. Podolsky, and N. Rosen. "Can quantum-mechanical description of physical reality be considered complete?" In: *Physical Review* **47**.10 (1935), p. 777.

[19] R. Horodecki et al. "Quantum entanglement". In: *Reviews of Modern Physics* **81**.2 (2009), p. 865.

[20] B. Hensen et al. "Loophole-free Bell inequality violation using electron spins separated by 1.3 kilometres". In: *Nature* **526**.7575 (2015), p. 682.

[21] P. Lodahl, S. Mahmoodian, and S. Stobbe. "Interfacing single photons and single quantum dots with photonic nanostructures". In: *Reviews of Modern Physics* **87**.2 (2015), p. 347.

[22] C. Sayrin et al. "Nanophotonic optical isolator controlled by the internal state of cold atoms". In: *Physical Review X* **5**.4 (2015), p. 041036.

[23] A. Sipahigil et al. "An integrated diamond nanophotonics platform for quantum optical networks". In: *Science* **354**.6314 (2016), p. 6875.

[24] G. Shan et al. "Vertical-external-cavity surface-emitting lasers and quantum dot lasers". In: *Frontiers of Optoelectronics* **5**.2 (2012), pp. 157–170.

[25] T. Sogabe, Q. Shen, and K. Yamaguchi. "Recent progress on quantum dot solar cells: a review". In: *Journal of Photonics for Energy* **6**.4 (2016), p. 040901.

[26] A. Rogalski. "Insight on quantum dot infrared photodetectors". In: *Journal of Physics: Conference Series*. Vol. 146. 1. IOP Publishing. 2009, p. 012030.

[27] S. Gasiorowicz. *Quantum Physics*. John Wiley & Sons, 2007.

[28] J. Handsteiner et al. "Cosmic Bell test: measurement settings from Milky Way stars". In: *Physical Review Letters* **118**.6 (2017), p. 060401.

[29] N. Zettili. *Quantum Mechanics Concepts and Applications*. 2009.

[30] E. Schrödinger. "Die gegenwärtige Situation in der Quantenmechanik". In: *Naturwissenschaften* **23**.49 (1935), pp. 823–828.

[31] L. Masanes, T. D. Galley, and M. P. Müller. "The measurement postulates of quantum mechanics are operationally redundant". In: *Nature Communications* **10**.1 (2019), p. 1361.

[32] M. F. Pusey, J. Barrett, and T. Rudolph. "On the reality of the quantum state". In: *Nature Physics* **8**.6 (2012), p. 475.

[33] S. Barnett. *Quantum Information*. Vol. 16. Oxford University Press, 2009.

[34] B. R. Martin and G. Shaw. *Mathematics for Physicists*. John Wiley & Sons, 2015.

[35] G. Teschl. "Mathematical Methods in Quantum Mechanics". In: *Graduate Studies in Mathematics* **99** (2009).

[36] M. L. Boas. *Mathematical Methods in the Physical Sciences*. John Wiley & Sons, 2006.

[37] N. Bohr. "Über die serienspektra der elemente". In: *Zeitschrift für Physik A Hadrons and Nuclei* **2**.5 (1920), pp. 423–469.

[38] J. M. Finn. *Classical Mechanics*. Jones & Bartlett Publishers, 2009.

[39] S. Lipschutz and M. Lipson. *Schaum's Outline of Theory and Problems of Linear Algebra*. Erlangga, 2001.

[40] J. J. Sakurai and E. D. Commins. *Modern Quantum Mechanics, Revised Edition*. 1995.

[41] R. Bennett, T. M. Barlow, and A. Beige. "A physically motivated quantization of the electromagnetic field". In: *European Journal of Physics* **37**.1 (2015), p. 014001.

[42] S. M. Dutra. *Cavity Quantum Electrodynamics: The Strange Theory of Light in a Box*. John Wiley & Sons, 2005.

[43] R. Loudon. *The Quantum Theory of Light*. OUP Oxford, 2000.

[44] L. H. Ryder. *Quantum Field Theory*. Cambridge University Press, 1996.

[45] J. D. Bjorken and S. D. Drell. *Relativistic Quantum Mechanics*. McGraw-Hill, 1965.

[46] M. O. Scully and M. S. Zubairy. *Quantum Optics*. AAPT, 1999.

[47] M. Fox. *Optical Properties of Solids*. 2002.

[48] R. Eisberg and R. Resnick. *Quantum Physics of Atoms, Molecules, Solids, Nuclei, and Particles*. John Wiley & Sons, 1985.

[49] T. Phipps and J. Taylor. "The magnetic moment of the hydrogen atom". In: *Physical Review* **29**.2 (1927), p. 309.

[50] P. A. M. Dirac. "The quantum theory of the electron". In: *Proceedings of the Royal Society of London. Series A, Containing Papers of a Mathematical and Physical Character* **117**.778 (1928), pp. 610–624.

[51] M. A. Nielsen and I. Chuang. *Quantum Computation and Quantum Information*. 2002.

[52] Y.-Y. Jau et al. "Entangling atomic spins with a Rydberg-dressed spin-flip blockade". In: *Nature Physics* **12**.1 (2016), p. 71.

[53] C. H. Bennett et al. "Teleporting an unknown quantum state via dual classical and Einstein-Podolsky-Rosen channels". In: *Physical Review Letters* **70**.13 (1993), p. 1895.

[54] C. H. Bennett et al. "Concentrating partial entanglement by local operations". In: *Physical Review A* **53**.4 (1996), p. 2046.

[55] J. Von Neumann. *Mathematische Grundlagen der Quantenmechanik*. Vol. 38. Springer-Verlag, 2013.

[56] C. H. Bennett et al. "Mixed-state entanglement and quantum error correction". In: *Physical Review A* **54**.5 (1996), p. 3824.

[57] S. Hill and W. K. Wootters. "Entanglement of a pair of quantum bits". In: *Physical Review Letters* **78**.26 (1997), p. 5022.

[58] W. K. Wootters. "Entanglement of formation of an arbitrary state of two qubits". In: *Physical Review Letters* **80**.10 (1998), p. 2245.

[59] E. T. Jaynes and F. W. Cummings. "Comparison of quantum and semiclassical radiation theories with application to the beam maser". In: *Proceedings of the IEEE* **51**.1 (1963), pp. 89–109.

[60] C. Gerry, P. Knight, and P. L. Knight. *Introductory Quantum Optics*. Cambridge university press, 2005.

[61] B. H. Bransden, C. J. Joachain, and T. J. Plivier. *Physics of Atoms and Molecules*. Pearson Education India, 2003.

[62] P. Kok and B. W. Lovett. *Introduction to Optical Quantum Information Processing*. Cambridge University Press, 2010.

[63] A. Kurcz et al. "Rotating wave approximation and entropy". In: *Physics Letters A* **374**.36 (2010), pp. 3726–3732.

[64] Y. Wang and J. Y. Haw. "Bridging the gap between the Jaynes–Cummings and Rabi models using an intermediate rotating wave approximation". In: *Physics Letters A* **379**.8 (2015), pp. 779–786.

[65] A. Ridolfo et al. "Photon blockade in the ultrastrong coupling regime". In: *Physical Review Letters* **109**.19 (2012), p. 193602.

[66] J.-T. Shen and S. Fan. "Coherent photon transport from spontaneous emission in one-dimensional waveguides". In: *Optics Letters* **30**.15 (2005), pp. 2001–2003.

[67] S. A. Maier. *Plasmonics: Fundamentals and Applications*. Springer Science & Business Media, 2007.

[68] H.-P. Breuer, F. Petruccione, et al. *The Theory of Open Quantum Systems*. Oxford University Press on Demand, 2002.

[69] G. Lindblad. "On the generators of quantum dynamical semigroups". In: *Communications in Mathematical Physics* **48**.2 (1976), pp. 119–130.

[70] H. M. Wiseman and G. J. Milburn. *Quantum Measurement and Control*. Cambridge University Press, 2009.

[71] P. Pearle. "Simple derivation of the Lindblad equation". In: *European Journal of Physics* **33**.4 (2012), p. 805.

[72] A. Reigue et al. "Probing electron-phonon interaction through two-photon interference in resonantly driven semiconductor quantum dots". In: *Physical Review Letters* **118**.23 (2017), p. 233602.

[73] I. de Vega and D. Alonso. "Dynamics of non-Markovian open quantum systems". In: *Reviews of Modern Physics* **89**.1 (2017), p. 015001.

[74] B. Schumacher and M. Westmoreland. *Quantum Processes Systems, and Information*. Cambridge University Press, 2010.

[75] B. Krummheuer, V. M. Axt, and T. Kuhn. "Theory of pure dephasing and the resulting absorption line shape in semiconductor quantum dots". In: *Physical Review B* **65**.19 (2002), p. 195313.

[76] G. Agarwal. *Quantum Optics*. Quantum Optics. Cambridge University Press, 2013.

[77] J. R. Johansson, P. D. Nation, and F. Nori. "QuTiP: An open-source Python framework for the dynamics of open quantum systems". In: *Computer Physics Communications* **183**.8 (2012), pp. 1760–1772.

[78] H. Torrey. "Transient nutations in nuclear magnetic resonance". In: *Physical Review* **76**.8 (1949), p. 1059.

[79] S. Wolfram et al. *Mathematica*. Cambridge University Press, 1996.

[80] M. Collett and C. Gardiner. "Squeezing of intracavity and traveling-wave light fields produced in parametric amplification". In: *Physical Review A* **30**.3 (1984), p. 1386.

[81] C. Gardiner and M. Collett. "Input and output in damped quantum systems: Quantum stochastic differential equations and the master equation". In: *Physical Review A* **31**.6 (1985), p. 3761.

[82] D. F. Walls and G. J. Milburn. *Quantum Optics*. Springer Science & Business Media, 2007.

[83] K. F. Riley, M. P. Hobson, and S. J. Bence. *Mathematical Methods for Physics and Engineering: a Comprehensive Guide*. Cambridge University Press, 2006.

[84] F. G. Smith and T. A. King. *Optics and Photonics: An Introduction*. 2001.

[85] T. M. Barlow, R. Bennett, and A. Beige. "A master equation for a two-sided optical cavity". In: *Journal of Modern Optics* **62**.sup2 (2015), S11–S20.

[86] S. Barnett and P. Radmore. "Quantum theory of cavity quasimodes". In: *Optics Communications* **68**.5 (1988), pp. 364–368.

[87] R. Lang, M. O. Scully, and W. E. Lamb Jr. "Why is the laser line so narrow? A theory of single-quasimode laser operation". In: *Physical Review A* **7**.5 (1973), p. 1788.

[88] U. Fano. "Effects of configuration interaction on intensities and phase shifts". In: *Physical Review* **124**.6 (1961), p. 1866.

[89] T. Lancaster and S. J. Blundell. *Quantum Field Theory for the Gifted Amateur*. OUP Oxford, 2014.

[90] P. Coleman. *Introduction to Many-Body Physics*. Cambridge University Press, 2015.

[91] F. J. Dyson. "The S matrix in quantum electrodynamics". In: *Physical Review* **75**.11 (1949), p. 1736.

[92] M. D. Schwartz. *Quantum Field Theory and The Standard Model*. Cambridge University Press, 2014.

[93] S. Fan, Ş. E. Kocabaş, and J.-T. Shen. "Input-output formalism for few-photon transport in one-dimensional nanophotonic waveguides coupled to a qubit". In: *Physical Review A* **82**.6 (2010), p. 063821.

[94] D. L. Hurst and P. Kok. "Analytic few-photon scattering in waveguide QED". In: *Physical Review A* **97**.4 (2018), p. 043850.

[95] S. Xu and S. Fan. "Input-output formalism for few-photon transport: A systematic treatment beyond two photons". In: *Physical Review A* **91**.4 (2015), p. 043845.

[96] T. Caneva et al. "Quantum dynamics of propagating photons with strong interactions: a generalized input–output formalism". In: *New Journal of Physics* **17**.11 (2015), p. 113001.

[97] T. Shi, D. E. Chang, and J. I. Cirac. "Multiphoton-scattering theory and generalized master equations". In: *Physical Review A* **92**.5 (2015), p. 053834.

[98] T. Shi and C. Sun. "Lehmann-Symanzik-Zimmermann reduction approach to multiphoton scattering in coupled-resonator arrays". In: *Physical Review B* **79**.20 (2009), p. 205111.

[99] S. Xu, E. Rephaeli, and S. Fan. "Analytic properties of two-photon scattering matrix in integrated quantum systems determined by the cluster decomposition principle". In: *Physical Review Letters* **111**.22 (2013), p. 223602.

[100] T. F. See, C. Noh, and D. G. Angelakis. "Diagrammatic approach to multiphoton scattering". In: *Physical Review A* **95**.5 (2017), p. 053845.

[101] T. Shi, Y. Chang, and J. J. García-Ripoll. "Ultrastrong coupling few-photon scattering theory". In: *Physical Review Letters* **120**.15 (2018), p. 153602.

[102] W. Konyk and J. Gea-Banacloche. "Quantum multimode treatment of light scattering by an atom in a waveguide". In: *Physical Review A* **93**.6 (2016), p. 063807.

[103] S. D. Barrett and P. Kok. "Efficient high-fidelity quantum computation using matter qubits and linear optics". In: *Physical Review A* **71**.6 (2005), p. 060310.

[104] A. Roulet, H. N. Le, and V. Scarani. "Two photons on an atomic beam splitter: Nonlinear scattering and induced correlations". In: *Physical Review A* **93**.3 (2016), p. 033838.

[105] B. Q. Baragiola and J. Combes. "Quantum trajectories for propagating Fock states". In: *Physical Review A* **96**.2 (2017), p. 023819.

[106] K. A. Fischer et al. "Scattering into one-dimensional waveguides from a coherently-driven quantum-optical system". In: *Quantum* **2** (2018), p. 69.

[107] A. Branczyk. "Non-classical states of light". In: *PhD Thesis* (2010).

[108] I. Suslov. "Divergent perturbation series". In: *Journal of Experimental and Theoretical Physics* **100**.6 (2005), pp. 1188–1233.

[109] G.-C. Wick. "The evaluation of the collision matrix". In: *Physical Review* **80**.2 (1950), p. 268.

[110] M. Spivak. *Calculus*. Cambridge University Press, 1994.

[111] J.-T. Shen and S. Fan. "Strongly correlated two-photon transport in a one-dimensional waveguide coupled to a two-level system". In: *Physical Review Letters* **98**.15 (2007), p. 153003.

[112] I. Shomroni et al. “All-optical routing of single photons by a one-atom switch controlled by a single photon”. In: *Science* **345**.6199 (2014), pp. 903–906.

[113] A. Reiserer, S. Ritter, and G. Rempe. “Nondestructive detection of an optical photon”. In: *Science* **342**.6164 (2013), pp. 1349–1351.

[114] A. M. Dawes et al. “All-optical switching in rubidium vapor”. In: *Science* **308**.5722 (2005), pp. 672–674.

[115] T. Tsoi and C. Law. “Single-photon scattering on Λ-type three-level atoms in a one-dimensional waveguide”. In: *Physical Review A* **80**.3 (2009), p. 033823.

[116] D. Witthaut and A. S. Sørensen. “Photon scattering by a three-level emitter in a one-dimensional waveguide”. In: *New Journal of Physics* **12**.4 (2010), p. 043052.

[117] M. Bradford and J.-T. Shen. “Single-photon frequency conversion by exploiting quantum interference”. In: *Physical Review A* **85**.4 (2012), p. 043814.

[118] K. Koshino et al. “Theory of deterministic down-conversion of single photons occurring at an impedance-matched Λ system”. In: *New Journal of Physics* **15**.11 (2013), p. 115010.

[119] S. Xu and S. Fan. “Generalized cluster decomposition principle illustrated in waveguide quantum electrodynamics”. In: *Physical Review A* **95**.6 (2017), p. 063809.

[120] M. Pletyukhov and V. Gritsev. “Scattering of massless particles in one-dimensional chiral channel”. In: *New Journal of Physics* **14**.9 (2012), p. 095028.

[121] S. Weinberg. *The Quantum Theory of Fields*. Vol. 2. Cambridge university press, 1995.

[122] J. R. Taylor. *Scattering theory: the quantum theory of nonrelativistic collisions*. Courier Corporation, 2006.

[123] J.-F. Huang et al. “Controlling single-photon transport in waveguides with finite cross section”. In: *Physical Review A* **88**.1 (2013), p. 013836.

[124] D. L. Hurst et al. “Nonreciprocal Transmission and Reflection of a Chirally Coupled Quantum Dot”. In: *Nano Letters* **18**.9 (2018), pp. 5475–5481.

[125] D. Hallett et al. “Electrical control of nonlinear quantum optics in a nano-photonic waveguide”. In: *Optica* **5**.5 (2018), pp. 644–650.

[126] P. Lodahl et al. “Chiral quantum optics”. In: *Nature* **541**.7638 (2017), p. 473.

[127] I. Söllner et al. “Deterministic photon–emitter coupling in chiral photonic circuits”. In: *Nature Nanotechnology* **10**.9 (2015), pp. 775–778.

[128] C. Junge et al. “Strong coupling between single atoms and nontransversal photons”. In: *Physical Review Letters* **110**.21 (2013), p. 213604.

[129] B. Lang, R. Oulton, and D. M. Beggs. “Optimised photonic crystal waveguide for chiral light–matter interactions”. In: *Journal of Optics* **19**.4 (2017), p. 045001.

[130] A. Ramsay. “A review of the coherent optical control of the exciton and spin states of semiconductor quantum dots”. In: *Semiconductor Science and Technology* **25**.10 (2010), p. 103001.

[131] A. C. Phillips. *Introduction to Quantum Mechanics*. John Wiley & Sons, 2013.

[132] M. Bayer et al. “Fine structure of neutral and charged excitons in self-assembled In (Ga) As/(Al) GaAs quantum dots”. In: *Physical Review B* **65**.19 (2002), p. 195315.

[133] R. Coles et al. “Chirality of nanophotonic waveguide with embedded quantum emitter for unidirectional spin transfer”. In: *Nature Communications* **7** (2016), p. 11183.

[134] A. Nysteen. “Few-photon Non-linearities in Nanophotonic Devices for Quantum Information Technology”. In: *PhD Thesis* (2015).

[135] M. N. Makhonin et al. “Waveguide coupled resonance fluorescence from on-chip quantum emitter”. In: *Nano Letters* **14**.12 (2014), pp. 6997–7002.

[136] A. Auffèves-Garnier et al. “Giant optical nonlinearity induced by a single two-level system interacting with a cavity in the Purcell regime”. In: *Physical Review A* **75**.5 (2007), p. 053823.

[137] L. Allen and J. H. Eberly. *Optical Resonance and Two-Level Atoms*. Vol. 28. Courier Corporation, 1987.

[138] H. Thyrrestrup et al. “Quantum Optics with Near-Lifetime-Limited Quantum-Dot Transitions in a Nanophotonic Waveguide”. In: *Nano Letters* **18**.3 (2018), pp. 1801–1806.

[139] C. Matthiesen, A. N. Vamivakas, and M. Atatüre. “Subnatural linewidth single photons from a quantum dot”. In: *Physical Review Letters* **108**.9 (2012), p. 093602.

[140] S. A. Empedocles and M. G. Bawendi. “Influence of spectral diffusion on the line shapes of single CdSe nanocrystallite quantum dots”. In: *The Journal of Physical Chemistry B* **103**.11 (1999), pp. 1826–1830.

[141] A. Javadi et al. “Single-photon non-linear optics with a quantum dot in a waveguide”. In: *Nature Communications* **6** (2015), p. 8655.

[142] Lumerical. *FDTD Solutions*. 2016.

[143] A. Melliti et al. “Radiative recombination lifetime of excitons in self-organized InAs/GaAs quantum dots”. In: *Solid State Communications* **128**.6-7 (2003), pp. 213–217.

[144] J. M. Hvam, K. Leosson, and D. Birkedal. “Coherence and dephasing in self-assembled quantum dots”. In: *Nanotechnology, 2003. IEEE-NANO 2003. 2003 Third IEEE Conference on*. Vol. 1. IEEE. 2003, pp. 122–125.

[145] J. Ishi-Hayase et al. “Negligible pure dephasing in InAs self-assembled quantum dots”. In: *Japanese Journal of Applied Physics* **46**.9S (2007), p. 6352.

[146] H. S. Dutta et al. “Coupling light in photonic crystal waveguides: A review”. In: *Photonics and Nanostructures-Fundamentals and Applications* **20** (2016), pp. 41–58.

[147] M. Fox. *A Student’s Guide to Atomic Physics*. Student’s Guides. Cambridge University Press, 2018.

[148] S. Fan. “Sharp asymmetric line shapes in side-coupled waveguide-cavity systems”. In: *Applied Physics Letters* **80**.6 (2002), pp. 908–910.

[149] J. D. Joannopoulos et al. *Photonic Crystals: Molding the Flow of Light*. Princeton university press, 2011.

[150] M. Arcari et al. “Near-unity coupling efficiency of a quantum emitter to a photonic crystal waveguide”. In: *Physical Review Letters* **113**.9 (2014), p. 093603.

[151] B. Lang, D. M. Beggs, and R. Oulton. “Time-reversal constraint limits unidirectional photon emission in slow-light photonic crystals”. In: *Philosophical Transactions of the Royal Society A: Mathematical, Physical and Engineering Sciences* **374**.2075 (2016), p. 20150263.

[152] N. Ha et al. “Size-dependent line broadening in the emission spectra of single GaAs quantum dots: Impact of surface charge on spectral diffusion”. In: *Physical Review B* **92**.7 (2015), p. 075306.

[153] A. G. Fowler et al. “Surface codes: Towards practical large-scale quantum computation”. In: *Physical Review A* **86**.3 (2012), p. 032324.

[154] M. J. Burek et al. “Fiber-coupled diamond quantum nanophotonic interface”. In: *Physical Review Applied* **8**.2 (2017), p. 024026.

[155] M. K. Bhaskar et al. “Quantum nonlinear optics with a germanium-vacancy color center in a nanoscale diamond waveguide”. In: *Physical Review Letters* **118**.22 (2017), p. 223603.

[156] W. K. Wootters. "Quantum entanglement as a quantifiable resource". In: *Philosophical Transactions of the Royal Society of London. Series A: Mathematical, Physical and Engineering Sciences* **356**.1743 (1998), pp. 1717–1731.

[157] R. McDermott et al. "Quantum–classical interface based on single flux quantum digital logic". In: *Quantum Science and Technology* **3**.2 (2018), p. 024004.

[158] D. Kielpinski, C. Monroe, and D. J. Wineland. "Architecture for a large-scale ion-trap quantum computer". In: *Nature* **417**.6890 (2002), p. 709.

[159] N. Ledentsov et al. "Quantum dot heterostructures: fabrication, properties, lasers". In: *Semiconductors* **32**.4 (1998), pp. 343–365.

[160] J. Metz and S. Barrett. "Effect of frequency-mismatched photons in quantum-information processing". In: *Physical Review A* **77**.4 (2008), p. 042323.

[161] R. Stockill et al. "Phase-tuned entangled state generation between distant spin qubits". In: *Physical Review Letters* **119**.1 (2017), p. 010503.

[162] J. Busch et al. "Entangling distant quantum dots using classical interference". In: *Physical Review A* **78**.4 (2008), p. 040301.

[163] G. Z. Cohen and L. Sham. "Rapid creation of distant entanglement by multiphoton resonant fluorescence". In: *Physical Review B* **88**.24 (2013), p. 245306.

[164] M. Massimi. *Pauli's Exclusion Principle: The Origin and Validation of a Scientific Principle*. Cambridge University Press, 2005.

[165] P. Michler. *Single Quantum Dots: Fundamentals, Applications and New Concepts*. Vol. 90. Springer Science & Business Media, 2003.

[166] S. Barnett and P. M. Radmore. *Methods in Theoretical Quantum Optics*. Vol. 15. Oxford University Press, 2002.

[167] J. S. Bell. "On the Einstein Podolsky Rosen paradox". In: *Physics Physique Fizika* **1**.3 (1964), p. 195.

[168] R. Raussendorf and H. J. Briegel. "A one-way quantum computer". In: *Physical Review Letters* **86**.22 (2001), p. 5188.

[169] S. Mahmoodian, P. Lodahl, and A. S. Sørensen. "Quantum networks with chiral-light–matter interaction in waveguides". In: *Physical Review Letters* **117**.24 (2016), p. 240501.

[170] E. Rephaeli and S. Fan. "Dissipation in few-photon waveguide transport". In: *Photonics Research* **1**.3 (2013), pp. 110–114.

[171] S. Hughes. "Enhanced single-photon emission from quantum dots in photonic crystal waveguides and nanocavities". In: *Optics Letters* **29**.22 (2004), pp. 2659–2661.

[172] P. P. Rohde and T. C. Ralph. "Frequency and temporal effects in linear optical quantum computing". In: *Physical Review A* **71**.3 (2005), p. 032320.

[173] A. Nysteen, D. P. McCutcheon, and J. Mørk. "Strong nonlinearity-induced correlations for counterpropagating photons scattering on a two-level emitter". In: *Physical Review A* **91**.6 (2015), p. 063823.

[174] H. Lee, P. Kok, and J. P. Dowling. "A quantum Rosetta stone for interferometry". In: *Journal of Modern Optics* **49**.14-15 (2002), pp. 2325–2338.

[175] C.-K. Hong, Z.-Y. Ou, and L. Mandel. "Measurement of subpicosecond time intervals between two photons by interference". In: *Physical Review Letters* **59**.18 (1987), p. 2044.

[176] H. Zheng, D. J. Gauthier, and H. U. Baranger. "Waveguide QED: Many-body bound-state effects in coherent and Fock-state scattering from a two-level system". In: *Physical Review A* **82**.6 (2010), p. 063816.

[177] A. Einstein. "Zur quantentheorie der strahlung". In: *Phys. Z.* **18** (1917), pp. 121–128.

[178] A. Nysteen et al. "Limitations of two-level emitters as nonlinearities in two-photon controlled-phase gates". In: *Physical Review A* **95**.6 (2017), p. 062304.

[179] D. L. Hurst et al. "Generating maximal entanglement between spectrally distinct solid-state emitters". In: *arXiv preprint arXiv:1901.03631* (2019).

[180] R. M. Heath et al. "Nanoantenna enhancement for telecom-wavelength superconducting single photon detectors". In: *Nano Letters* **15**.2 (2015), pp. 819–822.

[181] D. Klyshko, A. Penin, and B. Polkovnikov. "Parametric luminescence and light scattering by polaritons". In: *Soviet Journal of Experimental and Theoretical Physics Letters* **11** (1970), p. 5.

[182] I. Merkulov, A. L. Efros, and M. Rosen. "Electron spin relaxation by nuclei in semiconductor quantum dots". In: *Physical Review B* **65**.20 (2002), p. 205309.

[183] L. Viola, E. Knill, and S. Lloyd. "Dynamical decoupling of open quantum systems". In: *Physical Review Letters* **82**.12 (1999), p. 2417.

[184] J. Iles-Smith et al. "Limits to coherent scattering and photon coalescence from solid-state quantum emitters". In: *Physical Review B* **95**.20 (2017), p. 201305.

[185] J. Iles-Smith et al. "Phonon scattering inhibits simultaneous near-unity efficiency and indistinguishability in semiconductor single-photon sources". In: *Nature Photonics* **11**.8 (2017), p. 521.

[186] A. Roulet and V. Scarani. "Solving the scattering of N photons on a two-level atom without computation". In: *New Journal of Physics* **18**.9 (2016), p. 093035.

[187] L.-M. Duan and H. Kimble. "Scalable photonic quantum computation through cavity-assisted interactions". In: *Physical Review Letters* **92**.12 (2004), p. 127902.

[188] J. Borregaard, A. Sørensen, and P. Lodahl. "Quantum Networks with Deterministic Spin-Photon Interfaces". In: *arXiv preprint arXiv:1811.08242* (2018).

[189] L. Ortiz-Gutiérrez et al. "Experimental Fock-State Superradiance". In: *Physical Review Letters* **120**.8 (2018), p. 083603.

[190] J. Combes, J. Kerckhoff, and M. Sarovar. "The SLH framework for modeling quantum input-output networks". In: *Advances in Physics: X* **2**.3 (2017), pp. 784–888.

[191] P. G. Kwiat et al. "Proposal for a loophole-free Bell inequality experiment". In: *Physical Review A* **49**.5 (1994), p. 3209.

[192] V. Vdovin and M. Tokman. "Generation of a two-mode squeezed vacuum field in forward four-wave-mixing process in an ensemble of Λ atoms". In: *Physical Review A* **87**.1 (2013), p. 012323.

[193] B. L. Schumaker. "Noise in homodyne detection". In: *Optics Letters* **9**.5 (1984), pp. 189–191.

[194] K. A. Stroud and D. J. Booth. *Advanced Engineering Mathematics*. Macmillan International Higher Education, 2011.

[195] H. J. Weber and G. B. Arfken. *Essential Mathematical Methods for Physicists, ISE*. Elsevier, 2003.

[196] H. Kleinert. *Path Integrals in Quantum Mechanics, Statistics, Polymer Physics, and Financial Markets*. World scientific, 2009.

[197] F. J. Dyson. "Divergence of perturbation theory in quantum electrodynamics". In: *Physical Review* **85**.4 (1952), p. 631.

[198] C. M. Bender and S. A. Orszag. *Advanced Mathematical Methods for Scientists and Engineers I: Asymptotic Methods and Perturbation Theory*. Springer Science & Business Media, 2013.

[199] M. E. Peskin and D. V. Schroeder. *An Introduction To Quantum Field Theory (Frontiers in Physics)*. Westview Press Incorporated, 1995.